OCULAR STRUCTURES AND VISUAL FUNCTION IN CHILDHOOD EMMETROPIA AND MYOPIA: IMPLICATIONS FOR MYOPIA CONTROL TREATMENT

A thesis presented to the graduate faculty of New England College of Optometry in partial fulfillment of the requirements for the degree of Master of Science

Yan Wang

May, 2026

OCULAR STRUCTURES AND VISUAL FUNCTION IN CHILDHOOD EMMETROPIA AND MYOPIA: IMPLICATIONS FOR MYOPIA CONTROL TREATMENT

Yan Wang

This manuscript has been read and accepted by the Thesis Committee in satisfaction with the thesis requirement for the degree of Master of Science

5/11/2026
Date

DocuSigned by:
Fuensanta Vera-Diaz
1502BB240B7D484...
Fuensanta A. Vera-Diaz, OD, PhD, FAAO, FARVO
Graduate Faculty Advisor

DocuSigned by:
Kristen L. Kerber
459AE881FB8A4ED...
Kristen L. Kerber, OD, MSc, FAAO
Internal Examiner

Firmado por:
Beatriz Redondo
1BCAE67560B2477...
Beatriz Redondo, BSc Optom, PhD
External Examiner

5/11/2026
Date

DocuSigned by:
78A8AD972399447...
Athanasios Panorgias, MSc, PhD
Director of Graduate Studies

OCULAR STRUCTURES AND VISUAL FUNCTION IN CHILDHOOD EMMETROPIA AND MYOPIA: IMPLICATIONS FOR MYOPIA CONTROL TREATMENT

Yan Wang

New England College of Optometry, 2026

ABSTRACT

Purpose: To characterize ocular structures and visual functions in children with early-to-moderate myopia (MYOP) undergoing myopia-control treatment compared with controls with emmetropia (EM), and to determine how baseline characteristics may influence treatment response and progression.

Methods: In this prospective longitudinal study, children with MYOP (N=13) were compared to EM controls (N=10). Assessments included a clinical exam, on- and off-axis biometry, corneal biomechanics, wide-field OCT, optical aberrations, pattern ERG (pERG) using naturalistic stimuli, and psychophysical measures of contrast sensitivity and useful field of view (UFOV). Linear mixed models were used for repeated spatial and longitudinal measures, and ANCOVA/MANCOVA for baseline group comparisons with adjustments for age and axial length (AXL), as appropriate.

Results: At baseline, central AXL was greater in MYOP than EM (24.88 ± 0.74 mm vs. 23.41 ± 0.68 mm; $p < 0.001$), whereas anterior segment geometry, posterior thickness profiles, and corneal biomechanics were largely comparable between groups (choroid

thickness p = 0.107; retina thickness p = 0.458, hysteresis: p = 0.569). Optically, peripheral defocus (DEF) differed by refractive group (F = 11.07, p = 0.004) and varied by retinal area (Group × Area interaction F = 7.12, p < 0.001). Horizontal coma showed only a weak overall group effect (F = 4.480, p = 0.049), whereas spherical aberration (SA, Z12) varied by retinal area (F = 5.720, p = 0.002) but not by refractive group. Strehl ratio (SR) including all aberrations showed no main group effect (p = 0.330) but significant area-dependent differences (Group × Area: p < 0.001), while SR including only high-order aberrations showed significant effects of group (p = 0.002), area (p = 0.004), and their interaction (p < 0.001). Functionally, central (Pillai's trace = 0.429, F = 2.249, p = 0.124) and peripheral (Pillai's trace = 0.278, F = 0.960, p = 0.470) contrast sensitivity as well as pERG responses were preserved in MYOP (density p = 0.814; latency p = 0.107). Conversely, MYOP showed reduced peripheral acuity on UFOV (F = 10.557, p = 0.007) and altered temporal processing strategy (F = 4.897, p = 0.018). Longitudinally, broader structural measures remained stable, while descriptive optics suggested reduced DEF and modest increase in SA over follow-up.

Conclusions: Early-to-moderate pediatric myopia was characterized primarily by ocular elongation and region-dependent differences in peripheral optical quality, with limited baseline differences in gross ocular structure (increased individual variability in posterior corneal astigmatism in MYOP), corneal biomechanics, contrast sensitivity, or pERG responses. In contrast, children with myopia showed poorer performance on peripheral visual tasks and descriptive treatment-associated shifts in DEF and SA. These findings help define the anatomical and sensory context in which children adapt to myopia-control optics and may help explain inter-individual differences in treatment response.

Outline

List of Tables

List of Figures

1. General Background

Myopia has exhibited a steady rise in prevalence over recent decades, with global myopia rates increasing by approximately 5% per decade (Holden et al., 2016). By the year 2050, it is anticipated that nearly half of the world's population will have myopia (Holden et al., 2016). While historically regarded as a benign refractive error, myopia now stands at the forefront of ocular health concerns. The National Academy of Sciences defines myopia as a disease since robust evidence links myopia to various ocular pathologies, including retinal detachment, glaucoma, and myopic maculopathy (National Academies of Sciences, Engineering, and Medicine, 2024; Troilo et al., 2019). Consequently, myopia has emerged as a significant public health challenge and a socio-economic burden on a global scale.

In response to this growing crisis, both research and clinical communities have directed their efforts towards developing strategies aimed at slowing down the progression of myopia. Various strategies have been developed to slow down the progression of myopia, including pharmacological interventions such as low-dose atropine eye drops, as well as optical methods involving specially designed ophthalmic lenses and contact lenses like orthokeratology (Wildsoet et al., 2019). While these approaches have demonstrated positive effects in managing myopia progression in children, their effectiveness remains unpredictable (Bao et al., 2022; Chen et al., 2022; Ha et al., 2022; Vera-Diaz et al., 2023; Weng et al., 2022). Furthermore, there is evidence suggesting that the quality of a child's vision may be compromised after utilizing these treatments.

For example, these strategies have been associated with visual discomfort, light disturbance, high order aberration, lower contrast sensitivity and changes in the accommodative and vergence systems (Berntsen, 2018; Cooper et al., 2013; Kang, McAlinden, & Wildsoet, 2017; Lipson, Boland, & McAlinden, 2022; Nti & Berntsen, 2020; Sankaridurg et al., 2021; Song et al., 2021; Wildsoet et al., 2019). The impact on vision is influenced by the specific myopia control approach employed and is likely influenced by individual structural and functional characteristics, including neural adaptation (Corpus & Piñero, 2022).

Previous studies have indicated that low-dose atropine eye drops used for myopia control have minimal impact on accommodation, pupil diameter, and visual acuity (VA) in children, although these are dose-dependent and may be significant with the highest doses used in clinic (0.05%) (Chen et al., 2022; Ha et al., 2022; Polling et al., 2016). Nevertheless, the potential effects of low-dose atropine on reading, eye movements, visual search, and other aspects of temporal vision have not been explored before and will be assessed in this study.

The corneal reshaping that occurs with orthokeratology lenses decreases corneal asphericity, increasing the corneal and total high order aberrations, particularly primary spherical aberration (SA) (Ding et al., 2022; Mathur & Atchison, 2009). Although these higher-order aberrations have been shown to have no clinically significant impact on high-contrast acuity, they do significantly reduce low-contrast vision. However, they may improve visual function. Han et al. (2018), in a randomized study of 240 myopic children demonstrated that long-term orthokeratology improves accommodative accuracy and facility. Additionally, Song et al. (2021) found that switching to orthokeratology lenses led to distance and near exophoric shifts, improvements in accommodative function, stereopsis, ocular motility, and a decrease

in the binocular horizontal vergence range. However, the potential effects of orthokeratology lenses on reading, visual search, and other aspects of temporal and peripheral vision have not been previously investigated and will therefore be examined in this study.

Multifocal and dual-focus lenses may also increase high order aberrations, typically causing positive SA and reduced low-contrast VA (Huang et al., 2022; Nti & Berntsen, 2020; Papadogiannis et al., 2022). These lens designs have been shown to reduce accommodative response and also induce changes in binocular vision (Schmid, Gifford, & Atchison, 2023; Vera et al., 2023). Other potential consequences of the use of these lenses such as reading, visual search and other aspects of temporal and peripheral vision have not been previously examined and will be evaluated in this study.

In terms of spectacle-based strategies, several visual functions have been found to be affected, including peripheral visual acuity. For instance, Lu et al. (2020) demonstrated that children wearing Defocus Incorporated Multiple Segments (DIMS) lenses experienced reduced VA for the mid-peripheral defocus area, which could not be adapted within a week. Similarly, Gao et al. (2021) showed that Highly Aspherical Lenslet (HAL) lenses, when used for peripheral vision, decreased high-contrast VA by 0.07 logMAR and reduced low-contrast VA by 0.14 logMAR. However, no changes in the accommodation and vergence system were observed with spectacle-based strategies (Lam et al., 2020; Vera-Diaz et al., 2023).

With the 2025 U.S. FDA market authorization of the Essilor® Stellest® lens (Paris, France), HAL spectacle lenses may see broader adoption in academic and clinical practice in the

United States, as 5-year longitudinal evidence from Li et al. (2025) supports their efficacy in slowing myopia progression and axial elongation.

Previous studies observed that retinal function exhibits distinct variations between myopic and non-myopic eyes. Some have documented a reduction in amplitude of the retinal response, coupled with a minor postponement in the peak response time, in myopic eyes (Chen, Brown, & Schmid, 2006; Ho, Kee, & Chan, 2012; Koh et al., 2014; Park et al., 2013). These observations become increasingly pronounced with higher refractive errors, characterized by a decrement in amplitudes ranging from 5 to 10% per millimeter of axial elongation (Kader, 2012; Sachidanandam, Ravi, & Sen, 2017). While the impact of myopia and axial elongation on retinal function is broadly acknowledged, the scientific community has yet to reach a consensus on whether the central or peripheral retina is more influenced and where the response is predominantly affected. Furthermore, there is a notable scarcity of studies that concentrate on the alterations in retinal activity resulting from myopia treatment.

Queirós et al. (2020) investigated the impact of 60 days of orthokeratology treatment on pattern electroretinography (pERG) and visual evoked potentials (VEP). They observed a slight increase in retinal and cortical response amplitude with pERG and VEP, respectively, but these differences were not statistically significant during the 60-day treatment period. A comparable observation was made in a preliminary study where participants with myopia wore a specially engineered multifocal contact lens for a duration of 30 minutes (Amorim-de-Sousa et al., 2023). However, given the non-optimal nature of both the procedure (which involved the use of single vision followed by multifocal contact lenses) and the limited

number of participants (Lipson, Boland, & McAlinden, 2022), additional research is needed to establish more compelling evidence.

Regarding atropine, the existing scientific literature is limited, and the results that have been reported are controversial, underscoring the necessity for more comprehensive research (Chan et al., 2022; Gupta, Chakraborty, & Verkicharla, 2022; Vera-Diaz et al., 2023). On the other hand, Fernandes et al. (2026) reported that myopia-control spectacle lenses (both HAL and DIMS) induced short-term retinal electrophysiological changes in young myopic adults, with significant increases in pattern ERG amplitudes after 30 minutes of wear compared with baseline and variable persistence of these effects after 15 days depending on lens design.

Myopia development may also affect the cornea's biomechanical properties, including corneal hysteresis (CH) (Chang, Chang, & Wang, 2010; Shen et al., 2008; Song et al., 2008). The cornea's biomechanical properties, crucial to its function and impact on vision, are determined by factors such as extracellular matrix components, collagen lamella organization, and osmotic pressure changes (Piñero & Alcón, 2015). A few studies have shown that a decrease in CH is associated with an increase in axial length (AXL) (Chang, Chang, & Wang, 2010; Shen et al., 2008; Song et al., 2008). This suggests that CH could potentially serve as a future benchmark for deciding when to initiate myopia control. Additionally, there has been limited research, primarily on orthokeratology lenses (Chen, Lam, & Cho, 2009; González-Méijome et al., 2008; Shen et al., 2008; Wan et al., 2018), on the changes in CH before and after myopia control treatment.

In order to address these current gaps in knowledge, this study aims to investigate and compare the impact of myopia control strategies on various ocular structures and visual functions. The objective is to obtain information on the treatment strategy that may result in superior visual functioning and performance. In addition, this research will undertake a comparative analysis of both subjective and objective data to determine the factors contributing to myopia progression and their relative and combined influence on the outcomes of the myopia control treatment. The results of these studies may enable more accurate predictions about the future implementation of appropriate myopia-control strategies and may also help clarify the mechanisms underlying these interventions. The study includes children who plan to enroll in myopia-control treatment programs at NECO's Myopia Control Clinic (MCC) and The Dimock Center (Dimock), along with emmetropic children who previously participated in the observational PICNIC study conducted through the Children's Vision Lab at the New England College of Optometry.

2. Specific Aims

The overall objective of my MS studies was to further understand the mechanism of action of myopia control treatments by evaluating the effect of those treatments on ocular structures and functions in children with myopia. The specific aims of my thesis are:

Aim 1: To evaluate the effect of any of the currently available myopia control treatments (low dose atropine, orthokeratology, multifocal soft contact lenses, or their combinations) **on ocular structures and visual functions in children.**

For this purpose, we measured the following specific variables three times: (1) at baseline (8 to 21 days from the consultation visit; before they start any myopia control treatment), (2) following their 6 month follow up (8 to 21 days after the clinic visit), and (3) after their 12 month follow up (8 to 21 days after the clinic visit):

(i) Optical quality (aberrations) on- and off-axis (across 60 degrees in the periphery)

(ii) Biometry, including anterior and posterior corneal topography

(iii) Retinal and choroidal thickness, and shape of the posterior retina

(iv) Corneal hysteresis (CH)

(v) Contrast sensitivity (on- and off-axis)

(vi) Effective field of view

(vii) Visual search

(viii) Retinal responses natural images with varying contrast presented at different eccentricities (using pattern ERGs)

Hypotheses: (1) All myopia control treatments will affect the overall optical quality of the eye and ocular structures. (2) Functional vision will not be affected by myopia control treatments. (3) Retinal responses measured with ERG will increase with the use of myopia control treatments.

Aim 2: To evaluate the effect of the ocular structures and visual functions described in Aim-1 on the effectiveness of the treatments in controlling myopia.

The data collected in Aim-1 was used to determine the effect of the assessed ocular structures and visual functions on the participants' myopia progression, measured as increase in AXL. This assessment will help us understand the factors influencing myopia progression and the effectiveness of myopia control treatments.

Hypothesis: A greater progression of myopia is anticipated to be associated with lower contrast sensitivity, better peripheral optical quality, and suboptimal retinal responses.

3. General Methods

This is a prospective longitudinal study evaluating ocular structures and visual performance as well as changes in behaviors when using various myopia control treatments. The study also aims to assess the effect of visual functions and behaviors on the effectivity of these myopia control treatments. The study was conducted on children who are interested in enrolling in a myopia control treatment program.

3.1. Participants

We recruited a group of children with myopia (MYOP) from patients who visited NECO's MCC or Dimock for consultation and among those who decided to begin a myopia control treatment (low dose atropine, orthokeratology, multifocal soft contact lenses, or a combination). All eligible children aged 5 to 17 years who enrolled at the MCC or Dimock between November 2023 and December 2025 were invited to participate. We also recruited a group of participants with emmetropia (EM) who served as reference group.

General Inclusion criteria:

- Be at least 5 years of age and no more than 17 years of age at enrollment.
- Best uncorrected or corrected VA +0.10 LogMAR (20/25 Snellen equivalent) or better in each eye.

General Exclusion criteria:

- Previous use of a myopia control treatment.

- History of ocular disease, amblyopia or strabismus that may presently affect visual functions.
- Current use of ocular or systemic drugs that may have visual consequences.

Specific Criteria for the Myopia Group:

- Spherical equivalent (SE) refraction in the right eye (OD) ranging from −0.25 D to −10.00 D, determined with cycloplegic subjective refraction.
- Intend to start a treatment for myopia progression control.

Specific Criteria for the Emmetropia Group:

- SE OD ranging from +1.50 D to 0.00 D, determined with cycloplegic retinoscopy.

Given the limited prior data in this area and the large number of planned outcome metrics, an a priori sample size calculation was not feasible, so enrollment was guided by feasibility rather than formal power considerations.

We enrolled 10 children with EM across two separate recruitment periods: the first cohort of 6 participants was recruited in summer 2024, and the second cohort of 4 participants was recruited from late 2025 through early 2026.

We recruited 16 children participant with MYOP. The following participants were excluded: MYOP01 was excluded because the participant exceeded the upper age limit at the baseline laboratory visit. MYOP10 and MYOP11 were excluded from the baseline analysis because

they withdrew before completing the baseline assessment. MYOP04, MYOP07, and MYOP09 withdrew after baseline, and MYOP06 withdrew after the 6-month follow-up. Additionally, MYOP08 had not completed Visit (V) 3a and V3b, and MYOP12–MYOP16 had not completed V2a and V2b at the time of data processing for this thesis; accordingly, these participants were excluded from the relevant longitudinal analyses. Any other detailed data exclusion will be discussed under each corresponding result section.

3.2. Study design

Participants with myopia (MYOP) were invited to complete three sessions at the Children's Vision Lab, each lasting approximately 2.5 hours. The first session served as the baseline assessment and was scheduled 8–21 days after the initial clinical consultation and prior to initiating any myopia-control treatment. The second session occurred 6 months after treatment initiation (typically within 8–21 days of the 6-month clinic visit), and the final session occurred 12 months after treatment initiation (within 8–21 days of the 12-month clinic visit). Emmetropic participants completed a single laboratory visit using the same procedures performed by the group with MYOP.

Prior to beginning the study, the purpose and details of the experiments were explained to each eligible participant, as well as their parents or guardians. Participants were asked to read and write their name on the Assent Form, and their parent or guardian to read and sign the Informed Consent Form. After any questions from the participant, parent or guardian had satisfactorily been answered, they were asked to sign the abovementioned documents. Consent was obtained during the child's consultation visit to NECO's MCC or Dimock.

3.3. Procedures

Participants received a comprehensive battery of tests in the lab that included measurements of eye structure, sensory response, and real-world performance. Each of the three visits began with a review of the history and an assessment of their habitual and best corrected VA to ensure that all experimental tests were conducted with the best optical correction.

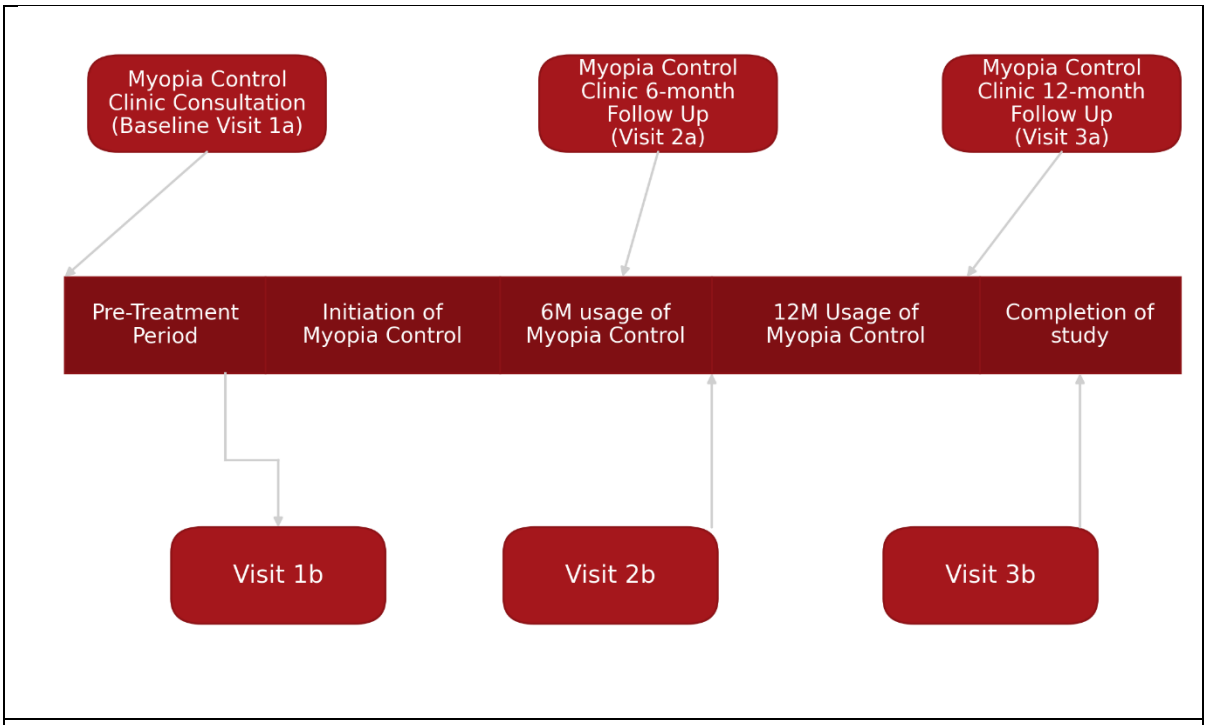

Figure 3. 1 Overview of the study design timeline for the patients with myopia.

The following experimental procedures were conducted, details for each procedure are provided in their relevant chapters:

- Chapter 4: Structural measurements were obtained using three devices: an IOLMaster 700 (ZEISS, Germany) for AXL and anterior segment length metrics and these were measured on- and off-axis; a Pentacam tomographer (OCULUS, Wetzlar, Germany) for corneal mapping; the biomechanical properties of the cornea (e.g. CH) are assessed using an Ocular Response Analyzer® G3 (Reichert, USA) (ORA).
- Chapter 5: Optical Quality: Corneal aberrations across the central ±30 degrees were measured using a fast-scanning Hartmann-Shack wavefront analyzer (Voptica, Spain) at viewing distances of 6 meters and 40 centimeters.
- Chapter 6: Retinal and choroidal thickness: wide-field Optical Coherence Tomography (OCT) scans were performed using the Spectralis system (Heidelberg Engineering, Germany). The protocol incorporated Enhanced Depth Imaging (EDI) to ensure accurate visualization of the choroid.
- Chapter 7: Retinal responses to blur were quantified using pERG with a naturalistic 'dead leaves' stimulus presented at varying eccentricities (0–12 degrees).
- Chapter 8: Visual performance was assessed at each visit using three specific tasks. The central contrast sensitivity test (identifying central grid orientations) was performed without eye-tracking. In contrast, both the peripheral contrast sensitivity test (locating peripheral patterns) and the effective field of view task (matching central and peripheral letters) were conducted using eye-tracking calibrated software.

By comparing these metrics across different visits, we were able to monitor changes throughout the course of their myopia control treatments.

3.4. General Data Processing and Analysis

Overview

Data collected across all structural, optical, and functional assessments were processed using a combination of proprietary device software, customized MATLAB scripts and excel spreadsheets. The overarching goal of the data processing phase was to extract reliable, standardized metrics for ocular anatomy, optical quality, and visual performance to facilitate longitudinal tracking and baseline comparisons between the myopic and emmetropic cohorts.

Biometry and Corneal Biomechanics (Chapter 4)

Structural dimensions of the anterior segment and AXL were extracted directly from the optical biometer at on-axis and off-axis (see Chapter 4) eccentricities. Corneal mapping data, including curvature and thickness profiles, were provided by the tomographer's software. For biomechanical assessments, the device provided automated extractions of CH, corneal resistance factor, and intraocular pressure metrics.

Optical Quality (Chapter 5)

Data captured by a peripheral scanning Hartmann-Shack wavefront analyzer were processed utilizing the instrument’s built-in software. The software extracted individual Zernike coefficients for each measured eccentricity, which were subsequently used to calculate global optical quality metrics, such as the overall Strehl ratio (SR), and a specific attention to defocus (DEF) and primary SA.

Retinal and Choroidal Thickness (Chapter 6)

Raw wide-field OCT B-scans were exported and analyzed using a custom MATLAB program. The software allowed for manual segmentation of the posterior pole to define the boundaries of the retina and choroid, followed by the automated extraction of thickness values at standardized spatial eccentricities (1, 3, 6, 10, and 14 mm).

Retinal Responses (Chapter 7)

Electrical signals recorded during the pERG testing were processed to quantify the retina's response to naturalistic 'dead leaves' stimuli. The Fourier-transformed signals were analyzed to extract response density and latency as the primary dependent variables across the tested foveal and parafoveal eccentricities.

Psychophysics (Chapter 8)

Behavioral data from the visual performance tasks were processed using customized MATLAB scripts. For both central and peripheral contrast sensitivity tests, the software fitted a contrast sensitivity function (CSF) to extract spatial frequency peaks, contrast sensitivity peaks, CSF acuity, and the area under the log CSF. For the effective field of view (UFOV) task, the scripts calculated UFOV Thresholds Size and stimulus response duration based on participant accuracy across the designated eccentricities.

4. Biometric Studies

4.1. Background

This chapter summarizes the rationale for collecting each biometric dataset and explains how each contributes to evaluating treatment-related changes in ocular structure or visual function and to identifying baseline predictors of myopia-control effectiveness.

Demographic variables (e.g., age, sex) and baseline clinical characteristics (e.g., refractive error, treatment modality) were collected to characterize the study cohort and contextualize longitudinal results. These data allowed us to assess comparability between groups and account for clinically relevant factors that might influence outcomes. Furthermore, documenting the treatment start date ensured that baseline and follow-up measurements were accurately aligned with the treatment duration.

IOLMaster 700 optical biometry was collected since AXL is the primary structural metric used to quantify myopia progression and therefore serves as the key outcome for myopia control treatment effectiveness in this thesis (Troilo et al., 2019). Additional anterior segment measures (e.g., central corneal thickness, anterior chamber depth, lens thickness, corneal radii) were also collected to characterize ocular structure and to test whether baseline ocular geometry is associated with subsequent axial elongation. On- and off-axis measurements (10° temporal, 10° nasal) were included to capture potential regional biometric differences related to eye shape that may differ by refractive group and/or change with myopia treatment (National Academies of Sciences, Engineering, and Medicine, 2024; Troilo et al., 2019).

Pentacam HR tomography was collected to quantify corneal structure (anterior/posterior curvature, pachymetry/thickness distribution, and topography) because corneal geometry can be altered by some myopia-control strategies and may influence downstream visual performance. In particular, orthokeratology-induced corneal reshaping is associated with changes in corneal asphericity and higher-order aberrations, making corneal mapping important for mechanistic interpretation of structural and functional outcomes (Ding et al., 2022; Mathur & Atchison, 2009). Tomography also provides a standardized, objective longitudinal tracking and safety monitoring in pediatric participants.

To assess corneal biomechanics, a non-contact air-pulse tonometer utilizing high-speed bidirectional applanation, ORA, was used. The evaluated metrics included CH, Corneal Compensated Intraocular Pressure (IOPcc), Goldmann-correlated Intraocular Pressure (IOPg), and Corneal Resistance Factor (CRF), with analyses based on the calculated average of three readings per participant at each visit. These measurements placed emphasis on CH, as prior work has reported associations between CH and AXL or myopia in children (Chang, Chang, & Wang, 2010; Shen et al., 2008; Song et al., 2008). This biomechanical data was collected to evaluate whether baseline CH might relate to subsequent myopia progression, potentially serving as a predictive factor for treatment response. Additionally, the ORA was utilized because corneal biomechanical changes have been actively investigated in the context of orthokeratology, supporting its inclusion when comparing structural effects across various myopia control treatment modalities (Chen, Lam, & Cho, 2009; González-Méijome et al., 2008; Piñero & Alcón, 2015; Song et al., 2008; Wan et al., 2018).

4.2. Methods

Participants and Demographics

Baseline evaluations included 16 participants in the MYOP group and 10 in the EM group. Longitudinal follow-up for the MYOP group is ongoing, with 6-month data completed for 5 participants and 12-month data for 3 participants. Demographic variables (name, date of birth, age, guardians, race, ethnicity, sex assigned at birth, pronouns) and MYOP treatment details (type, initiation date) were collected via guardians, clinical providers, and electronic health records (EHR).

Clinical Tests

Baseline ocular status was established using EHR data for comprehensive history (ocular, medical, family, allergies, medications). Clinical examination parameters included cover testing, near point of convergence (NPC), accommodative amplitudes (AMP), monocular estimation method (MEM), extraocular motility (EOM), and scotopic, photopic, and near pupil sizes. Structural and refractive assessments included topography, biometry, and refractive status via cycloplegic retinoscopy, autorefraction, and subjective refraction.

For the EM cohort, data for participants EM01–EM06 were retrieved from the PICNIC study (if within 21 days of the lab visit), whereas EM07–EM10 underwent cycloplegic refraction in the laboratory. All measurements were obtained from the right eye (OD), except for one participant who required left eye (OS) assessment due to mixed astigmatism OD.

On and Off-axis Ocular Length

An IOLMaster 700 was used to measure AXL, lens thickness (LT), anterior chamber depth (ACD), central corneal thickness (CCT), and corneal radius (CR1, CR2). Three readings were taken at three specific locations: on-axis (0°), 10° temporally, and 10° nasally. Off-axis measurements utilized external pinpoint LED targets calibrated with a pediatric head model to ensure consistent visual angles. Off-axis biometry was collected for all MYOP participants and EM07–EM10, while EM01–EM06 received only central optical biometry using a Lenstar 900 device (Haag-Streit, Switzerland) was obtained.

Anterior Segment Scheimpflug Tomography

A Pentacam® HR rotating Scheimpflug tomographer was used to acquire 3-dimensional data, extracting anterior/posterior curvature, thickness, anterior chamber biometry, and lens densitometry. The primary outcomes analyzed were posterior corneal astigmatism, eccentricity, and volume. Baseline group comparisons utilized ANCOVA with refractive group as the primary fixed effect, and age and SE as covariates. Longitudinal changes in the MYOP cohort were analyzed using linear mixed-effects models (LMMs) with visit number as a fixed effect, a random intercept per participant, and age and SE as covariates. Statistical significance was defined as a two-sided $p < 0.05$. Data from the right eye (OD) were used, except for participant MYOP14 for whom the left eye (OS) was tested.

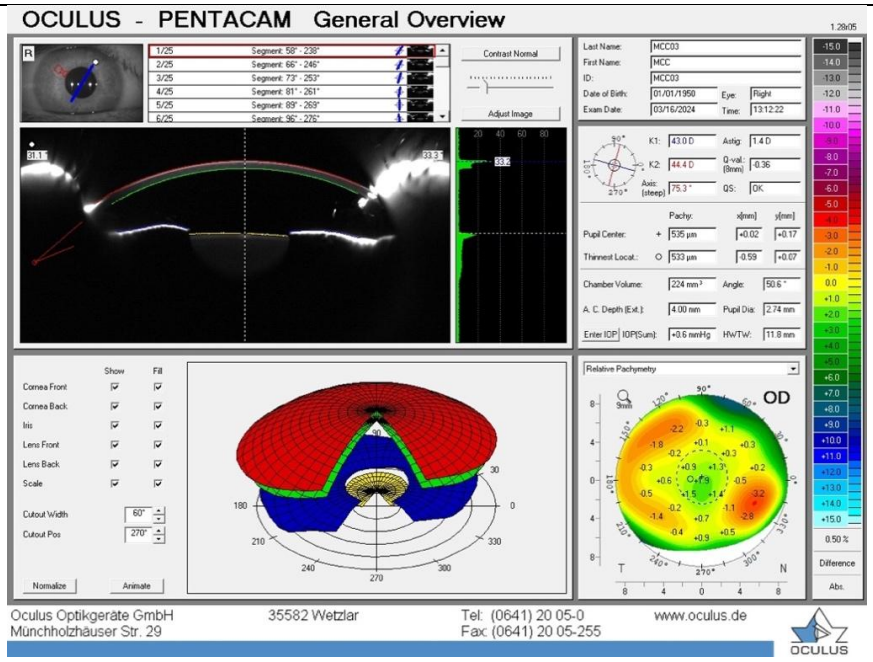

Figure 4. 1 Baseline tomography data image for participant MYOP03.

4.3. Results

Participants and Demographics

Across all participants, mean age at baseline was 11.14 ± 1.44 years, with 11 males and 12 females. In the MYOP group, mean age was 11.03 ± 1.56 years (6 males, 7 females), while the EM cohort had a mean age of 11.27 ± 1.35 years (5 males, 5 females). There was no difference in age between the groups (Mann–Whitney U = 58.00, p = 0.687). Among participants with MYOP, the distribution of myopia-control treatments included: atropine (n=7), atropine combined with spectacles (Stellest, n=1), multifocal soft contact lenses (Biofinity, n=2; MiSight; n=2), and orthokeratology (n=1), as detailed in Table 4.1.

Table 4. 1 Baseline demographic characteristics and clinical refractive profiles for all participants. Age at recruitment, sex assigned at birth, visual acuity in LogMAR units, and myopia control treatment at Visit 1. Refraction is expressed using power vectors, including spherical equivalent (SE or M), horizontal (J0), and vertical cross-cylinder (J45).

Participant	Age	Sex	M	J0	J45	VA	Treatment
MYOP02	10.13	Male	-1.75	-1.25	-2.25	0.00	Atropine
MYOP03	11.90	Female	-3.25	-3.00	-3.50	0.00	Atropine
MYOP04	7.38	Male	-2.75	-2.50	-3.00	+0.02	Atropine
MYOP05	11.42	Male	-5.00	-4.50	-5.50	0.00	Atropine
MYOP06	11.28	Female	-3.75	-2.25	-5.25	+0.10	MFSCL (Biofinity)
MYOP07	8.21	Male	-2.13	-2.00	-2.25	+0.10	MFSCL (MiSight)
MYOP08	11.37	Female	-2.25	-1.75	-2.75	+0.02	Atropine
MYOP09	12.42	Female	-3.13	-2.75	-3.50	0.00	MFSCL (Biofinity)
MYOP12	11.74	Female	-1.75	-1.50	-2.00	0.00	MFSCL (MiSight)
MYOP13	12.14	Male	-2.50	-2.25	-2.75	+0.02	Atropine
MYOP14	12.18	Female	-0.88	0.25	-2.00	+0.02	Atropine
MYOP15	11.15	Male	-3.25	-3.00	-3.50	+0.06	OrthoK
MYOP16	12.10	Female	-2.63	-2.00	-3.25	0.00	Atrop + Stellest
EM01	10.03	Male	1.00	1.25	0.75	0.00	N/A
EM02	9.30	Female	1.00	1.00	1.00	0.00	N/A
EM03	12.06	Female	0.88	1.00	0.75	0.00	N/A
EM04	11.84	Male	0.75	0.50	1.00	0.00	N/A
EM05	10.89	Female	0.88	1.00	0.75	0.00	N/A
EM06	11.39	Male	1.25	1.25	1.25	0.00	N/A
EM07	10.56	Male	1.00	1.25	1.00	0.00	N/A
EM08	10.51	Female	0.88	1.00	1.00	0.00	N/A
EM09	14.11	Female	0.63	1.00	0.75	0.00	N/A
EM10	12.05	Male	1.13	0.75	0.50	0.00	N/A

Clinical Tests

Baseline SE is summarized in Table 4.1. In the MYOP cohort (n = 13), mean SE OD was −2.69 ± 1.04 D (range: −5.00 to −0.88 D), and in the EM cohort (n = 10) +0.94 ± 0.18 D (range: +0.63 to +1.25 D). For VA, Mann–Whitney U showed a significant difference between groups, with poorer VA observed in the MYOP group (U = 100.00, p = 0.008). The groups were not significantly different in age (Mann–Whitney U test: U = 58.00, p = 0.687).

On- and Off-axis Ocular Length

Since participants EM01–EM06 underwent only central optical biometry, their data were excluded from all analyses in this subchapter to avoid cross-instrument comparisons.

Baseline Measurements (V1)

At baseline, the MYOP group exhibited longer dimensions across all measurements: central AXL (AXL-C) was 24.88 ± 0.74 mm (n=13) for MYOP and 23.41 ± 0.68 mm (n=4) for EM; 10° temporal AXL (AXL-T10) was 24.54 ± 0.67 mm (n=12) for MYOP and 23.36 ± 0.68 mm (n=4) for EM; and 10° nasal (AXL-N10) was 24.78 ± 0.69 mm (n=12) for MYOP; 23.43 ± 0.69 mm (n=4) for EM. Mann–Whitney U tests confirmed these differences (AXL-C: $p < 0.001$; AXL-T10: $p = 0.021$; AXL-N10: $p = 0.004$). Other anterior segment dimensions were largely comparable between the groups, as shown in Figure 4.2.

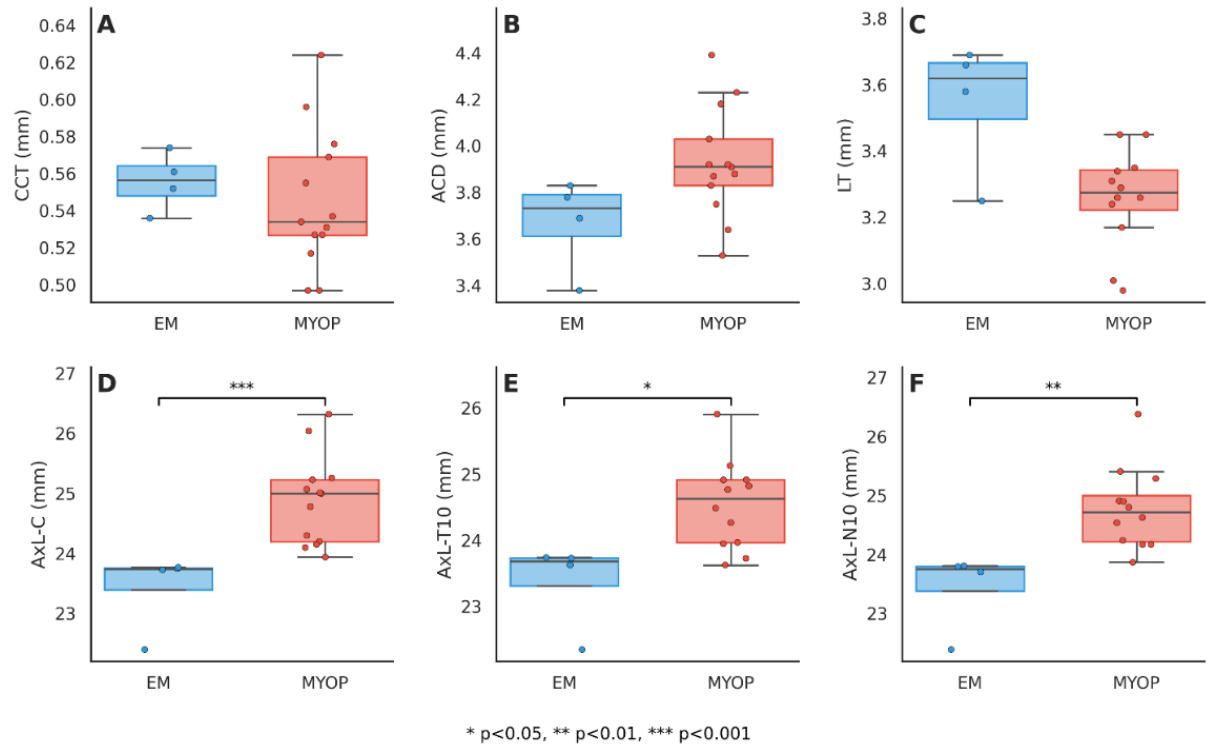

Figure 4. 2 Visit 1 (baseline) biometry outcomes for children with myopia (red) and emmetropia (blue). (A) central corneal thickness (CCT, mm), (B) anterior chamber depth (ACD, mm), (C) lens thickness (LT, mm), (D) central axial length (AXL-C, mm), (E) axial length at 10° temporal (AXL-T10, mm), and (F) axial length at 10° nasal (AXL-N10, mm). Boxplots represent the interquartile range and median, with whiskers indicating data spread and individual participant data points overlaid.

Longitudinal Changes (V1-3)

Over the follow-up period, the MYOP group appeared to exhibit progressive axial elongation across all eccentricities, which is visually summarized in Figure 4.3.

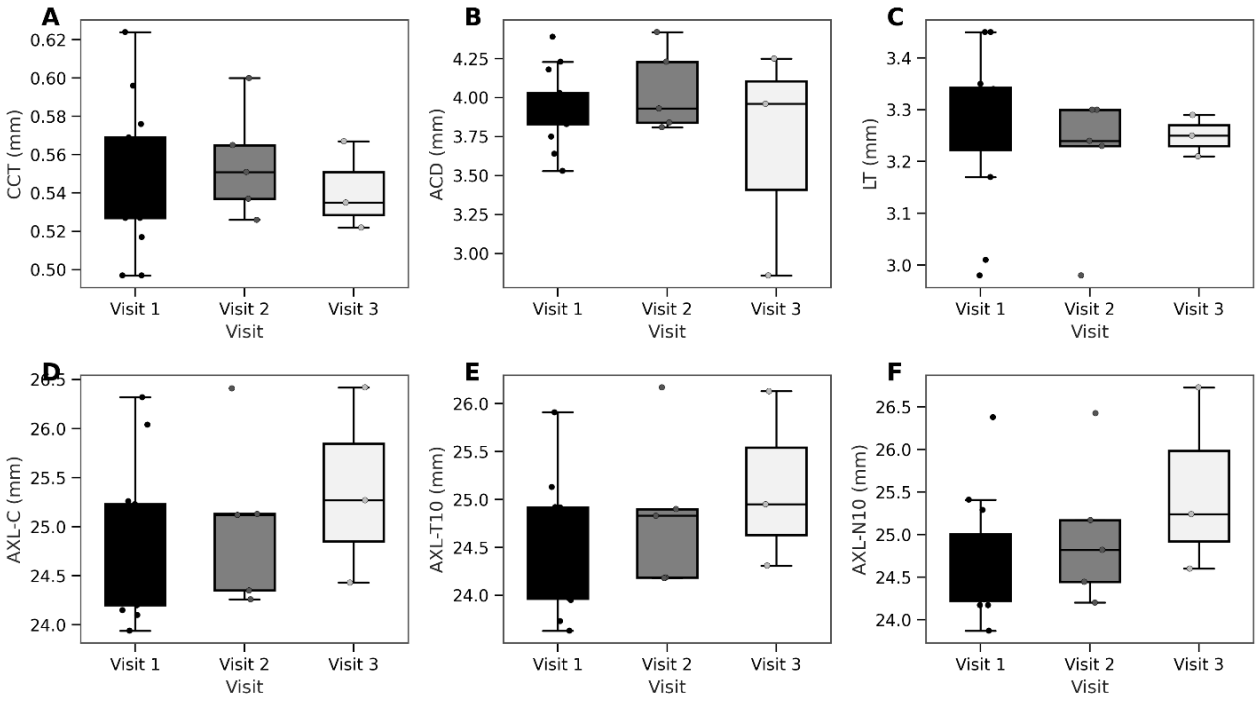

Figure 4. 3 Longitudinal biometry outcomes for the participants with myopia across three study visits. Panels show (A) central corneal thickness (CCT, mm), (B) anterior chamber depth (ACD, mm), (C) lens thickness (LT, mm), (D) central axial length (AXL-C, mm), (E) axial length at 10° temporal (AXL-T10, mm), and (F) axial length at 10° nasal (AXL-N10, mm) at Visit 1 (baseline), Visit 2 (6-month), and Visit 3 (12-month). There were no statistically significant ($p<0.05$) visit-to-visit differences for any metric.

Differences in sample sizes across the longitudinal timepoints reflect unavailable off-axis readings for some participants or visits. Despite the apparent upward trends in elongation, paired Wilcoxon comparisons across visits within each metric revealed no statistically significant visit-to-visit differences at an alpha level of 0.05. Note no longitudinal data was available for the EM group.

Anterior Segment Tomography

Data from MYOP13 were excluded from both the baseline and longitudinal analyses because this participant was unable to complete the test at the study visit.

Baseline Cross-Sectional Analysis (V1)

The baseline tomography cross-sectional analysis included 16 participants (4 EM, 12 MYOP). After controlling for age and M, ANCOVA analyses showed no differences between the refractive groups for the following parameters: posterior corneal astigmatism (adjusted effect = −0.93, p = 0.325), posterior corneal eccentricity (adjusted effect = −0.06, p = 0.471); or posterior corneal volume: (adjusted effect = 2.00, p = 0.736). A description of the baseline posterior corneal parameters for both groups is provided in Table 4.2. Among the evaluated baseline covariates, older age was significantly associated with lower posterior corneal astigmatism (β = −0.42, p = 0.006). However, neither age nor M significantly predicted posterior corneal eccentricity or volume, and M was not a significant predictor of any baseline posterior corneal metric.

Table 4. 2 Baseline posterior corneal parameters in emmetropic (EM) and myopic (MYOP) eyes. Posterior corneal astigmatism, eccentricity, and volume at the baseline visit for each group.

Measure	EM	MYOP
Posterior corneal astigmatism	−0.90±0.29	−1.70±1.26
Posterior corneal eccentricity	0.59±0.09	0.58±0.06
Posterior corneal volume	62.13±1.84	60.88±5.01

Longitudinal Assessment (V1–3)

The longitudinal posterior corneal parameters assessments are illustrated in Figure 4.4., and a summary across sequential follow-up visits is detailed in Table 4.3. LMMs adjusted for age and M revealed a significant decrease in posterior corneal eccentricity over time, showing an estimated slope of −0.023 per visit (95% CI: −0.044 to −0.001, p = 0.037). No significant longitudinal changes were observed for posterior corneal astigmatism (β = −0.053, p = 0.329) or volume (β = 0.020, p = 0.920).

Consistent with baseline findings, age remained a negative predictor of posterior corneal astigmatism in the longitudinal models (β = −0.55, p < 0.001). M showed no significant association with any of the posterior corneal parameters over time.

Table 4. 3 Longitudinal posterior corneal parameters in myopic eyes across visits. Posterior corneal astigmatism, posterior corneal eccentricity, and posterior corneal volume are summarized for the participants with myopia across sequential follow-up visits.

Measure	Visit 1 (n=12)	Visit 2 (n=5)	Visit 3 (n=3)
Posterior corneal astigmatism	−1.70±1.26	−2.08±0.77	−1.67±0.32
Posterior corneal eccentricity	0.58±0.06	0.60±0.06	0.59±0.07
Posterior corneal volume	60.88±5.01	62.10±6.00	59.73±5.45

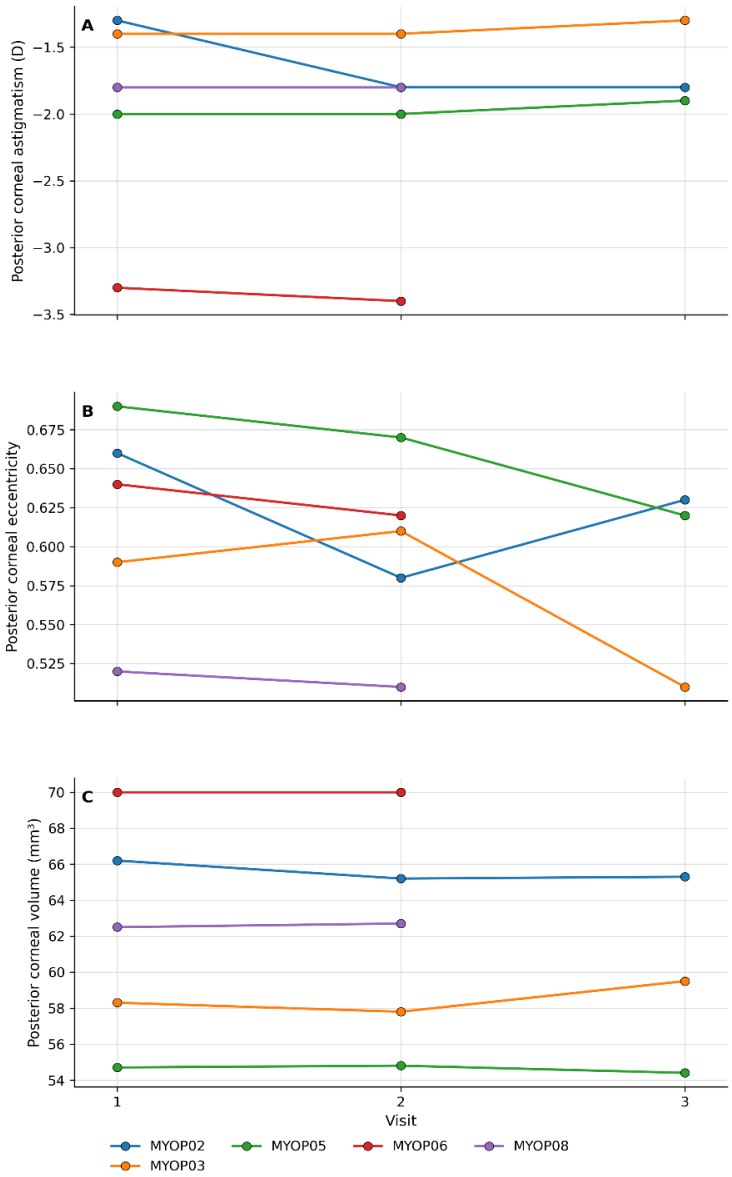

Figure 4. 4 Longitudinal posterior corneal parameters in eyes with myopia. A. shows posterior corneal astigmatism, B. posterior corneal eccentricity, and C. posterior corneal volume across visits 1–3 in the MYOP group participants with at least two visits. Each line represents an individual participant, and markers denote measured values at each available visit.

Corneal Biomechanical Properties

Both MYOP07 and EM03 were not able to perform this test at their baseline visit, and thus their data are not included in data analysis. At V1, the EM and MYOP groups showed similar corneal biomechanical values for all parameters (Figure 4.5 and Appendix Table A.2).

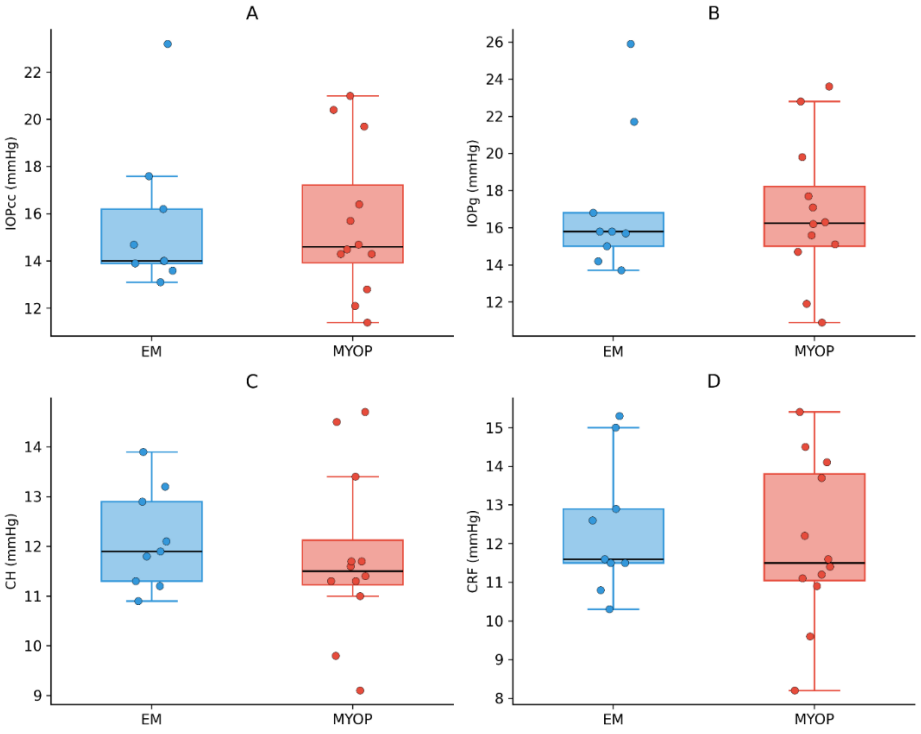

Figure 4. 5 Baseline corneal biomechanical properties and intraocular pressure profiles. Comparisons between participants with emmetropia (EM, blue) and participants with myopia (MYOP, red) at Visit 1. Panels display: (A) Corneal Compensated Intraocular Pressure (IOPcc), (B) Goldmann-correlated Intraocular Pressure (IOPg), (C) Corneal Hysteresis (CH), and (D) Corneal Resistance Factor (CRF). Boxplots represent the interquartile range (box) and median (central line), with whiskers indicating the data spread and individual participant data points overlaid.

An independent samples Welch's t-test indicated no difference in CH between the groups with EM and MYOP ($t = 0.580$, $p = 0.569$). This lack of significance was confirmed by a non-parametric Mann-Whitney U test ($U = 44.00$, $p = 0.499$).

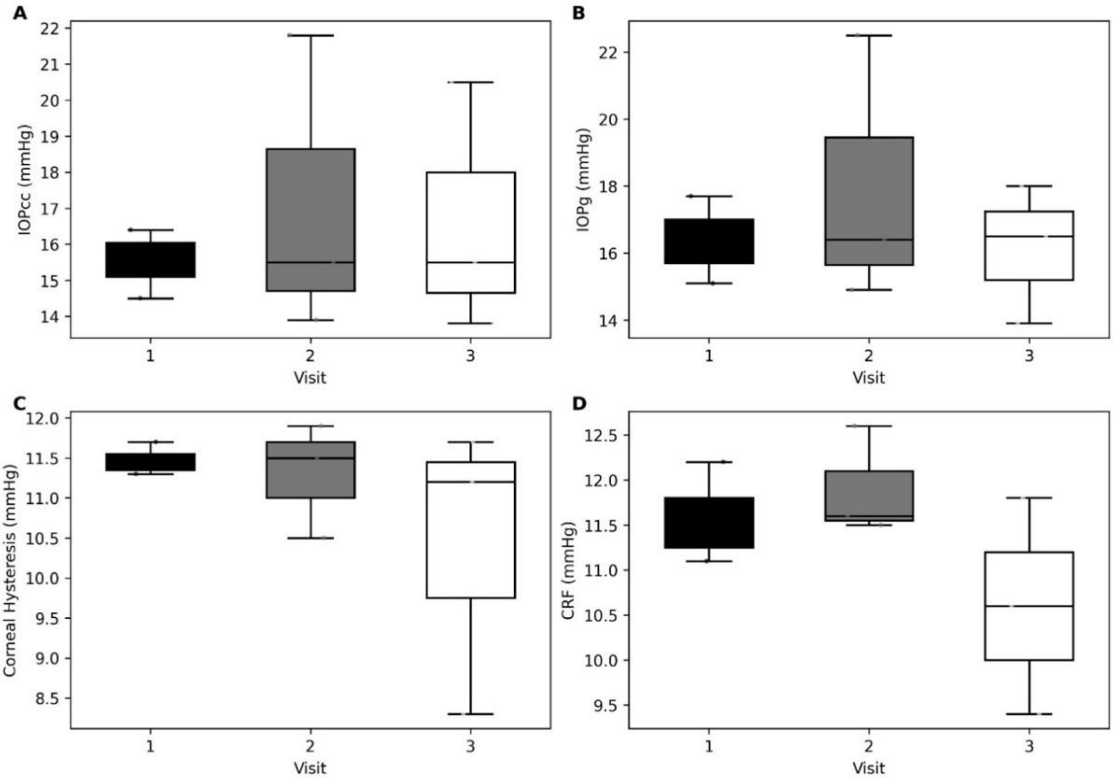

Figure 4. 6 Corneal biomechanical measurements for participants with myopia who have returned for a second or third visit. Panels display: (A) Corneal Compensated Intraocular Pressure (IOPcc), (B) Goldmann-correlated Intraocular Pressure (IOPg), (C) Corneal Hysteresis (CH), and (D) Corneal Resistance Factor (CRF). Boxplots represent the interquartile range (box) and median (central line), with whiskers indicating the data spread and individual participant data points overlaid.

Among MYOP participants with complete data (Figure 4.6), mean ± SD values were as follows: V1: IOPcc 15.53 ± 0.96 mmHg, IOPg 16.37 ± 1.30 mmHg, CH 11.47 ± 0.21 mmHg, CRF of 11.57 ± 0.57 mmHg; V2: IOPcc 17.07 ± 4.18 mmHg, IOPg 17.93 ± 4.03 mmHg, CH 11.30 ± 0.72 mmHg, CRF 11.90 ± 0.61 mmHg; V3: IOPcc 16.60 ± 3.48 mmHg, IOPg was 16.13 ± 2.07 mmHg, CH of 10.40 ± 1.84 mmHg, CRF of 10.60 ± 1.20 mmHg.

4.4. Discussion

Baseline Biometry

As anticipated, baseline optical biometry confirmed that participants with MYOP exhibited longer AXL compared to the control group with emmetropia across all conditions. Notably, similar magnitudes of axial elongation were observed centrally and at both 10° eccentricities tested, temporal and nasal. These results align with previous studies investigating peripheral biometry in young children, which similarly reported that within the near periphery (e.g., up to 20°), the myopic eye may exhibit a relatively uniform, global expansion in the posterior pole compared to emmetropic eyes (Faria-Ribeiro et al., 2013; Mutti et al., 2019). While the broader literature indicates that more pronounced regional asymmetries in eye shape, such as significant nasal-temporal differences in relative peripheral eye length, often emerge at larger eccentricities (over 30°) as myopia progresses (Atchison, Pritchard, & Schmid, 2006), these results indicate that the stretching of the eye globe remains largely symmetric within this narrow 10-degree macular range in pediatric myopia. Despite these differences in overall posterior eye length, anterior ocular dimensions, such as CCT, ACD, and LT, were largely comparable between the refractive groups at baseline. However, baseline VA differed significantly between groups, with the MYOP cohort demonstrating poorer logMAR VA than the EM group, suggesting that functional visual differences were present even in the absence of marked anterior segment structural differences. This indicates that prior to initiating myopia control interventions, the MYOP cohort demonstrated normal anterior

segment geometry that did not fundamentally differ from their EM peers, providing a standardized baseline for monitoring safety and treatment-induced changes.

Baseline Tomography

The present analysis indicates that posterior corneal shape metrics, specifically eccentricity and volume, were broadly similar between the EM and MYOP groups at baseline, exhibiting substantial overlap. However, posterior corneal astigmatism demonstrated a notably broader distribution in the MYOP compared to the relatively narrow range observed in EM eyes. While the average posterior corneal profile remains comparable between refractive groups, eyes in the MYOP group exhibited greater individual variation in posterior toricity, supporting Hu et al.'s conclusion that posterior astigmatism is significantly linked to the severity of myopia (Hu et al., 2025). From a clinical perspective, this diverse astigmatic profile is highly relevant to overall corneal optics and warrants longitudinal monitoring.

Corneal Biomechanics

Corneal biomechanical properties were evaluated because previous literature links lower CH to increased AXL and myopia progression (Chang, Chang, & Wang, 2010; Shen et al., 2008; Song et al., 2008). However, baseline ORA-derived metrics were similar between the participants with MYOP and EM. Because the cohorts were closely age-matched, direct comparative tests were used rather than a LMM to preserve degrees of freedom and statistical power. Furthermore, because the sample sizes were small, formal statistical tests for normality lack the power to definitively confirm a normal distribution. The Welch's t-test and

non-parametric tests were applied to the baseline CH data, and neither indicated a statistically significant difference between the two refractive groups. These results suggest the myopic cohort did not possess an inherently different or weaker biomechanical profile compared to their emmetropic peers prior to initiating treatment. This is consistent with previous literature demonstrating that biomechanical properties of the mild-to-moderate myopic cornea are stable and comparable to emmetropes (Plakitsi et al., 2011).

Longitudinal Structural and Biomechanical Changes

Over the follow-up visits, the myopic cohort demonstrated increased central AXL at each subsequent visit, consistent with the expected trajectory of pediatric myopia (Holden et al., 2016; Wildsoet et al., 2019). However, comprehensive analysis over the 12-month period revealed no statistically significant differences in overarching ocular structural parameters, which could be due to the early nature of the childhood or the small number of repeated visits. In addition, participants who contributed to the V2 and V3 datasets were exclusively undergoing low-dose atropine or multifocal soft contact lens treatments. These interventions likely modify retinal image quality or accommodation rather than physically compressing the anterior segment, thereby not expecting changing in CH or anterior segment integrity during follow-up (Lee et al., 2025). On the other hand, orthokeratology intentionally induce transient epithelial reshaping that mechanically alters corneal asphericity and topography (Ding et al., 2022; Mathur & Atchison, 2009). Only one participant undergoing orthokeratology was recruited into this study (MYOP15), and longitudinal follow-up data for this individual has not yet been obtained. The biomechanical findings must be viewed as

descriptive rather than confirmatory. Longitudinal statistical testing for the ORA data was not performed because the limited longitudinal sample (n=3) violates the assumptions and statistical power required. The longitudinal component of this dataset must be interpreted with caution due to the limited subset of MYOP participants with repeated measures.

Posterior Corneal Dynamics

While raw individual measurements for posterior cornea parameters showed apparent visit-to-visit fluctuations, modeling identified a subtle but significant decrease in posterior corneal eccentricity over time. Conversely, posterior corneal volume and astigmatism showed no longitudinal progression, reflecting modest and highly individualized short-term variations rather than consistent structural remodeling. These findings suggest that posterior corneal configuration is not the primary anatomical feature distinguishing children with MYOP from EM (Lee et al., 2025). Nevertheless, the greater variability in posterior astigmatism and the subtle longitudinal shifts in eccentricity indicate that the posterior cornea is not entirely static. This aligns with recent topographic studies demonstrating that posterior corneal asphericity flattens and posterior astigmatism actively fluctuates in response to physiological ocular growth and the increasing severity of myopia (An et al., 2025; Hu et al., 2025).

Limitations and Future Directions

Future studies utilizing a larger population size, balanced longitudinal follow-up, and continued formal inferential modeling are necessary to definitively determine whether these observed structural dynamics represent true biological progression or sampling variability.

Predictive Value of Baseline Metrics

A secondary aim of this study was to evaluate whether baseline ocular structure could predict the effectiveness of myopia control treatments. Current analyses revealed no significant correlations between baseline structural metrics, including AXL, corneal geometry, and biomechanical properties, and the subsequent rate of axial elongation. Despite the lack of predictive baseline correlations, the longitudinal trend of the data confirmed progressive axial elongation across all measured axes over the follow-up period. For example, central AXL steadily increased from baseline (24.88 ± 0.74 mm to 25.05 ± 0.86 mm at 6 months, and 25.37 ± 1.00 mm at 12 months). In contrast, overarching anterior ocular structural parameters and corneal biomechanics (such as CH) remained stable across the follow-up period, likely due to the specific optical and pharmacological treatments utilized by the returning participants. Consequently, the baseline characteristics do not currently serve as predictive for treatment efficacy in this study. However, meaningful predictive trends may still emerge once a more robust longitudinal dataset is established. To better understand the individual variability inherent in myopia control outcomes, future research must prioritize strategies to maximize participant retention and follow-up adherence, in addition to exploring alternative structural and functional biomarkers.

5. Optical Quality

5.1. Background

Myopia control interventions intentionally modify retinal image formation to slow axial elongation, often altering the eye's optical quality. For instance, the corneal reshaping inherent to orthokeratology decreases corneal asphericity and increases higher-order aberrations, particularly spherical aberration (Ding et al., 2022; Mathur & Atchison, 2009), which significantly reduces low-contrast acuity without impacting high-contrast vision. Similarly, multifocal and dual-focus soft contact lenses typically induce positive spherical aberration, reduce low-contrast visual acuity (Huang et al., 2022; Kang, McAlinden, & Wildsoet, 2017; Papadogiannis et al., 2022). These lens designs have also been shown to reduce accommodative response and induce changes in binocular vision (Schmid, Gifford, & Atchison, 2023; Vera et al., 2023). In contrast, pharmacological interventions like low-dose atropine generally have minimal impact on accommodation, pupil diameter, and visual acuity in children, although these are dose-dependent and may be significant with the highest doses used in clinic (0.05%) (Chen et al., 2022; Ha et al., 2022; Weng et al., 2022).

This chapter evaluates these optical changes to determine their impact on visual function and treatment efficacy, with a special emphasis placed on isolating the effects of defocus (DEF) and primary spherical aberration (SA). These specific higher-order aberrations were targeted because they are intentionally altered by the aforementioned optical myopia control treatments (Ding et al., 2022; Huang et al., 2022; Mathur & Atchison, 2009; Papadogiannis

et al., 2022; Schmid, Gifford, & Atchison, 2023; Vera et al., 2023), allowing for a mechanistic understanding of how these interventions manipulate retinal image quality.

5.2. Methods

Total ocular aberrations were assessed for the right eye of all participants using a fast-scanning, high-resolution Hartmann-Shack wavefront analyzer. To evaluate optical quality under different accommodative demands, aberrations were measured at viewing distances of 6 meters (“distance”) and 40 centimeters (“near”); however, only the distance data are presented in this analysis. During data acquisition, participants were instructed to fixate on the smallest resolvable circle within the 'Radgrating' target (Figure 5.1) to ensure stable accommodation and fixation. The instrument's scanning protocol covered a visual field range of ±30 degrees eccentricity along the horizontal meridian.

Following data acquisition, the instrument’s automated software extracted individual Zernike coefficients, which were subsequently processed to calculate the SR. The SR is a global metric of optical quality, defined as the ratio of the peak intensity of the eye's point spread function (PSF) to that of a diffraction-limited optical system. Distance aberrations with correction were evaluated across four retinal areas of interest: Central (±5°), temporal retina (-5 to -10°), nasal retina (+5 to +10°), and far-temporal retina (-10 to -15°). The extracted metrics included Z4 (DEF), Z8 (Horizontal Coma), Z12 (SA), SR with all aberrations (SR-All), and SR with only high-order aberrations (SR-onlyHOAs). Data were processed utilizing customized MATLAB scripts to compute normalized Area Under the Curve (AUC) values for these regional metrics.

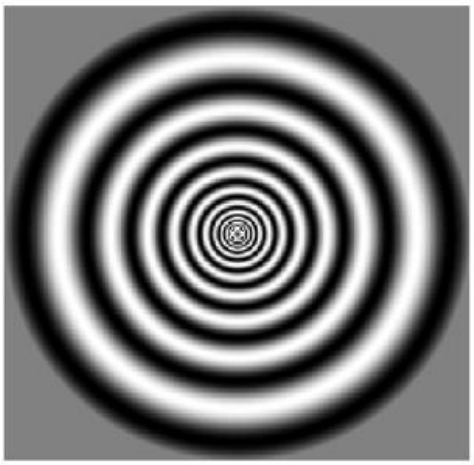

Figure 5. 1 Radgrating fixation target used when measuring aberrations.

Statistical Analysis

To address non-normality and right-skewness, particularly evident in DEF (Z4) and SR metrics, the normalized AUC data were log-transformed prior to modeling (e.g., lnZ4, lnSR-All, ln SR-onlyHOAs). For SR-All and for SR-onlyHOAs, a small constant (0.0005) was added prior to transformation to account for zero values. Linear mixed models (LMM) were constructed to test the effects of refractive group, area, and the group × area interaction. Initial models evaluated age as a covariate. In the final analysis, simplified LMMs were utilized, treating retinal area as the repeated factor within each subject and applying a compound symmetry covariance structure. Age and random intercepts were removed from the final models to maximize model stability and parsimony since age was not significant and its inclusion did not improve the interpretation of the results.

5.3. Results

Baseline Visit

Data for participants MYOP04, MYOP07, and EM07 were not included in baseline analysis due to not being able to complete the testing during their visit. At baseline (V1), eccentricity-dependent profiles for DEF, horizontal coma, SA, SR-All, and SR-onlyHOAs were evaluated for the EM (n=9) and MYOP (n=11) groups (Figure 5.2). Across the sampled retinal profile, the MYOP group exhibited a higher mean DEF AUC compared to the EM group (1.443 ± 1.303 μm versus 0.338 ± 0.267 μm). At the fovea, DEF AUC remained higher in MYOP (1.422 ± 0.913 μm) compared to EM (0.160 ± 0.142 μm).

In contrast, horizontal coma profiles were largely comparable between the groups, with overall means of -0.019 ± 0.071 in the MYOP group and -0.035 ± 0.068 in the EM group. Central horizontal coma was also similar (-0.019 ± 0.048 in MYOP vs. -0.011 ± 0.058 in EM), indicating minimal group separation for this metric.

For primary SA, the profile-averaged mean was slightly higher in the MYOP group (0.045 ± 0.047) compared to the EM group (0.032 ± 0.038). However, at the central location, SA values were similar (0.034 ± 0.073 in MYOP vs. 0.039 ± 0.039 in EM), suggesting greater group separation across the broader peripheral profile than at the fovea.

Regarding global image quality, the groups demonstrated different SR profiles across the retina. The mean for SR-All was 0.056 ± 0.026 in EM and 0.015 ± 0.017 in MYOP, with central values of 0.085 ± 0.040 and 0.011 ± 0.011, respectively. Similarly, the profile-

averaged mean for SR-onlyHOAs was 0.091 ± 0.054 in EM compared to 0.077 ± 0.066 in MYOP, with central values of 0.167 ± 0.111 and 0.101 ± 0.090, respectively.

Overall, as illustrated in Figure 5.2, the most pronounced descriptive difference between groups was for DEF, whereas coma showed substantial overlap and SA exhibited modest, eccentricity-dependent differences. For global image quality, the EM group generally demonstrated higher SR when low order aberrations were included, as expected, and the difference was more pronounced in the temporal retina. Conversely, group differences in the SR that only included HOAs were complex and region-specific: the MYOP group exhibited fewer HOAs in the near temporal regions, but poorer quality (higher HOAs) nasally.

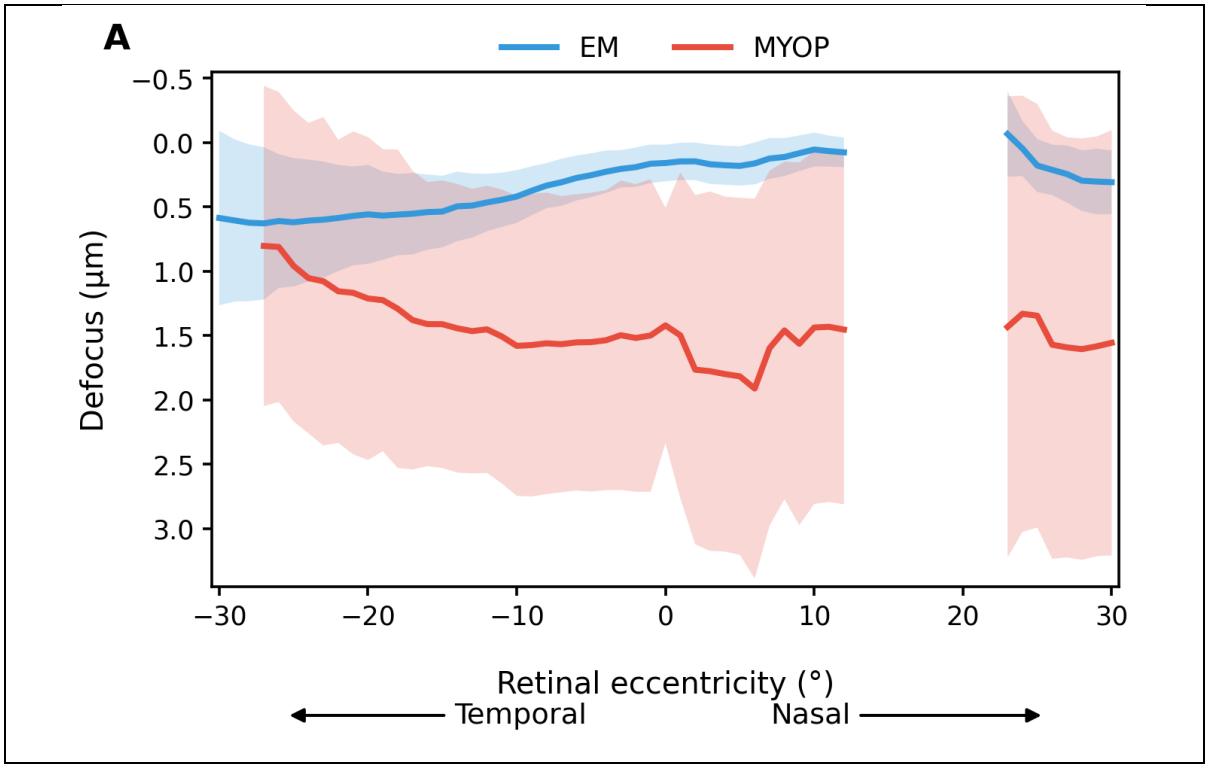

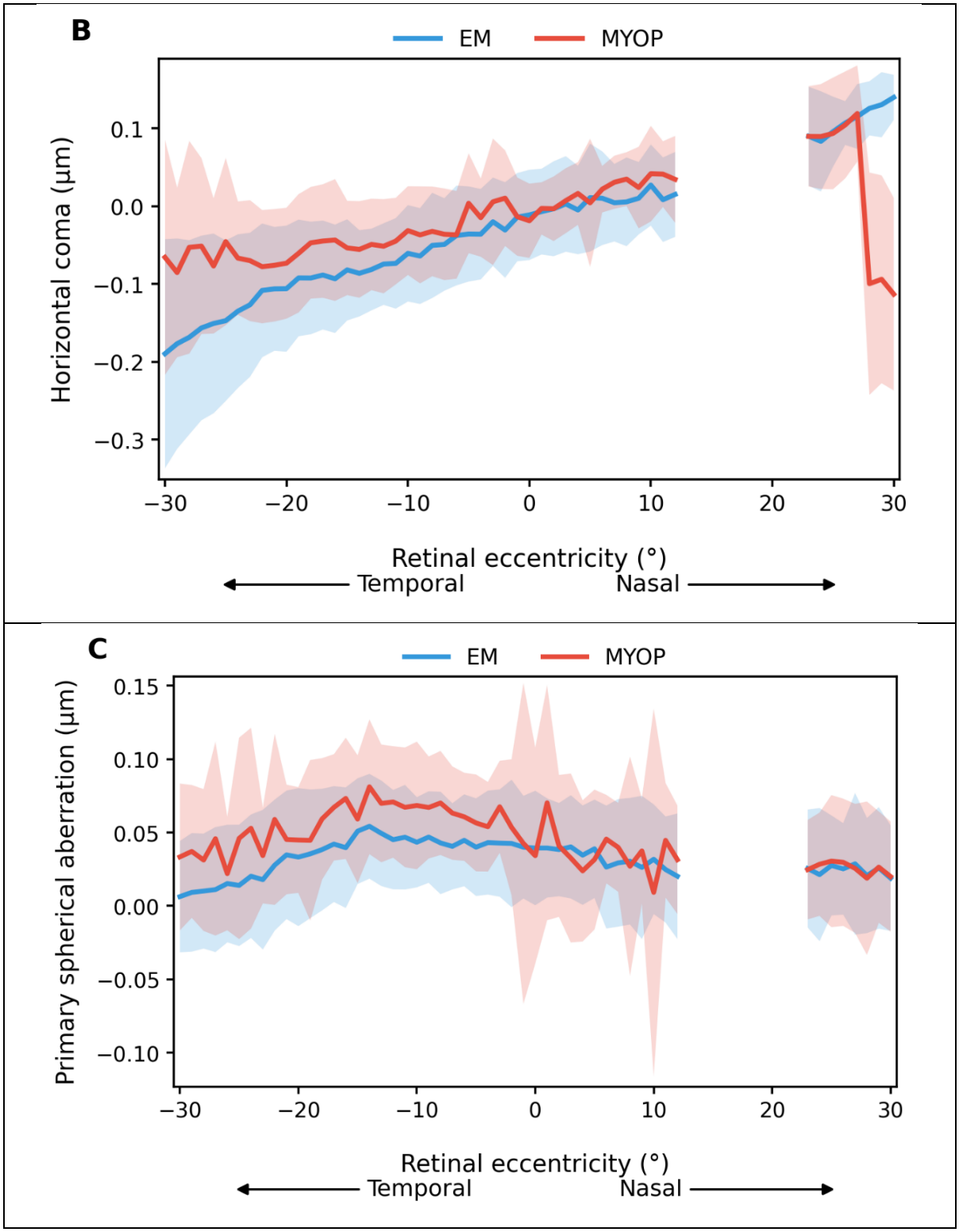
B
EM
MYOP
Horizontal coma (µm)
0.1
0.0
−0.1
−0.2
−0.3
−30
−20
−10
0
10
20
30
Retinal eccentricity (°)
Temporal
Nasal
C
EM
MYOP
Primary spherical aberration (µm)
0.15
0.10
0.05
0.00
−0.05
−0.10
−30
−20
−10
0
10
20
30
Retinal eccentricity (°)
Temporal
Nasal

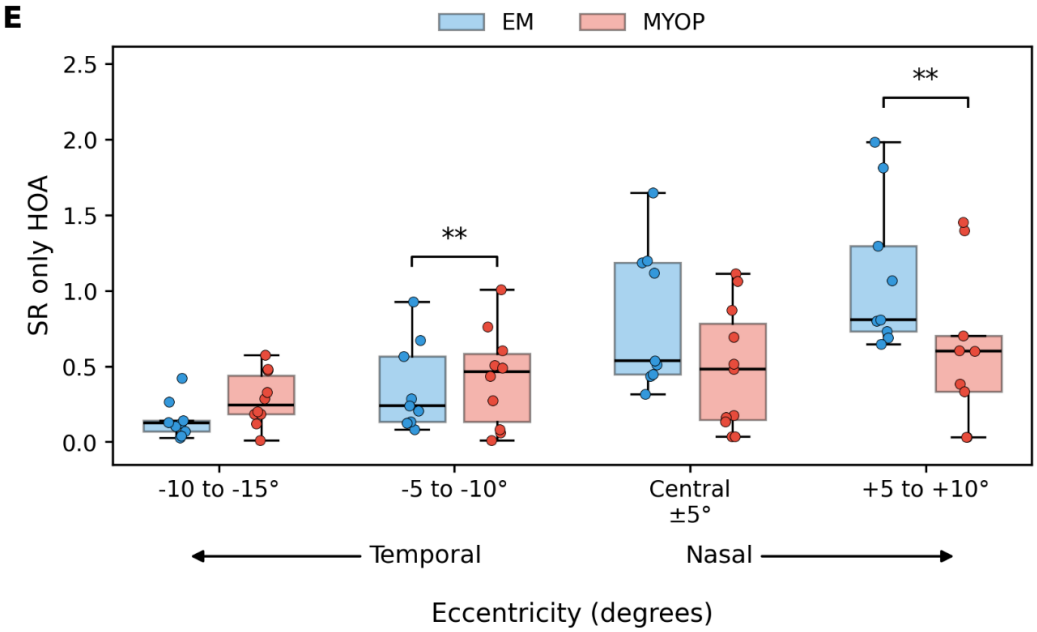

Figure 5. 2 Eccentricity-dependent optical profiles in emmetropic (EM) and myopic (MYOP) groups. (A) Defocus with inverted Y-axis. (B) Horizontal coma. (C) Primary spherical aberration. (D) Strehl Ratio (SR) with all aberrations (SR-All). (E) Strehl Ratio with only high-order aberrations (SR-onlyHOAs). A-C: solid lines represent the mean and shaded regions ±1 SD at each eccentricity. D & E: boxplots represent the interquartile range and median, whiskers indicate the spread and individual data points are overlaid.

To statistically evaluate these trends, LMM with retinal area (AUC) as the repeated factor were conducted for the aberrations log-transformed metrics. As before, initial models found that age was not a significant covariate for any metric (all $p > 0.05$). Removing age slightly improved the model fit without altering the pattern of significant effects (with the exception of lnZ8_AUC); therefore, the simplified models were retained for final interpretation.

For DEF (lnZ4_AUC), the model revealed significant main effects of refractive group ($F = 11.07$, $p = 0.004$) and retinal area ($F = 14.65$, $p < 0.001$), as well as a significant refractive

group × retinal area interaction ($F = 7.12$, $p < 0.001$). This confirms that DEF differed significantly between groups and that the magnitude of this difference varied across the visual field. For horizontal coma (lnZ8_AUC), there was a small overall main effect of group ($F = 4.48$, $p = 0.049$), but the main effect of retinal area ($p = 0.114$) and interaction ($p = 0.612$) were not significant.

This provides only weak evidence of an overall group difference and no evidence of area-dependent group effects for coma. For SA (lnZ12_AUC), there was a significant main effect of retinal area ($F = 5.72$, $p = 0.002$), whereas refractive group and the interaction term were not significant. Pairwise comparisons indicated significant regional variation, specifically between the temporal -5° to -10° region and the nasal +5° to +10° region ($p = 0.015$), as well as between the far-temporal -10° to -15° region and the nasal +5° to +10° region ($p = 0.002$). While SA varied spatially, it did not differ between the cohorts.

For SR with all aberrations (lnSR-All_AUC), there were significant effects for refractive group ($p = 0.002$), retinal area ($p = 0.004$), and refractive group × retinal area interaction ($p < 0.001$). The overall estimated marginal means differed significantly between refractive groups, and Welch's t-test showed a significant difference between the groups at -5 to -10° ($p = 0.001$), Central ±5° ($p < 0.001$), and +5 to +10° ($p < 0.001$) region. These results suggest that overall optical quality differed between groups overall, and that the pattern of these differences was dependent on retinal location.

However, for SR with only HOAs (lnSR-onlyHOAs_AUC), there was no significant main effect of refractive group ($p = 0.330$), although both the retinal area and the refractive group

× retinal area interaction were highly significant ($p < 0.001$), indicating that the spatial profile of HOAs differed between the groups. Pairwise area comparisons revealed multiple significant regional differences, with the lowest values occurring in the temporal and far-nasal periphery ($p = 0.004$).

Longitudinal data (V1-3)

Longitudinal eccentricity-dependent optical profiles were evaluated for the subset of the MYOP cohort that completed all three study visits (MYOP02, MYOP03, and MYOP05) (Figure 5.3). Due to declining number of participants across the follow-up visits (V1 n=11; V2 n=5; V3 n=3), these patterns represent preliminary descriptive observations rather than definitive longitudinal results.

Across all sampled eccentricities, the mean Z4 profile decreased from 1.812 ± 1.733 μm at V1, to 1.024 ± 0.622 μm at V2, and 0.730 ± 0.497 μm at V3.

Mean Z8 remained relatively stable over time (-0.016 ± 0.105 at V1; -0.018 ± 0.114 at V2; 0.000 ± 0.114 at V3).

Mean Z12 showed a subtle upward trend following treatment initiation, progressing from 0.050 ± 0.043 at V1, to 0.059 ± 0.039 at V2, and 0.056 ± 0.069 at V3.

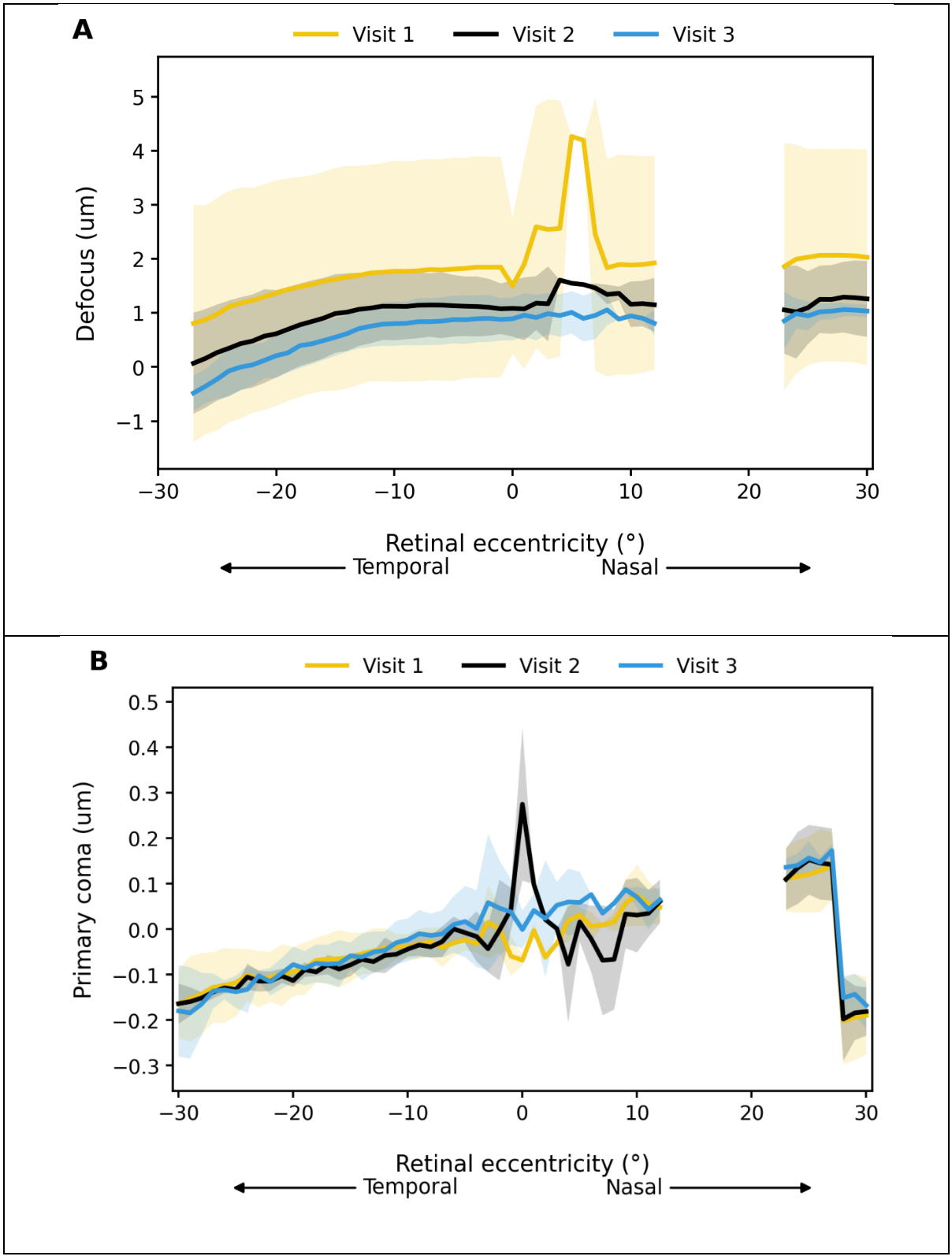
A
Visit 1
Visit 2
Visit 3
Defocus (um)
5
4
3
2
1
0
−1
−30
−20
−10
0
10
20
30
Retinal eccentricity (°)
Temporal
Nasal
B
Visit 1
Visit 2
Visit 3
Primary coma (um)
0.5
0.4
0.3
0.2
0.1
0.0
−0.1
−0.2
−0.3
−30
−20
−10
0
10
20
30
Retinal eccentricity (°)
Temporal
Nasal

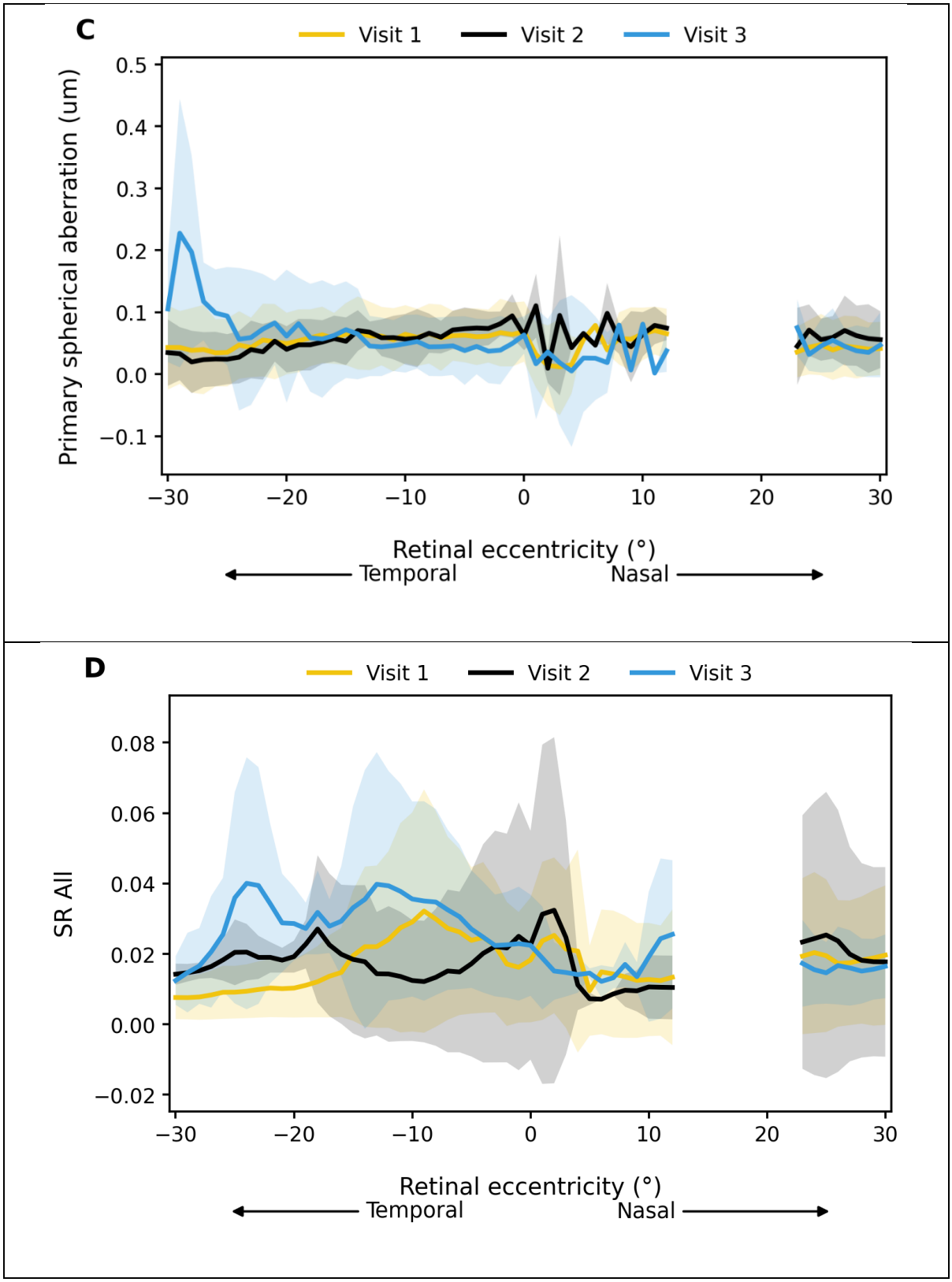
C
Visit 1
Visit 2
Visit 3
Primary spherical aberration (um)
0.5
0.4
0.3
0.2
0.1
0.0
−0.1
−30
−20
−10
0
10
20
30
Retinal eccentricity (°)
Temporal
Nasal
D
Visit 1
Visit 2
Visit 3
SR All
0.08
0.06
0.04
0.02
0.00
−0.02
−30
−20
−10
0
10
20
30
Retinal eccentricity (°)
Temporal
Nasal

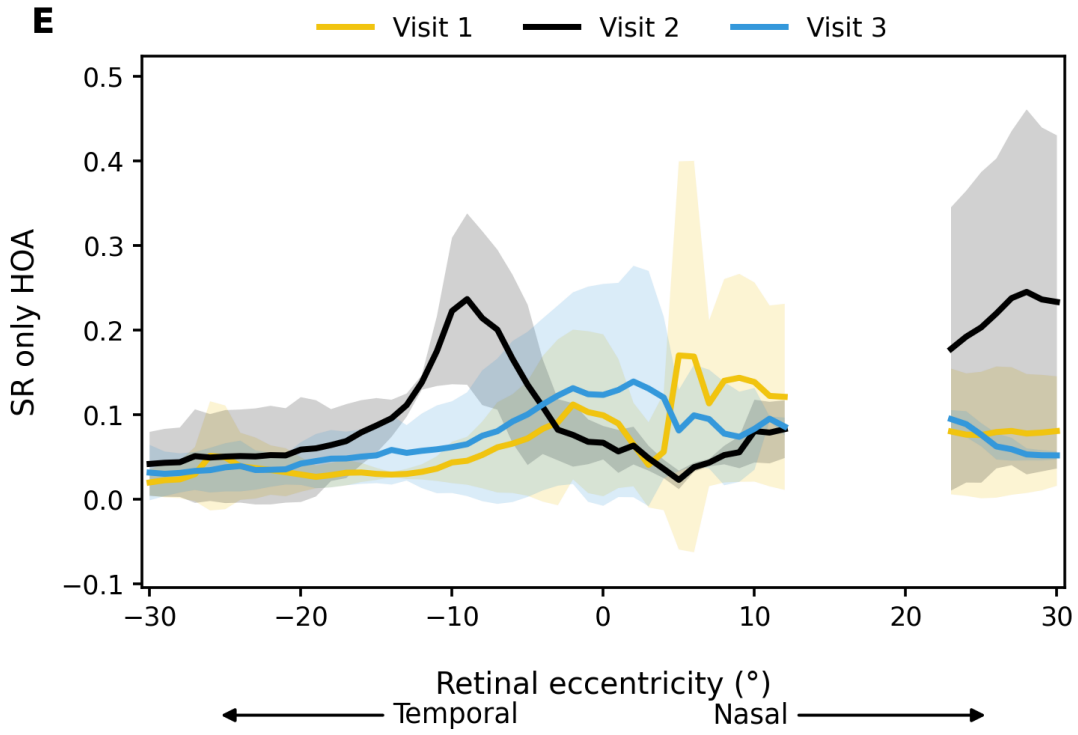

Figure 5. 3 Retinal aberration profiles for participants with myopia who completed all three study visits (n = 3, MYOP02, MYOP03, and MYOP05). (A) Defocus, (B) Horizontal coma, (C) Primary spherical aberration, (D) Strehl Ratio (SR) with all aberrations (SR-All). (E) Strehl Ratio with only high-order aberrations (SR-onlyHOAs), plotted as a function of retinal eccentricity. In each panel, solid lines represent the mean for each visit, and shaded regions ± 1 SD around the mean at each eccentricity.

Regarding overall image quality, mean SR-All exhibited modest improvement from 0.017 ± 0.017 at V1 to 0.024 ± 0.018 at V3. On the other hand, SR-onlyHOAs fluctuated, measuring 0.067 ± 0.073 at V1, 0.107 ± 0.101 at V2, and 0.072 ± 0.062 at V3.

Overall, as depicted in Figure 5.3, aberration profiles remained strongly dependent on eccentricity at each visit. The most notable longitudinal change occurred in DEF, while the remaining optical metrics displayed smaller magnitude variations over the 12-month period.

5.4. Discussion

This analysis evaluated whether early-to-moderate pediatric myopia is associated with altered spatial profiles of optical quality prior to (baseline) and during early follow up optical myopia-control therapies. At baseline, the clearest differences between groups were observed for DEF, whereas SA showed regional variation without a refractive group effect. These results are highly consistent with previous findings demonstrating that peripheral DEF profiles significantly distinguish MYOP from EM eyes, while foundational HOAs often exhibit similar regional patterns regardless of refractive status (Atchison, Pritchard, & Schmid, 2006; Romashchenko, Rosén, & Lundström, 2020; Vera-Diaz et al., 2025).

Baseline Optical Quality and Aberrations

At baseline, the most robust aberration result emerged from the DEF analysis, which demonstrated a significant refractive-group difference that varied by retinal area. Rather than a simple, uniform global shift across the visual field, participants with MYOP exhibited distinct regional DEF profiles compared to participants with emmetropia. This is broadly consistent with the longitudinal findings from the PICNIC study (Vera-Diaz et al., 2025), which demonstrated that relative peripheral DEF is significantly more negative in children at high risk for myopia and in those who have already developed myopia. Furthermore, similar to the spatial dependence observed in the current data, the PICNIC study confirmed that these relative peripheral DEF differences increase primarily with eccentricity in the temporal retina.

In contrast, HOAs such as horizontal coma and SA were more comparable between the refractive groups in this study. Horizontal coma showed weak evidence for an overall group difference, and no evidence of spatially varying group effects. This lack of significant refractive group differences in foundational HOAs across the visual field aligns closely with the findings of the PICNIC study and other recent investigations in pediatric cohorts (Romashchenko, Rosén, & Lundström, 2020; Vera-Diaz et al., 2025). These previous studies similarly demonstrated that while myopic children differ substantially from emmetropes in peripheral DEF, their baseline spatial profiles for HOAs, such as SA and coma, remain largely similar prior to the initiation of targeted optical treatments (Atchison, Pritchard, & Schmid, 2006; Vera-Diaz et al., 2025). However, the finding that SA showed no evidence of refractive-group differences at baseline diverges slightly from the study by Vera-Diaz et al. (2025), which reported that SA was generally less positive in children at high risk for myopia (who had not yet developed myopia). The comparability of SA between the MYOP and EM groups in the current study is nonetheless highly relevant for clinical myopia management. Because treatments such as orthokeratology and highly aspheric multifocal lenses intentionally induce positive SA to slow axial elongation (Ding et al., 2022; Huang et al., 2022; Kang, McAlinden, & Wildsoet, 2017; Mathur & Atchison, 2009; Papadogiannis et al., 2022), establishing that these specific myopic children do not possess inherently different baseline SA profiles provides a useful baseline reference for monitoring treatment-induced optical changes.

The global optical quality metrics provided further insight into these group dynamics. Children with MYOP show lower SR values, indicating worse overall optical quality, which

is driven by their myopic DEF. When the SR is calculated using only high-order aberrations (SR-onlyHOAs), there was no significant overall effect of refractive group, but a significant refractive group-by-area interaction, with MYOP showing better HOAs at the near temporal periphery but higher HOAs at the nasal periphery.

This complex, area-dependent spatial variation in high-order optical quality provides nuanced context to recent longitudinal findings from the PICNIC study (Vera-Diaz et al., 2025). The PICNIC study evaluated a larger group of young children and found that myopic and high-risk children exhibited higher high-order SR (better optical quality) than low-risk children, with the largest differences occurring specifically in the near periphery within ±20 degrees. Furthermore, the study revealed that primary SA was less positive in children with or at high risk for myopia, and that their relative peripheral DEF became progressively more negative over time, particularly at the mid-temporal retina. Our finding that myopes show better HOAs specifically in the near temporal periphery aligns directly with their observation that HOAs are lower in the near peripheral retina. Ultimately, both studies strongly converge on the core conclusion that childhood myopia is characterized by significant, area-dependent spatial variations in high-order optics across the peripheral visual field, which may play a critical role in providing optical signals for emmetropization.

Longitudinal Optical Changes

When examining the longitudinal data for distance aberrations with correction, it is important to establish that targeted myopia-control therapies were actively initiated by V2. Following treatment initiation, descriptive profiles suggested a decrease in DEF and a small increase in

primary SA across the subsequent follow-up visits, whereas horizontal coma remained relatively stable. These patterns are qualitatively consistent with optical changes expected during myopia-control treatment, which intentionally alter peripheral image quality and induce positive SA (Ding et al., 2022; Huang et al., 2022; Kang, McAlinden, & Wildsoet, 2017; Mathur & Atchison, 2009; Papadogiannis et al., 2022). However, given the progressive reduction in sample size across follow-up visits, dropping from 11 participants at baseline to 5, and finally to only 3 who completed all visits, these longitudinal findings must be interpreted cautiously. They represent preliminary descriptive observations rather than definitive treatment effects. Future prospective evaluations with larger, well-retained cohorts are necessary to reliably distinguish true treatment-induced optical modulation from normal biological variation and to draw robust conclusions regarding the underlying mechanisms of these therapies.

Overall, these findings confirm that the off-axis optical environment in childhood myopia is distinctly characterized by unique spatial profiles of DEF and HOAs. This pre-existing optical landscape must be carefully considered when prescribing clinical interventions that intentionally manipulate the peripheral visual field.

6. Retinal and Choroidal Thickness

6.1. Background

Robust evidence links myopia to various ocular pathologies, including retinal detachment, glaucoma, and myopic maculopathy (National Academies of Sciences, Engineering, and Medicine, 2024), making accurate in vivo assessment of the posterior segment critical for understanding the structural implications of myopia progression and control. To enhance the visibility of the choroid, this study implemented specific imaging strategies, including Enhanced Depth Imaging (EDI) that positions the OCT instrument closer to the eye, thereby shifting the zero-delay line and region of highest sensitivity deeper into the scan towards the choroid (Spaide, Koizumi, & Pozzoni, 2008). Additionally, a wide-field objective lens was utilized to facilitate the quantification of choroidal thickness (ChT) beyond the macular region, spanning a field of 55 degrees (Hoseini-Yazdi et al., 2019). Finally, to address inherent imaging artifacts, the system's eye-tracking capabilities allowed for the averaging of multiple B-scans at an identical location to reduce image noise and enhance signal quality (Alonso-Caneiro, Read, & Collins, 2011).

6.2. Methods

Posterior segment imaging was performed on the right eye using a wide-field Spectralis OCT to quantify choroidal (ChT) and retinal thickness (RT) (Figure 6.1.). To optimize structural visibility, images were acquired using Enhanced Depth Imaging (EDI) and high-resolution. The protocol utilized a custom radial scan, employing the TruTrack™ eye-tracking system to

average 16 B-scans per location and ensure high signal quality (Alonso-Caneiro, Read, & Collins, 2011).

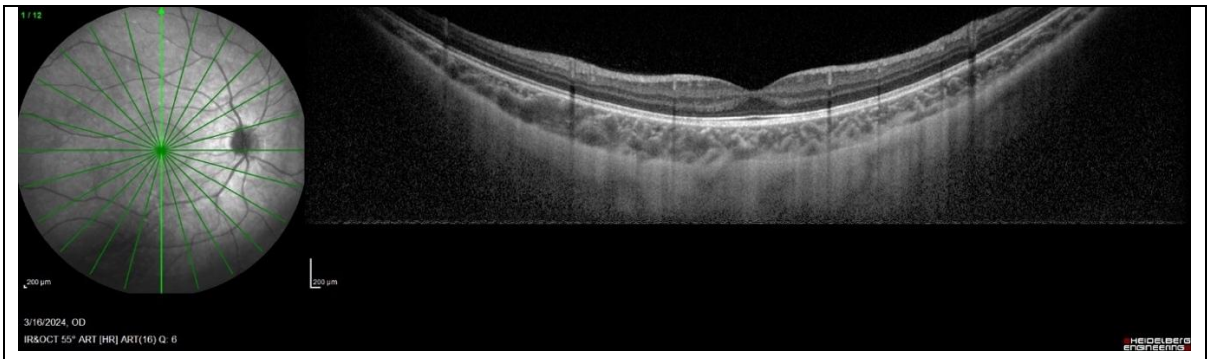

Figure 6. 1 Baseline wide-field Spectral-Domain OCT scan. Representative imaging (participant MCC03, right eye) demonstrating the 55-degree radial acquisition pattern on the infrared fundus view (left) and the 90 degrees Enhanced Depth Imaging (EDI) B-scan across the posterior pole (right).

Raw OCT scan data were exported and processed using a customized MATLAB program (Widefield Choroid, Version 40, provided by the University of Houston College of Optometry). Within this software, the posterior pole was manually segmented to delineate two primary structural zones: RT and ChT. A total of 12 radial B-scans were segmented per eye for each study visit. In instances where scan quality was locally compromised or specific layer boundaries were indistinct, manual approximation lines were drawn to interpolate the missing areas (Figure 6.2). Following the completion of all segmentations across the radial scans, the software automatically extracted the RT and ChT values at specific spatial

eccentricities (1, 3, 6, 10, and 14 mm) and compiled them into a standardized dataset for subsequent statistical analysis.

Prior to statistical evaluation, the extracted dataset was screened for quality control. As a strict exclusion criterion, all negative ChT and RT values, which represent physically impossible biological dimensions resulting from automated or manual segmentation artifacts, were excluded from the dataset. (e.g. RT of EMM03 at 14mm, was removed prior to analysis due to a negative value artifact)

At V1, ChT and RT was analyzed using a linear mixed model (LMM) with eccentricity (1, 3, 6, 10, and 14 mm) specified as a within-subject factor and refractive group (EMM vs. MYOP) as a between-subject factor; age and AXL were included as covariates.

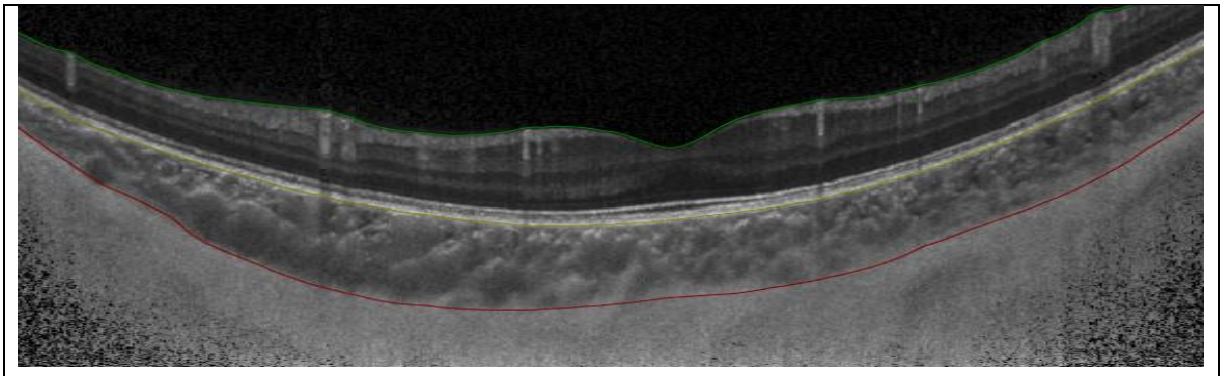

Figure 6. 2 Image processing interface, with green line marks the boundary of ILM, Yellow line marks the Basement Membrane, and the redline marks the boundary of choroid.

6.3. Results

Baseline data for participants MYOP02 and MYOP07 were not included due to being unable to finish the test during the visit.

Choroidal Thickness (ChT) at Baseline

A strong main effect of eccentricity on ChT was notes for the group ($F(4,19) = 59.456$, $p < 0.001$), indicating systematic thinning toward more peripheral retinal locations (Table 6.1).

The overall main effect of refractive group was not statistically significant ($F(1,21.334) = 2.824$, $p = 0.107$), and neither age ($p = 0.355$) nor AXL ($p = 0.585$) contributed significantly to ChT in this model. However, the Refractive Group × Eccentricity interaction showed borderline evidence for location-dependent group differences ($F(4,19) = 2.762$, $p = 0.058$), indicating systematic thinning of the choroid toward more peripheral retinal locations.

Table 6. 1 Type III tests of fixed effects for Choroidal Thickness (ChT).
(Visit 1 Linear Mixed Model, LMM), SE = Spherical Equivalent.

Effect	Numerator df	Denominator df	F	p-value
Refractive Group	1	21.334	2.824	0.107
Eccentricity	4	19.000	59.456	< 0.001
Age	1	17.000	0.903	0.355
AXL	1	17.000	0.310	0.585
Refractive Group × Eccentricity	4	19.000	2.762	0.058

Estimated marginal means (EMM, adjusted to Age = 11.32 years and AXL = 24.07 mm) indicated that the emmetropia group had thicker choroids than the MYOP group at all eccentricities (e.g., 1 mm: 341.49 vs 298.20 μm; 14 mm: 255.64 vs 209.77 μm), consistent with a generalized thinning with MYOP (Table 6.2).

Table 6. 2 Estimated marginal means (EMMs) of Choroidal Thickness (ChT) (μm) by refractive group and eccentricity.
(adjusted to Age = 11.325 and axial length, AXL = 24.070), SE = Spherical Equivalent.

Eccentricity (mm)	Emmetrope EMM (SE)	df	95% CI	Myope EMM (SE)	df	95% CI
1	341.488 (19.257)	20.996	301.441 to 381.535	298.200 (18.201)	20.686	260.313 to 336.087
3	336.340 (17.587)	20.862	299.751 to 372.930	294.163 (16.594)	20.588	259.612 to 328.715
6	319.183 (15.959)	20.609	285.957 to 352.409	278.626 (15.023)	20.426	247.330 to 309.923
10	279.455 (14.650)	19.700	248.865 to 310.045	246.438 (13.759)	19.628	217.703 to 275.173
14	255.640 (14.828)	19.925	224.702 to 286.578	209.766 (13.930)	19.840	180.693 to 238.840

Given the near-significant interaction, simple-effects comparisons were conducted to evaluate refractive group differences at each eccentricity. Unadjusted pairwise comparisons showed no statistically significant group differences at any location (all $p \geq 0.063$, smallest $p = 0.063$ at 14 mm). To control the familywise error rate across the five eccentricity-specific contrasts, the Holm step-down procedure ($\alpha = 0.05$) was applied; none of the comparisons remained significant after adjustment (Table 6.3).

Table 6. 3 Simple effects: mean differences between refractive groups (Emmetrope, EMM, MYOP) in µm at each eccentricity (unadjusted and Holm-adjusted).
SE = Spherical Equivalent.

Eccentricity (mm)	Difference EMM − MYOP	SE	df	Unadjusted p-value	Adjusted p-value
1	43.288	28.813	23.319	0.146	0.460
3	42.177	26.698	22.680	0.128	0.460
6	40.557	24.667	21.580	0.115	0.460
10	33.017	23.066	19.921	0.168	0.168
14	45.874	23.281	20.221	0.063	0.315

Retinal Thickness (RT) at Baseline

RT varied strongly with eccentricity ($F(4, 2185.733) = 98.066$, $p < 0.001$), demonstrating a systematic spatial profile across the posterior pole (Table 6.4).

Table 6. 4 Type-III tests of fixed effects for Retinal Thickness (µm) for the Visit 1 Linear Mixed Models (LMM).

Effect	Numerator df	Denominator df	F	p-value
RefractiveGroup	1	64.792	0.558	0.458
Eccentricity	4	20185.733	98.066	< 0.001
Age	1	17.035	3.978	0.062
AXL	1	17.584	2.444	0.136

EMM (adjusted for age = 11.32 years and AXL = 24.09 mm) indicated that RT was maximal at 3 mm (overall EMM = 342.49 µm, 95% CI: 336.65 to 348.32), intermediate at 6 mm

(EMM = 306.26 µm, 95% CI: 299.05 to 313.47), and lowest at 14 mm (EMM = 239.99 µm, 95% CI: 220.42 to 259.55), with 1 mm and 10 mm showing similar thickness (EMM = 281.17 µm and 283.00 µm, respectively) (Table 6.5). Pairwise comparisons across eccentricities (Bonferroni-adjusted) were consistent with these differences, with most location pairs differing significantly ($p < 0.001$), except 1 and 10 mm.

Table 6. 5 Estimated marginal means (EMMs) of Retinal Thickness (µm) by refractive group (Emmetropes = EM, Myopes = MYOP) and eccentricity. (adjusted to Age = 11.3177 and AXL = 24.0870).

Eccentricity (mm)	EM EMM (SE)	95% CI	MYOP EMM (SE)	95% CI
1	286.094 (7.485)	271.292 to 300.895	276.247 (7.047)	262.322 to 290.171
3	348.777 (5.058)	338.433 to 359.120	336.193 (4.689)	326.618 to 345.768
6	313.844 (5.985)	301.859 to 325.829	298.669 (5.594)	287.483 to 309.856
10	288.090 (7.066)	274.088 to 302.091	277.907 (6.642)	264.757 to 291.056
14	234.602 (14.879)	205.421 to 263.783	245.368 (13.902)	218.107 to 272.630

In contrast, there was no evidence that RT differed by refractive group after covariate adjustment. The main effect of group was not statistically significant ($F(1, 64.792) = 0.56$, $p = 0.46$), and the refractive group × eccentricity interaction was also not significant ($F(4, 12464.476) = 0.85$, $p = 0.49$), indicating that the eccentricity-dependent RT profile did not differ reliably between EM and MYOP. Consistent with this, simple-effects comparisons of

at each eccentricity showed no statistically significant group differences at any location (Table 6.6). Although adjusted EMMs suggested numerical differences per location, the contrasts were not statistically supported. Age showed a borderline association with RT ($F(1, 17.035) = 3.98$, $p = 0.06$; $\beta = -3.61$ µm/year, 95% CI: −7.43 to 0.21), while AXL was not significant ($F(1, 17.58) = 2.44$, $p = 0.14$).

Table 6. 6 Emmetrope (EM) vs Myope (MYOP) groups differences in Retinal Thickness (µm) at each eccentricity (unadjusted and Holm-adjusted).

Eccentricity (mm)	Difference (EM – MYOP)	SE	df	Unadjusted p-value	Adjusted p-value
1	9.847	10.953	95.877	0.371	0.993
3	12.584	7.866	25.900	0.122	0.500
6	15.174	9.023	44.852	0.100	0.500
10	10.183	10.408	79.414	0.331	0.993
14	−10.767	20.756	1166.404	0.604	0.993

ChT - Longitudinal Trends (V2 and V3)

Follow-up visits were incomplete; therefore, the n-to-visit patterns should be interpreted only as descriptive trajectories rather than population-level estimates of change. Across all participants with MYOP, the number of participants with ChT data was n=11 at V1, n=5 at V2, and n=3 at V3. Subject-level trajectory plots (Figure 6.3) at meaningful eccentricities illustrate heterogeneous ChT patterns across visits. Depending on the eccentricity and time point, some showed apparent thickening while others exhibited thinning. As the figure shows, not all participants contributed to all visits, seen as truncated trajectories.

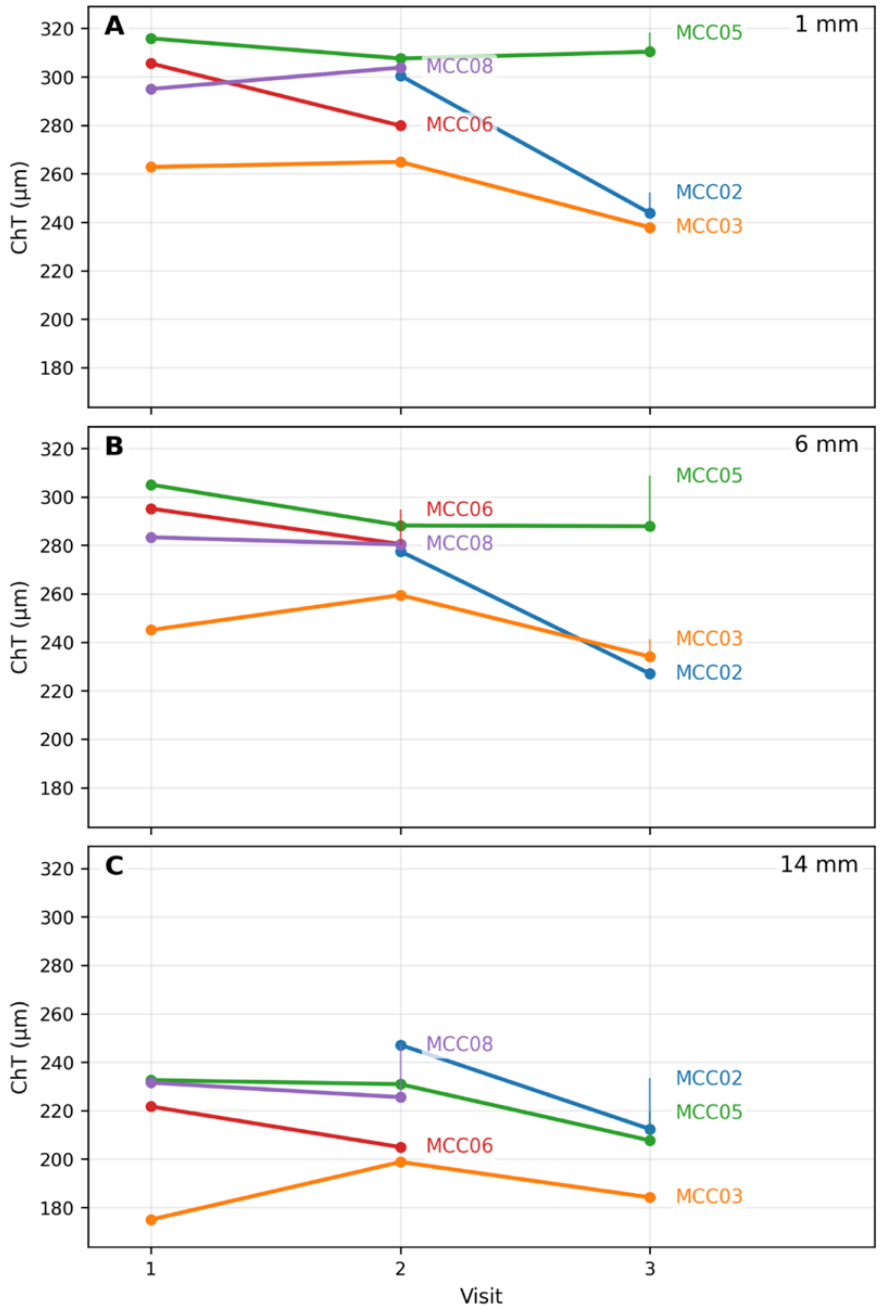

Figure 6. 3 Trajectories of choroidal thickness (ChT, µm) across visits in children with myopia. A–C: ChT at 1, 6, and 14 mm eccentricity, respectively. Each colored line represents one subject (MCC02, MCC03, MCC05, MCC06, MCC08) and connects measurements across visits (points). Not all participants contributed data at all visits.

To focus specifically on within-subject change, Δ-from-baseline plots were generated to display ChT difference at V2−V1 and V3−V1 by eccentricity for participants who had a V1 measurement at that same location. Because baseline-referenced change inherently requires a V1 data point, one subject (MCC02) who had follow-up data but no V1 baseline was displayed separately using Δ(V3−V2). This approach retains their longitudinal information without mixing definitions in the main Δ-from-V1 panels (Figure 6.4).

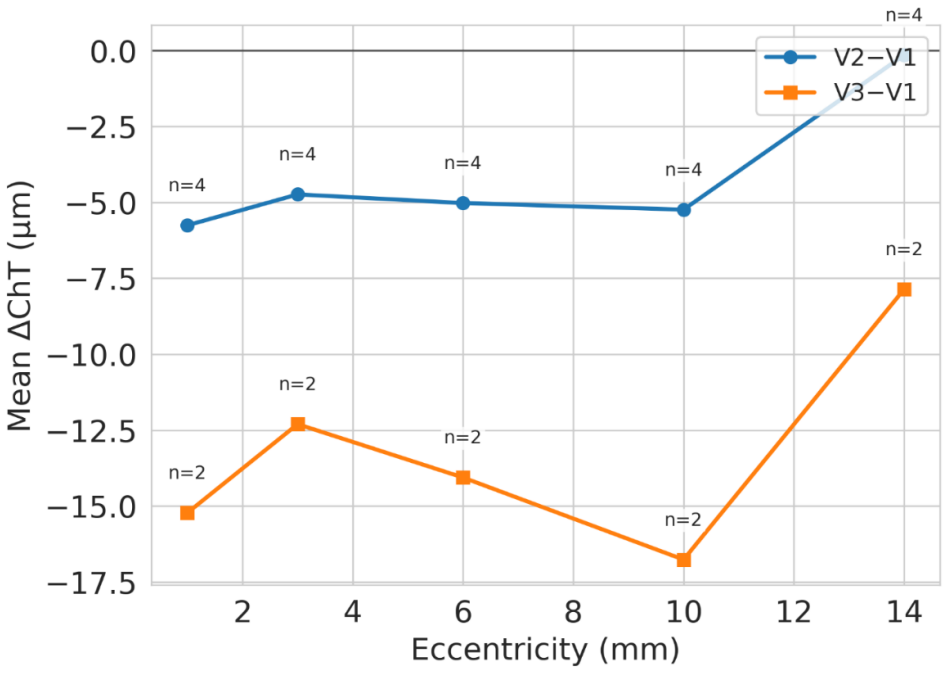

Figure 6. 4 Mean choroidal thickness change (ΔChT, µm) across eccentricity relative to baseline (Visit 1) in the group of children with myopia. Sample sizes (n) above each data point indicate the number of participants contributing data at that visit and eccentricity.

Group-level mean ChT by visit was summarized with uncertainty bands to show central tendency while reflecting the reality of limited follow-up (Figure 6.5). Error bars represent t-based 95% confidence intervals, and each visit is explicitly annotated with *n* so readers can see how the estimates at V2, and especially V3, are based on fewer participants than V1.

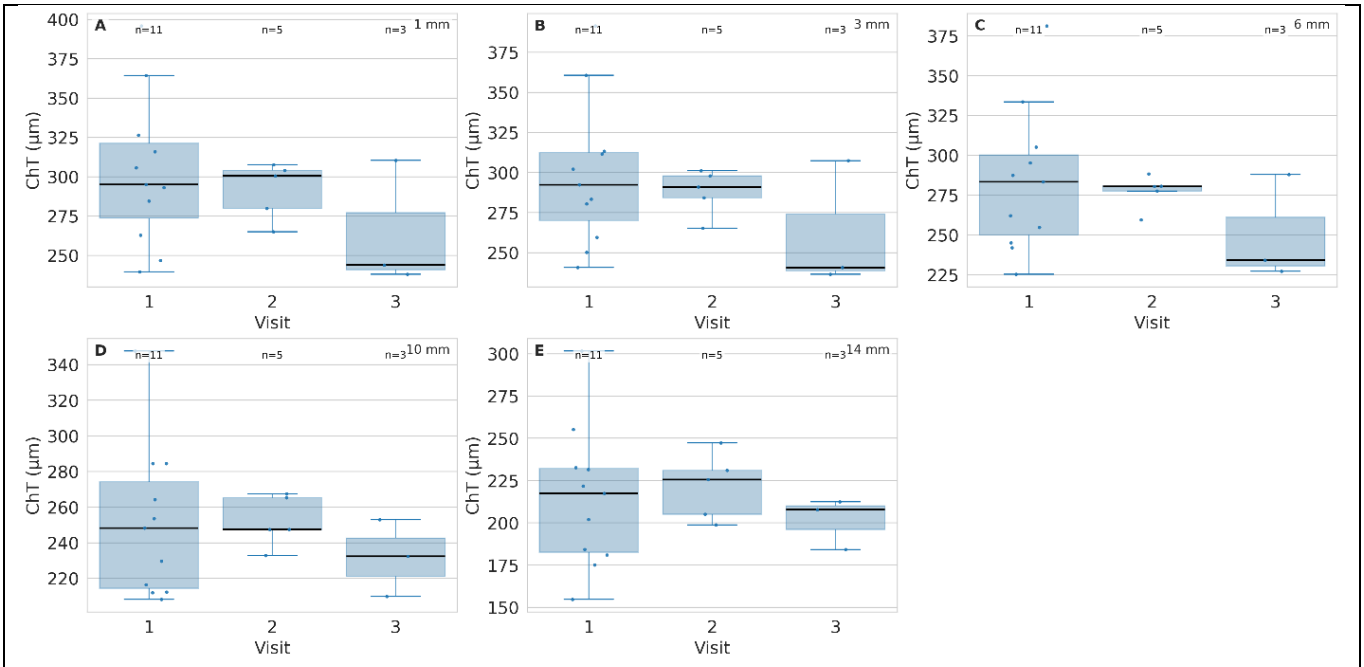

Figure 6. 5 Mean choroidal thickness (ChT) in participants with myopia across study visits, shown separately by eccentricity (Panels A–E: 1, 3, 6, 10, and 14 mm). Points indicate the mean ChT at each visit and error bars show 95% confidence intervals. Sample size varies by visit and eccentricity; n annotations indicate the number of participants contributing data at each time point. This plot is descriptive and should be interpreted cautiously given the varied samples across visits (V1 n=11, V2 n=5, V3 n=3).

Finally, heatmap profiles (Figure 6.6) organized by visit provide a compact view of eccentricity-dependent ChT within each subject. This visualization makes missingness

explicit (via blank cells) across V1, V2, and V3, visually highlighting the shrinking number of participants with available data across the panels (V1 > V2 > V3).

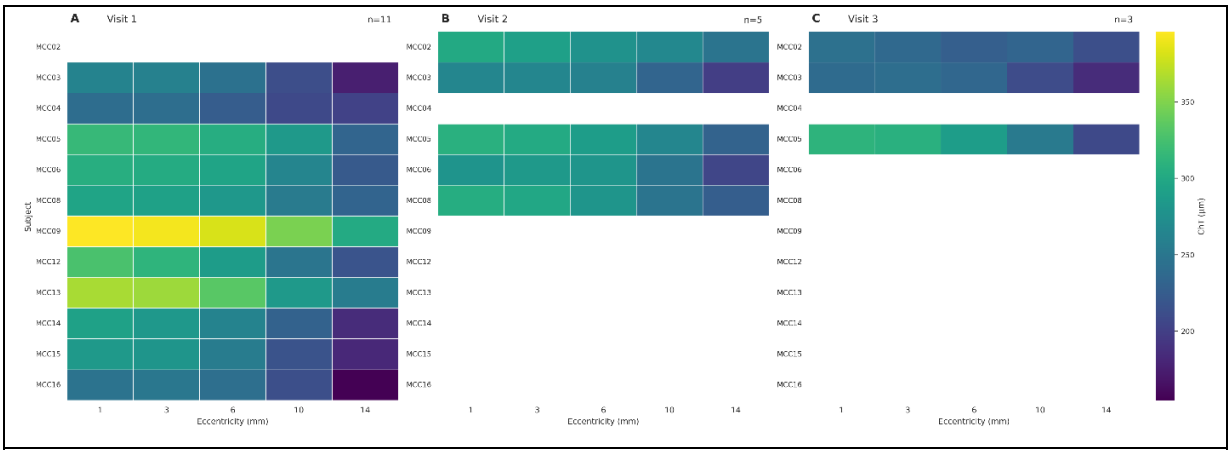

Figure 6. 6 Heatmap profiles of choroidal thickness (ChT, µm) across eccentricity in participants with myopia. Panels A–C show ChT for Visit 1 (n=11), Visit 2 (n=5), and Visit 3 (n=3), respectively. Rows correspond to participants and columns correspond to eccentricity (1, 3, 6, 10, 14 mm); color indicates ChT using a shared color scale across visits. Blank cells indicate missing measurements (no data for that subject–eccentricity–visit). The number of participants contributing to each visit is annotated, noting unequal samples across visits.

6.4. Discussion

Baseline Thickness Profiles

The evaluation of posterior segment structures using wide-field EDI OCT revealed pronounced spatial profiles across the 55-degree field for both the choroid and the retina. For ChT, all participants demonstrated significant, systematic thinning moving from the fovea toward the 14 mm peripheral locations, as expected based on established wide-field and pediatric topographical models (Fontaine et al., 2017; Hoseini-Yazdi et al., 2019; Jin et al.,

2016). This eccentricity-dependent attenuation aligns closely with established topographical models, such as those documented by Hoseini-Yazdi et al. (2019).

When comparing refractive groups, the group with MYOP exhibited a trend of generalized choroidal thinning relative to their peers with EM. However, there was no conclusive, statistically reliable evidence of refractive group differences at any specific eccentricity once multiplicity was controlled. This lack of statistical divergence is likely due to a combination of limited sample size and the specific demographic of the cohort. The participants with MYOP are young and present with early-to-moderate refractive error. Recent literature indicates that ChT is highly correlated with the degree of axial elongation (Fontaine et al., 2017; Hoseini-Yazdi et al., 2019; Jin et al., 2016; Zhu et al., 2023). However, it is critical to contextualize these prior findings by differentiating between central and peripheral measurements, as well as the age of the cohorts evaluated. For example, several large cross-sectional studies have successfully documented significant central choroidal thinning in children with myopia (Fontaine et al., 2017; Jin et al., 2016; Zhu et al., 2023). Conversely, comprehensive evaluations of peripheral or wide-field ChT have been predominantly conducted in young adult populations, where established MYOP demonstrate pronounced peripheral thinning compared to EM (Hoseini-Yazdi et al., 2019). Data evaluating wide-field peripheral ChT specifically in young pediatric cohorts at the onset of myopia remains limited. Therefore, our results suggest that substantial, absolute structural attenuation of the choroid is a progressive consequence of advanced axial elongation, rather than a defining feature universally detectable at the immediate clinical onset of the condition.

Similarly, baseline RT exhibited a strong, eccentricity-dependent profile that peaks at the 3 mm parafoveal region before steadily declining peripherally. This characteristic topographical distribution is highly consistent with established normative pediatric OCT data (Jin et al., 2016; Read, Alonso-Caneiro, & Vincent, 2017). Previous cross-sectional and longitudinal evaluations in young children have consistently demonstrated that RT naturally reaches its maximum within the parafoveal annulus (typically around 1.5 to 3.0 mm from the fovea) due to the high regional density of ganglion cells, before progressively tapering off into the perifovea and broader periphery (Jin et al., 2016).

Regarding whether RT is expected to change within these specific eccentricities at this age, the literature indicates a high degree of structural stability. Longitudinal pediatric studies have shown that overall macular and parafoveal RT changes by an average of less than 2 μm over 12 to 18 months, maintaining a highly stable profile even during periods of active, normal axial growth (Romashchenko, Rosén, & Lundström, 2020). However, when evaluating the impact of refractive error, studies evaluating both central and peripheral RT confirm that children with MYOP tend to exhibit subtle but statistically significant thinning specifically within these parafoveal and perifoveal eccentricities compared to their EM peers (Jin et al., 2016; Read, Alonso-Caneiro, & Vincent, 2017; Zhang et al., 2024). Therefore, the eccentricity-dependent RT profile observed in our cohort perfectly mirrors the expected structural anatomy of the pediatric retina, confirming that while subtle regional thinning may begin to manifest, the foundational retinal architecture and its spatial distribution remain highly stable during childhood myopia.

Longitudinal Structural Trajectories

The longitudinal assessment of ChT aimed to evaluate whether initiating myopia control treatments induces measurable structural changes over a 12-month period. Previous literature and experimental models suggest that certain interventions, such as orthokeratology or specialized myopia control contact lenses, may induce transient or sustained choroidal thickening, which is hypothesized to act as a compensatory biomarker for treatment efficacy (Amorim-de-Sousa et al., 2023; National Academies of Sciences, Engineering, and Medicine, 2024; Nickla & Wallman, 2009; Summers, 2013). However, the longitudinal trajectories observed here in participants with MYOP were characterized by high individual variation, a finding that must be heavily contextualized by the severely limited longitudinal sample size. With follow-up data available for only five participants at the 6-month visit and a mere three participants at the 12-month visit, the capacity to identify true group-level trends is fundamentally restricted. Within this very small subset, within-subject changes from baseline revealed that while some participants exhibited apparent choroidal thickening at specific eccentricities, others demonstrated continued thinning. Because the longitudinal dataset was constrained by this small number of participants, these patterns cannot be generalized and must be interpreted strictly as descriptive, individual-level observations rather than confirmatory trends. The pronounced variance within such a minimal sample underscores that if myopia control treatments do elicit a measurable choroidal response, the effect may be highly localized, temporally dynamic, or subject to significant individual differences. Future studies utilizing substantially larger, well-retained pediatric participants will be absolutely

essential to achieve the statistical power required to reliably separate true treatment-induced choroidal modulation from normal biological fluctuation and progressive myopic stretching.

7. Retinal Responses

7.1. Background

Myopia appears to be associated not only with structural ocular changes but also with measurable differences in retinal function compared with non-myopic eyes (Chen, Brown, & Schmid, 2006; Ho, Kee, & Chan, 2012; Koh et al., 2014; Park et al., 2013). Retinal electrophysiology (ERG) studies have reported reduced response amplitudes and small delays in peak timing in myopic eyes, with effects that become more evident as refractive error and AXL increase (Chen, Brown, & Schmid, 2006; Ho, Kee, & Chan, 2012; Kader, 2012; Koh et al., 2014; Park et al., 2013; Sachidanandam, Ravi, & Sen, 2017). Although the relationship between myopia/axial elongation and retinal function is widely recognized, it remains unclear whether functional differences are more prominent centrally or in the peripheral retina (Chen, Brown, & Schmid, 2006; Ho, Kee, & Chan, 2012; Kader, 2012; Koh et al., 2014; Park et al., 2013; Sachidanandam, Ravi, & Sen, 2017).

Importantly, there is limited literature evaluating whether myopia control interventions themselves modify retinal activity over time, despite the fact that these treatments intentionally alter retinal image quality and peripheral defocus (Amorim-de-Sousa et al., 2023; Chan et al., 2022; Gupta, Chakraborty, & Verkicharla, 2022; Kang, McAlinden, & Wildsoet, 2017; Nti & Berntsen, 2020; Queirós et al., 2020; Song et al., 2021; Wildsoet et al., 2019). Available evidence on treatment-related retinal changes is mixed and limited by short follow-up and/or small sample sizes (Amorim-de-Sousa et al., 2023; Queirós et al., 2020). For example, orthokeratology has been evaluated with pERG and Visual evoked potential

(VEP) over relatively short time periods with no statistically significant changes reported, and multifocal myopia-control contact lenses have also been studied over brief exposure durations (Amorim-de-Sousa et al., 2023; Queirós et al., 2020). Regarding atropine, the current evidence remains limited and sometimes inconsistent, and baseline electro retinal response has been suggested as a possible modifier of treatment efficacy (Chan et al., 2022; Gupta, Chakraborty, & Verkicharla, 2022; Vera-Diaz et al., 2023).

Given these gaps, an objective, repeatable measure of retinal function is valuable for assessing potential retinal-level effects of myopia-control interventions in children (Amorim-de-Sousa et al., 2023; Chan et al., 2022; Chen, Brown, & Schmid, 2006; Gupta, Chakraborty, & Verkicharla, 2022; Ho, Kee, & Chan, 2012; Kader, 2012; Koh et al., 2014; Park et al., 2013; Queirós et al., 2020; Sachidanandam, Ravi, & Sen, 2017). In this thesis, pERG was used to quantify retinal responses to clear versus blurred images using a novel “dead leaves” stimulus that better approximates natural image statistics than simple grating patterns (Panorgias et al., 2021). By presenting stimuli at different eccentricities, the protocol evaluates whether retinal responses to blur differ across retinal regions (Panorgias et al., 2021) and whether these responses change after initiation of myopia control treatment.

7.2. Methods

pERG was utilized to quantify the retina’s interpretation of images with all contrasts (0-100%) by directly monitoring electrical brain signals during image perception. To more accurately mirror natural contrast backgrounds compared to traditional checkboard images [68], the pERG protocol employed an arrangement of 'dead leaves' in a solid circle or ring

formation, as shown in Figure 7.1. By adjusting the radius and width of this stimulus, retinal responses were evaluated across different eccentricities (0 to 4 degrees foveally, 4 to 8 degrees, and 8 to 12 degrees). Evaluating these electrical responses before and after treatment allows for the indirect deduction of corresponding changes in the brain's sensory pathway.

Procedures

Prior to testing, the skin at the electrode sites was prepared by cleaning with alcohol pads followed by exfoliation with NuPrep Gel (D234). Disposable Skin Electrodes (D161) were then positioned at the right temporal canthus (serving as the reference electrode) and the inferior eyelid (serving as the active electrode). A ground connection was established on the forehead using a combination of D207 Wrist Snaps and D230 Red Dot Electrodes. All electrodes were accessories of the Espion E3 System (Diagnosys LLC, Lowell, MA, USA), which was utilized to record the pERG signals.

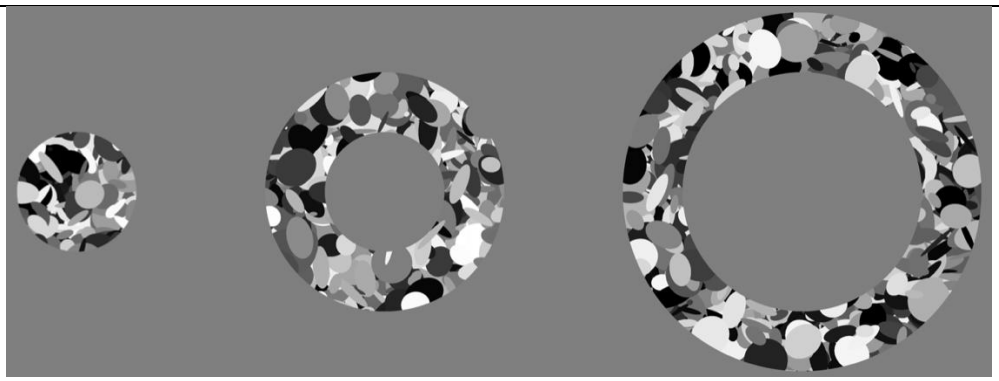

Figure 7. 1 Examples of pERG Stimuli at different eccentricities. Left: 0–4°, Middle: 4–8°, and Right: 8–12°. The participant fixates in the center of the image.

Stimuli were generated using custom MATLAB code and presented on an LG OLED C3 42-inch TV (Seoul, South Korea) that had been calibrated using a Datacolor Spyder (Rotkreuz, Switzerland). The display system was synchronized with the Espion E3 system via an Arduino Uno Rev3 (Ivrea, Italy). Before data collection commenced, electrode impedance was verified to ensure optimal contact, and the participant's fellow (untested) eye was fogged. During recording, a 50/60 Hz line filter was applied to minimize alternating wave interference from electrical sources.

Outcome Measures

Two primary outcome measures were extracted from the Fourier-transformed pERG recordings for each tested eccentricity: retinal response density and response latency.

- Response Density: Defined as the electrical signal amplitude divided by the specific stimulus area (measured in nV/deg^2), this metric represents the overall strength or magnitude of the retina's neural response to the naturalistic contrast stimulus.
- Latency: Defined as the implicit time (measured in milliseconds, ms) required for the retinal system to begin responding to the presented stimulus, providing a functional metric of temporal processing speed.

To ensure the reliability and validity of these extracted metrics, a strict data quality threshold was established prior to statistical evaluation. Specifically, any individual pERG recordings demonstrating a signal-to-noise ratio (SNR) of less than one were deemed unreliable and were entirely excluded from all subsequent analyses.

Statistical Analyses

To analyze the pERG data, a LMM was used to evaluate the effects of refractive group (EM/MYOP) and eccentricity (0-4°, 4°-8°, 8°-12°) on retinal response density, with age included as a covariate. A first-order autoregressive covariance structure was applied to account for correlations between adjacent eccentricities within the same participant. An identical LMM was utilized to evaluate the response latency data. When significant main effects of eccentricity were identified, Bonferroni-corrected pairwise comparisons were performed to characterize the functional differences between retinal locations.

7.3. Results

Participants and Demographics

Seventeen participants successfully completed the baseline pattern electroretinogram (pERG) testing, comprising 9 participants with EM (mean age 11.35 ± 1.40 years) and 8 with MYOP (mean age 10.51 ± 1.81 years). Baseline clinical characteristics and ocular biometry for these cohorts are summarized in Table 7.1.

Table 7. 1 Age and clinical data of all participants in the pattern electroretinography (pERG) test at Visit 1.
EMM = Emmetropia group, MYOP = Myopia group.

Group	N (number of participants)	Age (mean ± SD)	SE OD (mean ± SD)	AXL OD (mean ± SD)
EMM	9	11.35 ± 1.40	0.92 ± 0.18	23.18 ± 0.80
MYOP	8	10.51 ± 1.81	−3.05 ± 1.01	24.97 ± 0.84

Baseline Retinal Response Density

There was a strong and statistically significant main effect of Eccentricity ($F(2, 17.824) = 97.363$, $p < 0.001$) (Figure 7.2). Age-adjusted estimated marginal means revealed a monotonic decline in response density as distance from the fovea increased [4° = 3.771 (SE 0.194); 8° = 1.417 (SE 0.194); 12°: = 0.851 (SE 0.201). Bonferroni-corrected pairwise comparisons confirmed that response density at 4° was significantly higher than at 8° ($p < 0.001$) and 12° ($p < 0.001$), and density at 8° was significantly higher than at 12° ($p = 0.027$).

There was no significant main effect of refractive group on response density ($F(1, 11.339) = 0.058$, $p = 0.814$) (Figure 7.2) The EMM for both groups were similar (MYOP = 1.914, EM = 2.112, $p = 0.536$). The Refractive Group × Eccentricity interaction was also not significant ($F(2, 17.824) = 0.929$, $p = 0.413$), indicating that the eccentricity-dependent decline in sensitivity was similar for both groups. The inclusion of AXL as a covariate in a secondary model did not alter these results as AXL was not a significant predictor ($p = 0.802$), and the main effect of refractive group remained non-significant ($p = 0.872$).

As illustrated in Figure 7.2, there is a decline in response density moving from the central 4° out to the 12° periphery, a pattern shared equally by both the refractive cohorts. The overlapping interquartile ranges between the two groups at every eccentricity reinforce the LMM findings of no significant group differences.

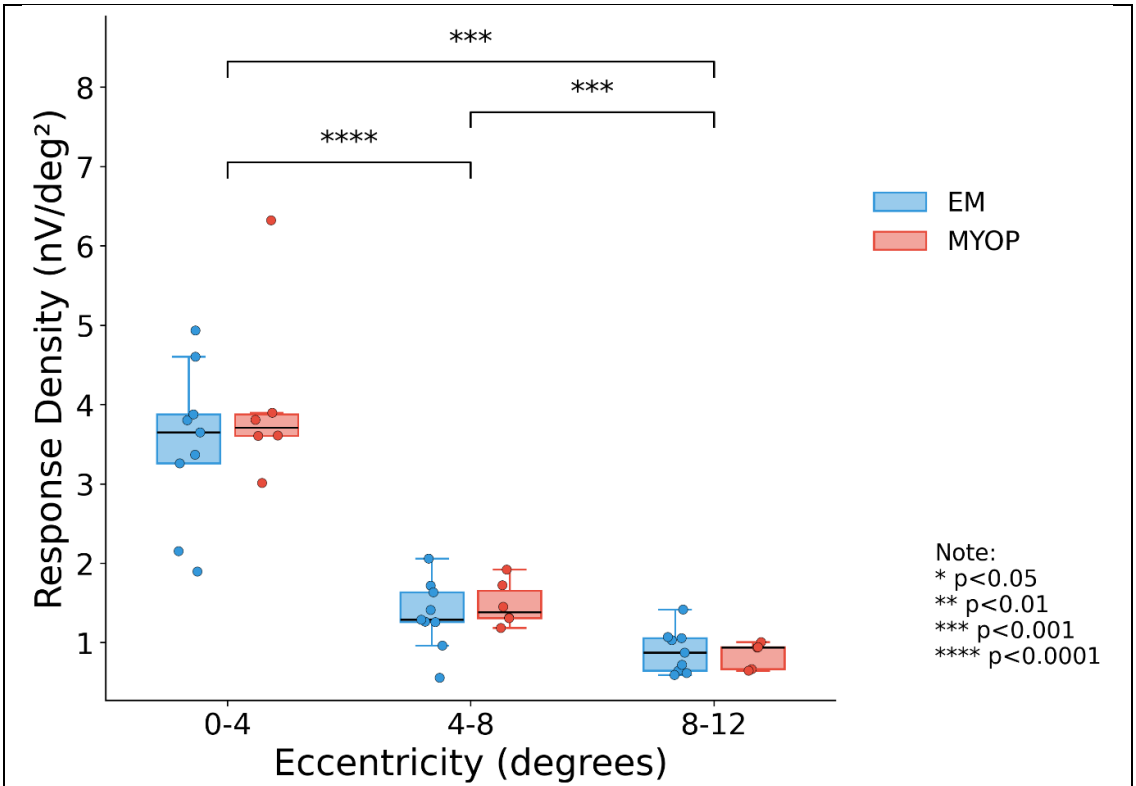

Figure 7. 2 Baseline comparisons of Response Density (nV/deg²) by eccentricity (4°, 8°, 12°), stratified by refractive group (emmetropia = EM in blue; myopia = MYOP in red). Boxes represent the interquartile range, the central line indicates the median, whiskers show the spread of the data, individual points represent each participant.

This uniform decline is further detailed in Table 7.2, which provides the raw descriptive statistics. While the MYOP group showed a slightly higher mean response density at 4° (4.04 ± 1.16 nV/deg²) compared to the EM group (3.50 ± 1.00 nV/deg²), the values rapidly converge at the 8° and 12° marks, confirming that spatial functional topography is preserved regardless of refractive status.

Table 7. 2 Baseline Response Density (mean ± SD) by eccentricity (degrees) and refractive group (EM = emmetropic group; MYOP = myopic group). Response density is defined as signal amplitude divided by stimulus area (nV/deg²). Values are reported as mean ± standard deviation, n indicates the number of participants contributing within each group.

Group	N (number of participants)	Eccentricity	Response Density
EM	9	4	3.50 ± 1.00
EM	9	8	1.35 ± 0.44
EM	9	12	0.89 ± 0.28
MYOP	6	4	4.04 ± 1.16
MYOP	6	8	1.48 ± 0.28
MYOP	5	12	0.84 ± 0.17

Baseline Retinal Response Latency

There was no significant main effect of refractive group ($F(1, 11.577) = 3.062$, $p = 0.107$). However, a trend toward shorter latencies in the MYOP group (8.402 ± 1.155 ms) compared to the EM group (11.576 ± 1.395 ms) was noted. Although it did not reach statistical significance, there was indeed a trend suggesting shorter latencies in MYOP (difference = −3.173, $p = 0.107$). The inclusion of age and AXL as covariates did not alter these results.

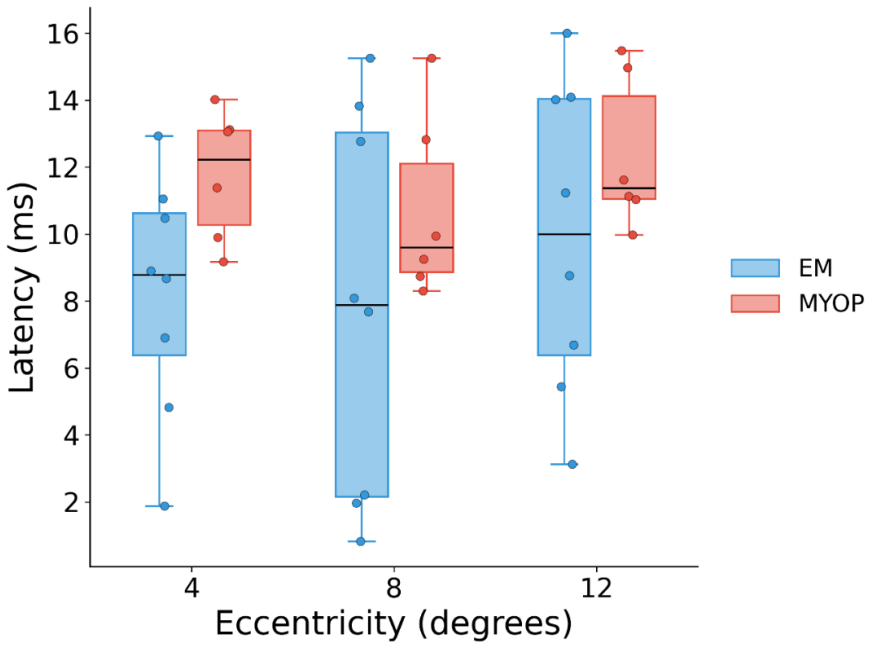

Figure 7. 3 Baseline comparisons of retinal response latency (ms) by eccentricity (4°, 8°, 12°), stratified by refractive group: Participants with emmetropia (EM, blue) and myopia (MYOP, red). Boxes represent the interquartile range, the central line indicates the median, whiskers show the spread of the data, individual points represent each participant.

A closer examination of the data distribution in Figure 7.3 reveals a high degree of variance in response timing across all participants, which helps explain the lack of statistical significance between the groups. The overlapping boxplots demonstrate that while individual latency ranges fluctuated widely, the overall timing behavior remains comparable across the central and peripheral retina. Table 7.3 breaks down the specific raw latency values. Together, the figure and table highlight that temporal processing of the "dead leaves" stimuli is highly variable but fundamentally intact across both refractive populations.

Table 7. 3 Baseline Latency (mean ± SD) by eccentricity (degrees) and refractive group (EM = emmetropic group; MYOP = myopic group). Latency is defined as the time for the system to begin responding to the stimulus (e.g., milliseconds). Values are reported as mean ± standard deviation, and **n** indicates the number of participants contributing within each group × eccentricity cell.

Group	Eccentricity	n	Latency
EM	4	8	8.20 ± 3.57
EM	8	8	7.83 ± 5.74
EM	12	8	9.92 ± 4.64
MYOP	4	6	11.78 ± 1.95
MYOP	8	6	10.72 ± 2.74
MYOP	12	6	12.36 ± 2.28

Longitudinal data were only available for two participants: MCC03 – three visits available, and MCC02 –two visits available. Given this, longitudinal analyses were not possible. Pattern ERG response density decreased over time for MCC03 at all eccentricities, with the largest reduction observed between Visit 1 and Visit 3 in the central 0–4° region (Figure 7.4). Peripheral rings (4–8° and 8–12°) showed smaller absolute changes and largely overlapping response densities across visits. Response latency was relatively stable across visits, with only minor visit-to-visit variability and no consistent tendency toward either shortening or

prolongation at any eccentricity. Together, these data suggest a modest decline in central amplitude over time in this subject without clear evidence of progressive latency delay.

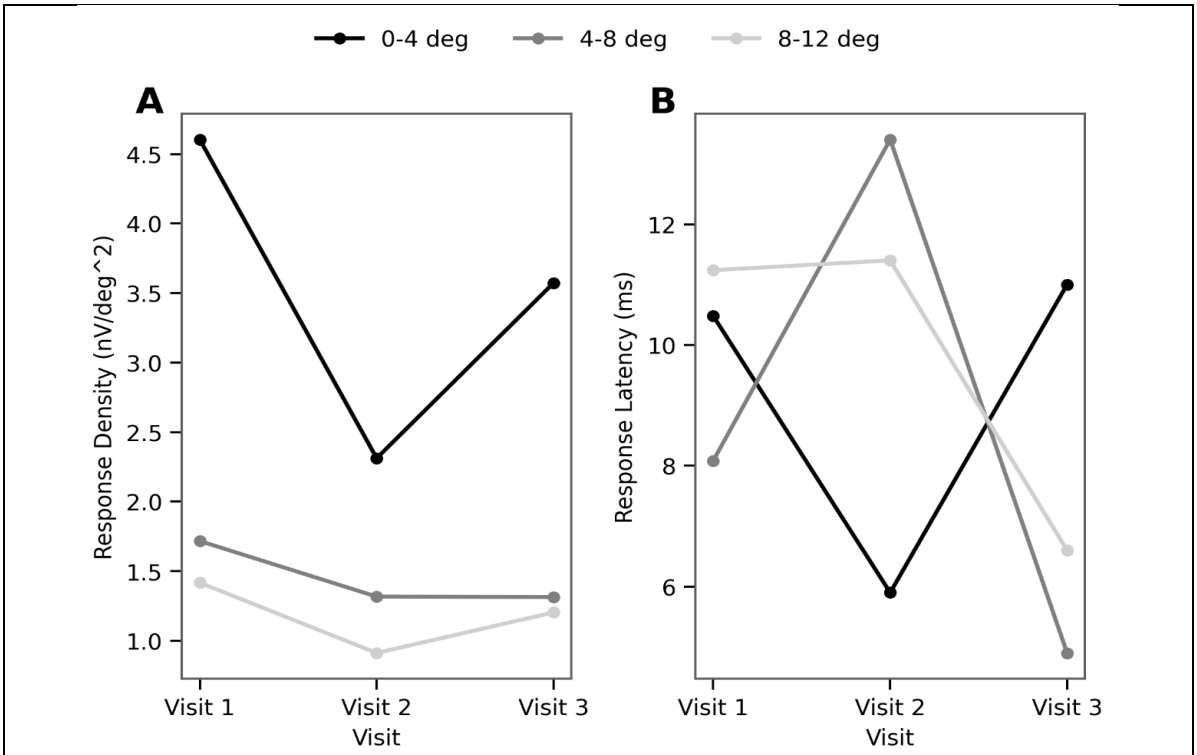

Figure 7. 4 Pattern ERG response density (A) and latency (B) in MCC03 across three visits. Black, dark gray, and light gray lines denote 0–4°, 4–8°, and 8–12° retinal eccentricities, respectively.

7.4. Discussion

The baseline pattern ERG evaluation revealed a pronounced reduction in retinal response density from the central 4° to the peripheral 12°. This strong spatial gradient aligns with the established topography of the human retina, specifically the rapid decline in retinal ganglion

cell (RGC) density moving away from the fovea (Curcio & Allen, 1990). However, we found no statistically reliable differences in pERG response density or latency between participants with MYOP and EM across these eccentricities. This absence of functional deficit contrasts with some broader pERG literature (Gupta, Chakraborty, & Verkicharla, 2022), which frequently reports reduced amplitudes and delayed implicit times in myopic eyes, often attributed to the mechanical stretching of the globe and subsequent alteration of RGC spacing. This discrepancy is likely driven by both our cohort's demographic and our methodological design. Our participants are young children presenting with early-to-moderate myopia prior to optical intervention. And at this early stage of axial elongation, the inner retina may not yet exhibit the profound functional attenuation seen in older adults or those with pathologic myopia. Furthermore, the use of a naturalistic, broad-band spatial stimulus in our pERG paradigm (Panorgias et al., 2021) likely elicits a different inner-retinal response than those by standard high-contrast reversing checkerboards. Consequently, these findings suggest that in the early stages of pediatric myopia, the fundamental spatial topography and temporal processing of the inner retina remain intact.

Another important finding from our baseline data was that the AXL of the eyes did not negatively affect how well the retina functioned. When we incorporated AXL into our statistical models, it did not change the results for either the strength (density) or the speed (latency) of the retinal response. This differs from what is often reported in studies of older adults or people with severe myopia, where the extreme physical stretching of a longer eye can thin out the retinal cells and weaken the electrical signal (Koh et al., 2014; Sachidanandam, Ravi, & Sen, 2017). However, the children with MYOP in our study are still

in the early stages of the condition. While their eyes are longer than those of their emmetropic peers, they have not stretched enough to cause any measurable damage to the retina. In fact, the speed of their retinal responses was completely normal, and even trended slightly faster than the emmetropic group. This confirms that before starting any myopia treatments, the neural pathways in the eyes of these young participants are healthy and fully functioning, giving us a solid, stable baseline to measure future changes against.

On the other hand, the analysis of latency revealed no statistically significant differences in implicit times between eyes with MYOP and those with EM ($p = 0.107$). This observation contrasts with some prior literature reporting significantly delayed retinal responses in myopic eyes (Chen, Brown, & Schmid, 2006; Ho, Kee, & Chan, 2012; Koh et al., 2014; Park et al., 2013; Sachidanandam, Ravi, & Sen, 2017). The lack of a statistically reliable difference in our findings is likely attributable to the small sample size of the current study, which limits the statistical power required to detect subtle temporal delays. While there was a numerical trend toward shorter implicit times in the myopic group (difference $\approx$ -3.17 ms), the limited sample size prevents drawing firm conclusions. Therefore, our results indicate that temporal processing speed for complex "dead leaves" stimuli is not overtly impaired in this early myopic cohort, but further research with a substantially larger sample size is needed to definitively determine if this functional preservation holds true or if subtle delays emerge as statistical power increases.

In summary, retinal response density to naturalistic blur is affected by retinal eccentricity but there does not seem to be an effect of MYOP, whereas there might be an effect of MYOP

retinal response latency that needs to be corroborated by a larger study. These findings suggest that the neural mechanisms encoding naturalistic contrast remain robust in the young myopic retina despite axial elongation.

8. Psychophysics

8.1. Background

Psychophysical measures provide a direct assessment of how optical and neural factors combine to determine real-world visual performance, and they complement the structural and optical quality outcomes reported in other chapters. Because myopia-control treatments intentionally modify retinal image formation (e.g., by inducing peripheral defocus, altering higher-order aberrations or contrast), it is important to quantify whether these interventions change visual function (Berntsen, 2018; Cooper et al., 2013; Kang, McAlinden, & Wildsoet, 2017; Lipson, Boland, & McAlinden, 2022; Nti & Berntsen, 2020; Sankaridurg et al., 2021; Song et al., 2021; Wildsoet et al., 2019). Contrast sensitivity is particularly relevant because it can reveal subtle losses in visual quality not detected by high-contrast acuity testing, and it can be affected by optical blur and increased aberrations (Ding et al., 2022; Huang et al., 2022; Kang, McAlinden, & Wildsoet, 2017; Lipson, Boland, & McAlinden, 2022; Mathur & Atchison, 2009; Nti & Berntsen, 2020; Papadogiannis et al., 2022; Song et al., 2021).

Prior work has shown that orthokeratology alters the corneal shape and is associated with increased HOAs (particularly SA) and reduced low-contrast acuity, while multifocal/dual-focus soft contact lenses may also reduce quality of vision and alter accommodative behavior (Ding et al., 2022; Huang et al., 2022; Kang, McAlinden, & Wildsoet, 2017; Lipson, Boland, & McAlinden, 2022; Mathur & Atchison, 2009; Nti & Berntsen, 2020; Papadogiannis et al., 2022; Sankaridurg et al., 2021; Schmid, Gifford, & Atchison, 2023; Song et al., 2021; Vera et al., 2023). Spectacle-based myopia-control designs have also been reported to influence

peripheral visual function, highlighting the need to consider off-axis vision when evaluating these treatments (Chen et al., 2022; Gao et al., 2021; Lam et al., 2020; Lu et al., 2020).

In addition to contrast sensitivity, tasks that investigate peripheral processing and attention, such as effective field of view and visual search, may detect functional impacts of myopia-control optics that are not captured by foveal measures alone (Berntsen, 2018; Cooper et al., 2013; Corpus & Piñero, 2022; Kang, McAlinden, & Wildsoet, 2017; Lipson, Boland, & McAlinden, 2022; Nti & Berntsen, 2020; Sankaridurg et al., 2021; Song et al., 2021; Wildsoet et al., 2019). Although some studies have described changes in accommodation and binocular vision with orthokeratology and multifocal contact lenses, potential effects on broader visual performance domains remain relatively underexplored, particularly in pediatric myopia-control cohorts (Kang, McAlinden, & Wildsoet, 2017; Lipson, Boland, & McAlinden, 2022; Nti & Berntsen, 2020; Schmid, Gifford, & Atchison, 2023; Vera et al., 2023). Therefore, this thesis includes a battery of psychophysical tests assessing central and peripheral contrast sensitivity and measures of effective field of view performance to evaluate whether myopia-control treatments are associated with measurable visual functional changes over time.

8.2. Methods

Contrast Sensitivity

Customized MATLAB scripts were utilized to measure the complete contrast sensitivity function (CSF) both on-axis and at 8 degrees eccentricity. For central CSF assessment, participants were instructed to identify the orientation of sinusoidal gratings varying in

contrast and spatial frequency while fixating centrally (Figure 8.1). The testing sequence consisted of five consecutive display panels. As picture shows, each panel presented an array of 16 circular stimuli, resulting in a cumulative total of 80 trials per test.

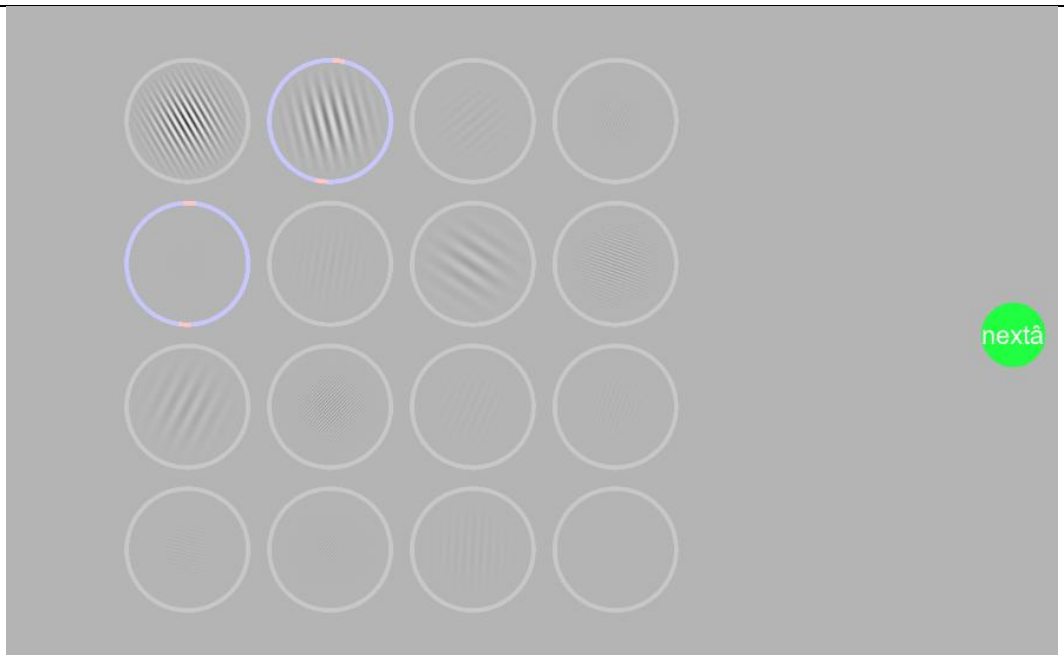

Figure 8. 1 Central Contrast Sensitivity Function (CSF) task interface. The visual display consists of a 4x4 array featuring 16 circular stimuli, each presenting a sinusoidal grating. The gratings systematically vary in both contrast and spatial frequency to assess the threshold. Participants are instructed to maintain central fixation while identifying the orientation of each grating by aligning the two pink rectangular markers with the orientation of the internal grating lines. The complete testing sequence progresses through five consecutive display panels (16 stimuli per window), yielding a total of 80 trials per session.

Peripheral CSF was measured at eight degrees eccentricity. Before the start of the peripheral contrast sensitivity test, a gaze calibration was conducted using a Gazepoint eyetracker (Gazepoint, Vancouver, Canada). This calibration enabled the recording of the participants'

eye movements throughout the entire procedure, to ensure that they used the peripheral retinal area chosen and they maintained a consistent eye-to-screen distance.

Participants were then presented with eight circles centrally positioned on the screen, as shown in Figure 8.2. They were instructed to fixate at the center of the area enclosed by these circles and click the mouse when ready. Subsequently, if they were indeed fixating centrally, a sinusoidal pattern, varying in contrasts and spatial frequency, appeared at one of the eight locations (up/down/left/right/up-right/up-left/bottom-right/bottom-left) at one of the peripheral locations (Figure 8.2).

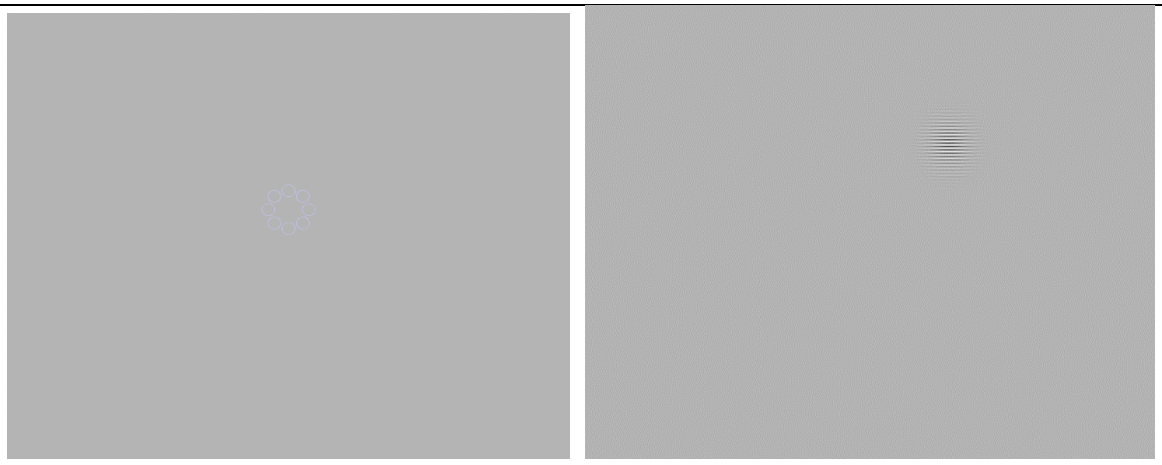

Figure 8. 2 Interface for the peripheral contrast sensitivity task. Left: The fixation screen displaying eight centrally positioned circles where the participant must maintain gaze. Right: The test screen showing a sinusoidal grating target appearing in the upper-right peripheral location. Participants are required to maintain central fixation while identifying the location of the target using the mouse cursor. position.

The task for the participant was to pinpoint the location of these images on the screen using the mouse cursor while maintaining fixation at the center of the screen. The collected

MATLAB data were then processed using customized MATLAB codes to extract spatial frequency peak (SFP), contrast sensitivity peak (CSP), the area enclosed by the fitted contrast sensitivity function (AULCSF), low spatial frequency contrast sensitivity (LSFCS), and contrast sensitivity function acuity peak (CSAV).

Effective Field of View

Another custom MATLAB script was utilized to measure the participants' effective field of view (UFOV) to evaluate peripheral processing and attention. This task required participants to determine whether a briefly presented foveal target letter matched the identity of a simultaneously presented peripheral letter located at 4, 8, or 16 degrees of eccentricity randomly, as shown in Figure 8.3.

To determine UFOV Threshold Size, the threshold optotype size was estimated independently for each specific eccentricity. Importantly, the central foveal target and the peripheral target were always the exact same size on any given trial; they were scaled together simultaneously as the adaptive test progressed. Therefore, UFOV Threshold Size specifically reflects the smallest optotype size that could be correctly identified as either the 'same' or 'different' at threshold performance for that designated peripheral location. Furthermore, the task evaluated temporal processing limits by directly factoring in response accuracy rather than measuring simple reaction times. For each trial, the participant's response regarding whether the targets were the same or different was explicitly recorded as either correct or incorrect. Using these accuracy data, the program dynamically varied both the stimulus duration and the stimulus size based on the correctness of the participant's

responses to previous size and duration combinations. This adaptive procedure identified the threshold stimulus duration required for accurate discrimination at each tested eccentricity.

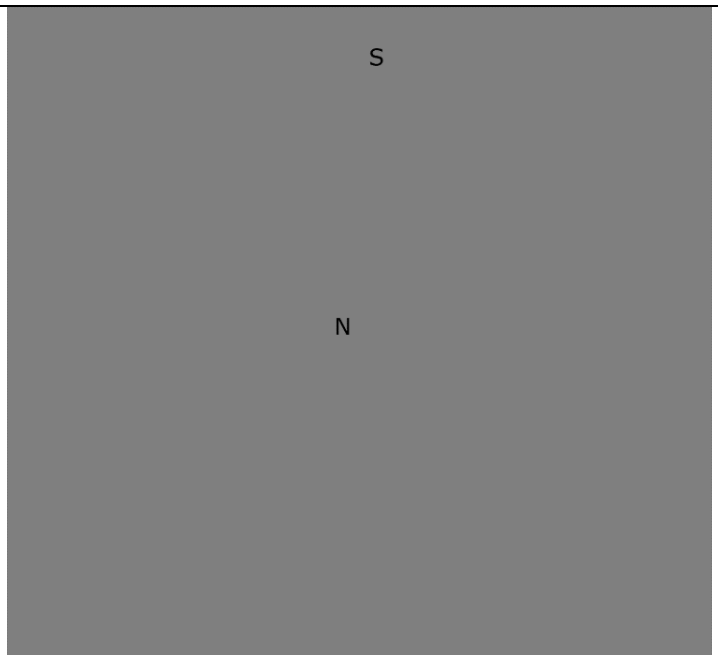

Figure 8. 3 Sample image for the effective field of view test. The participant was asked to fixate in the central target letter that was briefly presented while answering whether the peripheral letter is different or the same.

Data Processing

Raw data from the psychophysical tasks were processed using custom MATLAB scripts to extract key outcome measures for each participant.

- CSF: For both central and peripheral (8° eccentricity) tasks, the following metrics were derived from the fitted contrast sensitivity function:
    - Spatial Frequency Peak (SF Peak): SF at which sensitivity is maximal.

  - Contrast Sensitivity Peak (CS Peak): Maximum contrast sensitivity.
  - CSF Acuity: High-spatial-frequency cutoff, representing VA.
  - Area Under the Log CSF (AULCSF): A global measure of contrast sensitivity performance integrated across all spatial frequencies.
  - Low Spatial Frequency Contrast Sensitivity (LSFCS): Extracted specifically for the peripheral task to assess performance at lower spatial frequencies.

- Effective Field of View (UFOV):
  - UFOV Threshold Size: Minimum optotype size required to discriminate whether the simultaneously scaled central and peripheral targets were the same or different.
  - UFOV Response Time: the minimum stimulus presentation duration necessary to maintain accurate discrimination.

Statistical Analysis

Descriptive statistics, including means and standard deviations (Mean ± SD), were calculated for all outcome measures. The analysis focused on evaluating baseline differences in visual performance between the refractive groups at the baseline visit. Multivariate general linear models (MANCOVA) were used to test whether refractive group (EM vs. MYOP) was associated with CSF metrics, adjusting for age.

Separate models were run for central and peripheral CSF outcomes, and the dependent variables were SFPeak, CSPeak, AUCLCSF, and CSFAcuity. Central and peripheral outcomes were evaluated in separate a priori models; an alpha level of 0.05 was used for

each location. Because Box's M indicated unequal covariance matrices (p = 0.008), Pillai's trace was utilized as the robust multivariate test statistic. Significant multivariate effects were followed by univariate tests and Bonferroni-adjusted pairwise comparisons of estimated marginal means (EMM). A pre-specified sensitivity analysis additionally adjusted for AXL. For the UFOV tasks, a mixed-effects model was used with Eccentricity (4°, 8°, 16°) as the within-subject factor (repeated) and Refractive Group (EM vs. MYOP) as the between-subject factor, with age as a covariate. To account for multiple testing across the two primary UFOV outcomes (Threshold Size and Response Time), the Holm sequential decision rule was applied across the two primary p-values.

Longitudinal changes for the myopic cohort at 6 and 12 months were treated as descriptive and exploratory due to the limited sample size returning for follow-up visits.

8.3. Results

Contrast Sensitivity

The multivariate effect of refractive group on central CSF metrics was not significant after adjusting for age (Pillai's trace = 0.429, F(4,12) = 2.249, p = 0.124). In univariate follow-up tests, CSFAcuity differed by group after adjusting for age (F(1,15) = 9.744, p = 0.007), with higher CSFAcuity in EM than MYOP (difference = 5.813, SE = 1.862, 95% CI [1.844, 9.783]). Group differences were not detected for SFPeak (p = 0.999), CSPeak (p = 0.424), or AUCLCSF (p = 0.677). Age was positively associated with larger CSPeak (p = 0.005) and AUCLCSF (p = 0.016), and showed a trend for larger SFPeak (p = 0.064).

Table 8. 1 Central CSF estimated marginal means (EMMs) by refractive group (emmetropia = EM, myopia = MYOP).
SE = Spherical Equivalent.

Outcome	EM (SE)	MYOP (SE)	EM–MYOP diff	p (Bonf.)
Age-only model (Age = 11.226)				
SFPeak	2.645 (0.171)	2.644 (0.171)	0	0.999
CSPeak	2.453 (0.063)	2.380 (0.063)	0.073	0.424
AUCLCSF	2.728 (0.171)	2.624 (0.171)	0.103	0.677
CSFAcuity	21.079 (1.314)	15.266 (1.314)	5.813	0.007
Age + AXL model (Age = 11.226; AXL = 23.978)				
SFPeak	2.581 (0.224)	2.707 (0.224)	-0.126	0.741
CSPeak	2.387 (0.078)	2.446 (0.078)	-0.059	0.658
AUCLCSF	2.537 (0.211)	2.815 (0.211)	-0.278	0.441
CSFAcuity	19.914 (1.660)	16.430 (1.660)	3.484	0.228

In the sensitivity analysis where we additionally adjusted for AXL, the multivariate effect of refractive group remained non-significant (Pillai's trace = 0.141, $F(4,11) = 0.450$, $p = 0.771$), and no univariate group effects were significant (all $p \geq 0.228$), including CSFAcuity ($F(1,14) = 1.587$, $p = 0.228$) (Table 8.1). Age remained significantly associated with CSPeak ($p = 0.003$) and AUCLCSF ($p = 0.009$), whereas AXL was not a significant predictor of any outcome (all $p \geq 0.167$). Thus, the central CSFAcuity group difference observed in the age-only model was not robust to adjustment for AXL.

For peripheral CSF, the multivariate effect of refractive group was not significant (Pillai's trace = 0.278, $F(4,10) = 0.960$, $p = 0.470$) (Table 8.2). Univariate tests showed no significant group differences for SFPeak ($p = 0.271$), CSPeak ($p = 0.132$), or AUCLCSF ($p = 0.502$).

CSFAcuity showed a trend toward higher values in EM ($F(1,13) = 3.839$, $p = 0.072$). Age was not a significant predictor ($p = 0.768$), and when AXL was added, the multivariate effect of refractive group remained non-significant (Pillai's trace = 0.305, $F(4,9) = 0.986$, $p = 0.462$), and univariate group effects were non-significant for all outcomes (SFPeak $p = 0.365$; CSPeak $p = 0.165$; AUCLCSF $p = 0.942$; CSFAcuity $p = 0.217$) (Table 8.2). Neither age nor AXL significantly predicted peripheral CSF outcomes in these models.

Table 8. 2 Peripheral CSF Estimated Marginal Means (EMMs) by Group.
SE = Spherical Equivalent, EM = Emmetropes, MYOP = Myopes.

Outcome	**EM EMM (SE)**	**MYOP EMM (SE)**	**EM–MYOP difference**	**p (Bonf.)**
Age-only model (Age=11.226)				
SFPeak	2.837 (0.355)	2.293 (0.313)	0.544	0.271
CSPeak	2.750 (0.093)	2.551 (0.082)	0.199	0.132
AUCLCSF	1.320 (0.077)	1.249 (0.068)	0.071	0.502
CSFAcuity	59.922 (6.172)	43.783 (5.441)	16.14	0.072
Age + AXL model (Age=11.236; AXL=24.343)				
SFPeak	2.919 (0.479)	2.229 (0.402)	0.69	0.365
CSPeak	2.796 (0.124)	2.515 (0.104)	0.281	0.165
AUCLCSF	1.287 (0.103)	1.275 (0.087)	0.012	0.942
CSFAcuity	60.224 (8.359)	43.548 (7.027)	16.676	0.217

Effective Field of View (UFOV)

UFOV Threshold Size

At baseline, UFOV Threshold Size increased as a function of eccentricity for both the EM and MYOP cohorts. Across all eccentricities, the MYOP group exhibited higher (worse) thresholds compared to the EM group (Figure 8.4).

Mean threshold size values for the MYOP group worsen from 0.349 at 4°, to 0.460 at 8°, and 0.827 at 16° (medians: 0.220, 0.460, and 0.770, respectively). In contrast, the EM group maintained lower mean thresholds of 0.128 at 4°, 0.190 at 8°, and 0.638 at 16° (medians: 0.115, 0.190, and 0.685, respectively).

Mixed-effects modeling of UFOV Threshold Size (4°, 8°, 16°) demonstrated a significant effect of refractive group and eccentricity, with age included as a covariate. Myopes showed higher (worse) adjusted threshold values than emmetropes (EMM 0.565 vs 0.339; $F(1,12.160) = 10.557$, $p = 0.007$), and UFOV Threshold Size increased with eccentricity (EMMs: 0.238 at 4°, 0.386 at 8°, 0.732 at 16°; $F(2,25.875) = 45.426$, $p < 0.001$).

Pairwise comparisons indicated 16° > 4° ($p < 0.001$) and 16° > 8° ($p < 0.001$), while 4° vs 8° was not significant ($p = 0.110$). The refractive group × eccentricity interaction was not significant ($p = 0.859$), indicating that group differences were relatively consistent across eccentricities.

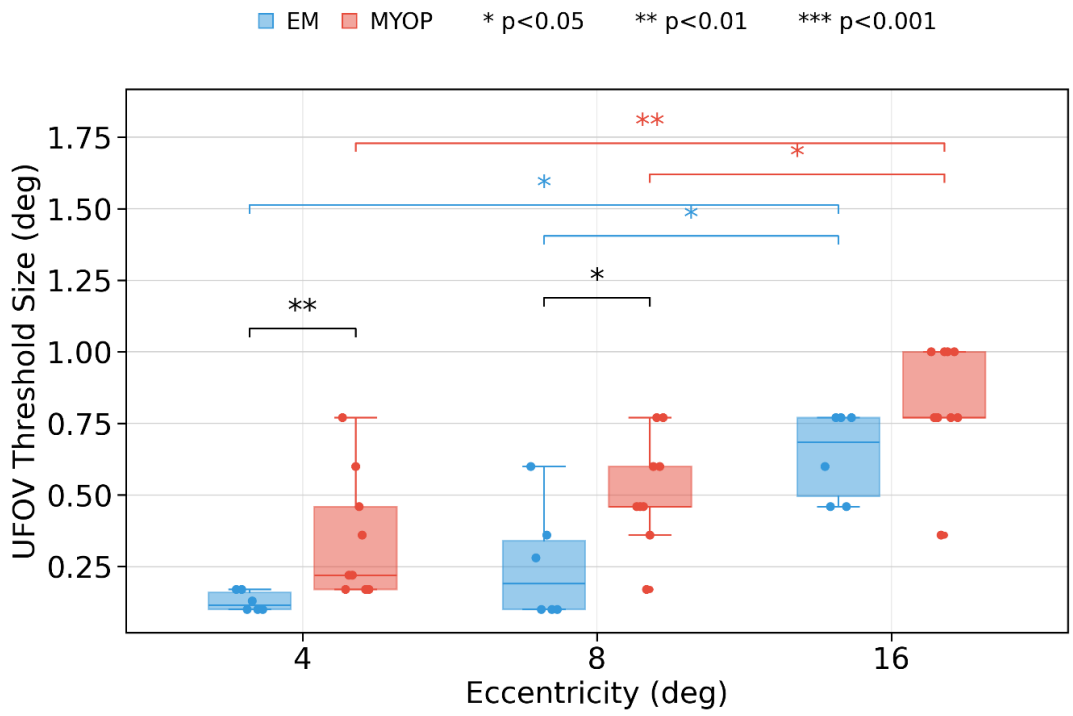

Figure 8. 4 UFOV threshold size at Visit 1 in emmetropic (EM) and myopic (MYOP) participants at 4°, 8°, and 16° eccentricities. Boxplots show the distribution of threshold size values for each group, with individual participant data points overlaid. Blue denotes EM and red-orange denotes MYOP. Horizontal brackets with asterisks indicate significant differences between groups at a given eccentricity or significant within-group differences across eccentricities, where present. Asterisk labels indicate significance level: * $p < 0.05$, ** $p < 0.01$, and *** $p < 0.001$.

UFOV Response Time

Response times also varied significantly across eccentricities, though the spatial patterns diverged notably between the groups (Figure 8.5). In EM, median response times (sec) increased progressively from the central to the peripheral locations (0.055 s at 4°, 0.085 s at 8°, and 0.260 s at 16°). Conversely, the MYOP group demonstrated a non-monotonic temporal profile, with median responses of 0.100 s at 4°, peaking at 0.260 s at 8°, and decreasing back to 0.100 s at 16°.

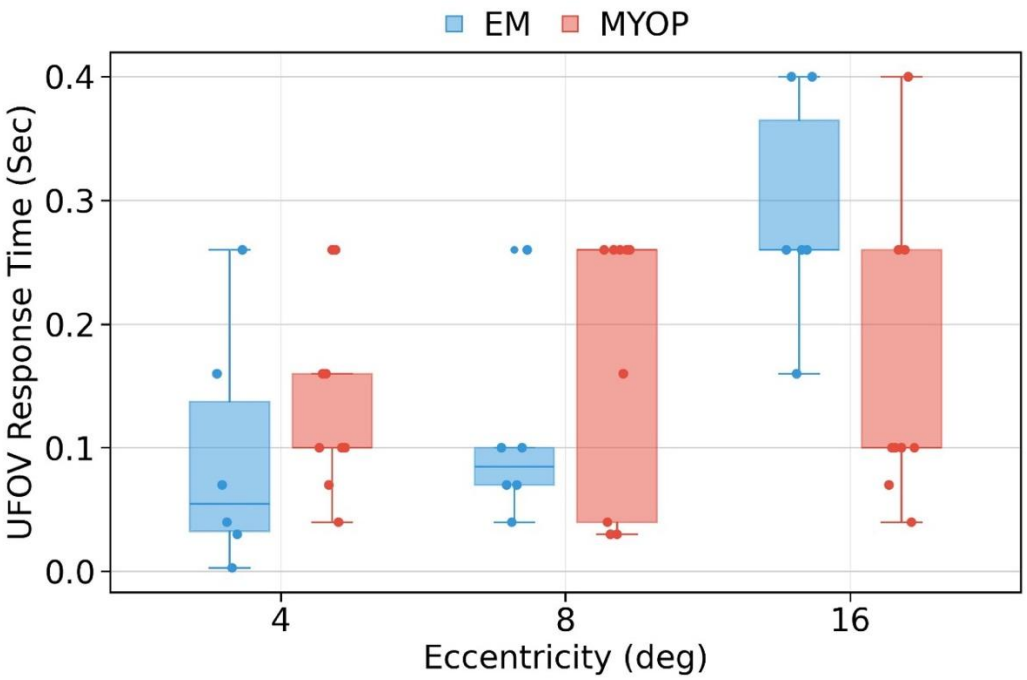

Figure 8. 5 Response time (sec) at Visit 1 in Emmetropic (EM) and Myopic (MYOP) participants at 4°, 8°, and 16° eccentricities. Boxplots show the distribution of UFOV response times for each group at each eccentricity, with EM shown in blue and MYOP shown in red. Boxes represent the interquartile range, the central line indicates the median, whiskers show the spread of the data, and individual points represent each.

For UFOV response time, mixed-effects modeling showed a significant effect of eccentricity ($F(2,20.305) = 5.129$, $p = 0.016$) and a significant refractive group × eccentricity interaction ($F(2,20.305) = 4.897$, $p = 0.018$), with no effect of age ($p = 0.934$). Across participants, response time increased at larger eccentricities (EMMs: 0.116 at 4°, 0.140 at 8°, 0.224 at 16°), with 16° significantly slower than 4° ($p = 0.026$). Importantly, the interaction indicated different eccentricity profiles by refractive group: EM showed a marked increase in response

time at 16° (0.290) relative to 4° and 8°, whereas MYOP showed comparatively stable response times across eccentricities (0.139, 0.173, 0.159).

Multiple Testing Control

To strictly evaluate whether group differences varied by eccentricity across both UFOV outcomes, the Holm sequential decision rule was applied to the Group × Eccentricity interactions ($\alpha = 0.05$). The UFOV–Time interaction remained statistically significant (Holm-adjusted $p = 0.04$), while the UFOV Threshold Size interaction did not (Holm-adjusted $p = 0.86$). This confirms robust distinct peripheral timing strategies utilized by EM and MYOP.

Table 8. 3 Mean ± standard deviation of UFOV Threshold Size (degrees) for the three participants with myopia that completed three visits at 4°, 8°, and 16° eccentricity.

Eccentricity (deg)	Visit 1	Visit 2	Visit 3
4°	0.387 ± 0.333	0.270 ± 0.095	0.200 ± 0.092
8°	0.460 ± 0.000	0.287 ± 0.070	0.333 ± 0.046
16°	0.847 ± 0.133	0.770 ± 0.000	0.770 ± 0.000

Longitudinal Data

The longitudinal dataset included three participants with MYOP who completed UFOV testing across all three study visits. As detailed in Table 8.3 and illustrated in Figure 8.6, UFOV Threshold Size consistently increased at greater eccentricities. For this specific longitudinal subset at baseline (V1), UFOV Threshold Size was 0.387 ± 0.333 at 4°, 0.460 ± 0.000 at 8°, and 0.847 ± 0.133 at 16°.

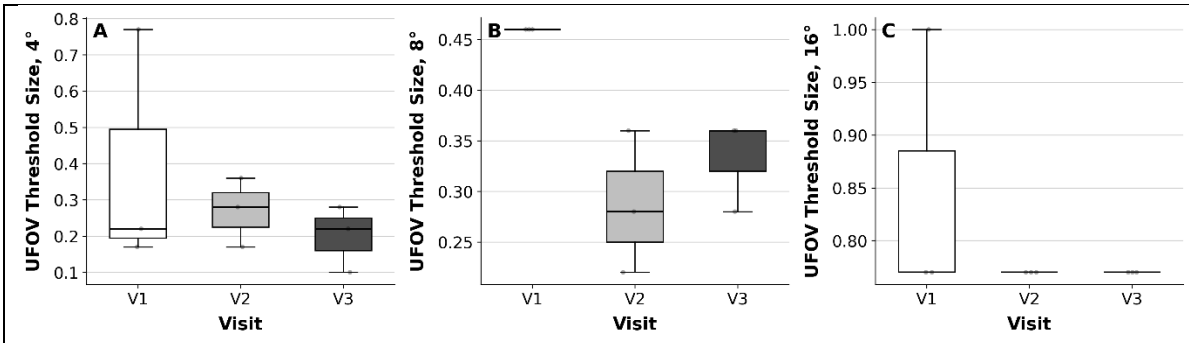

Figure 8. 6 UFOV Threshold Size (degree) measured at 4°, 8°, and 16° eccentricity across three visits (Visit 1–Visit 3). Panel A = 4° eccentricity, Panel B = 8° eccentricity, and Panel C = 16° eccentricity. Data are shown for the three participants with myopia that completed three visits (MCC02, MCC03, MCC05).

Over the 12-month follow-up period, central UFOV Threshold Size (4°) demonstrated a decrease in threshold, indicating improved acuity, from V1 (0.387 ± 0.333) to V3 (0.200 ± 0.092). In contrast, peripheral UFOV Threshold Size at 16° remained relatively stable across the same timeframe (V1 0.847 ± 0.133; V2 0.770 ± 0.000; V3 0.770 ± 0.000).

Regarding temporal processing (Figure 8.7), UFOV response times remained stable across visits at both the 4° (V1 0.140 ± 0.035 s; V2 0.113 ± 0.127 s; V3 0.153 ± 0.092 s) and 8° eccentricity (V1 0.110 ± 0.130 s; V2 0.120 ± 0.123 s; V3 0.117 ± 0.075 s). However, response times at 16° eccentricity slowed notably from baseline (0.090 ± 0.017 s) to follow-ups (V2 0.273 ± 0.121 s; V3 0.207 ± 0.092 s). This reflects a mean within-subject increase in response time of +0.117 s at 16° between V1 and V3 (Table 8.4).

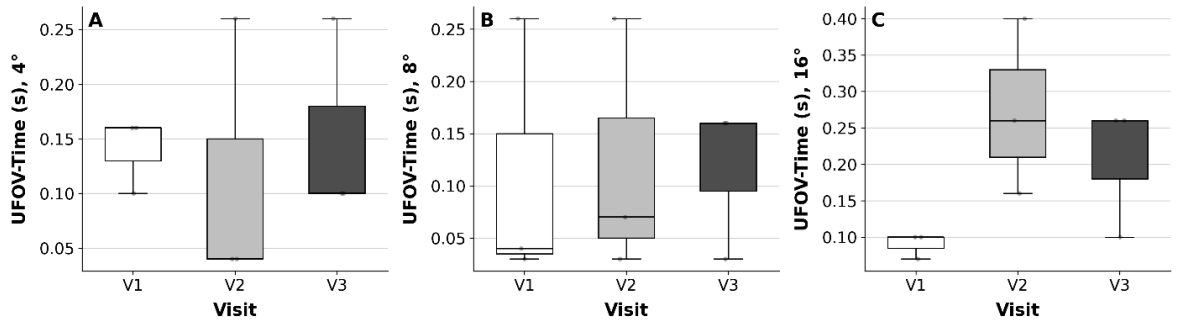

Figure 8. 7 UFOV response time (Time, sec) measured at 4°, 8°, and 16° eccentricity across three visits (Visit 1–Visit 3) in Test3. Panel A = 4° eccentricity, Panel B = 8° eccentricity, and Panel C = 16° eccentricity. Data are shown for the three participants with myopia that completed three visits: MCC02, MCC03, MCC05.

Table 8. 4 Mean ± standard deviation of UFOV response time (seconds) for the three participants with myopia that completed three visits at 4°, 8°, and 16° eccentricity.

Eccentricity (deg)	Visit 1	Visit 2	Visit 3
4°	0.140 ± 0.035	0.113 ± 0.127	0.153 ± 0.092
8°	0.110 ± 0.130	0.120 ± 0.123	0.117 ± 0.075
16°	0.090 ± 0.017	0.273 ± 0.121	0.207 ± 0.092

8.4. Discussion

The psychophysical evaluations in this study were designed to assess whether the optical and structural changes associated with pediatric myopia translate into measurable differences in functional vision and visual attention. For example, by evaluating contrast sensitivity and the effective field of view (UFOV) across central and peripheral retina, we identified distinct functional profiles between myopic and emmetropic children prior to the initiation of myopia control treatments.

Contrast Sensitivity

Our central CSF analysis revealed that participants with MYOP exhibited significantly lower high-spatial-frequency CS (CSF-Acuity) compared to their emmetropic peers when adjusting only for age. However, this functional gap disappeared entirely once AXL was introduced as a covariate. Furthermore, no significant group differences were observed for overarching metrics like the area under the log CSF (AULCSF) or peak contrast sensitivity in either the central or peripheral field. These findings suggest that the fundamental neural mechanisms governing contrast perception remain intact in young MYOP.

The observed reduction in unadjusted central CSF acuity is likely a direct consequence of the elongated eye rather than an inherent neural deficit (Chui et al., 2005). This establishes an important baseline: prior to treatment, these participants with MYOP possess robust contrast processing capabilities that are primarily limited by their ocular anatomy rather than neural attenuation (Vera-Diaz et al., 2025). This resilient functional baseline in children provides an important contrast to studies in young adults, which often report more pronounced degradation of contrast sensitivity, particularly when influenced by myopia-control interventions (Joslin et al., 2003; Kang, McAlinden, & Wildsoet, 2017; Lipson, Boland, & McAlinden, 2022). Research involving young adults has shown that treatments such as orthokeratology and multifocal soft contact lenses increase higher-order aberrations, specifically spherical aberration, which significantly reduces low-contrast visual acuity. For example, orthokeratology decreases corneal asphericity and increases total higher-order aberrations (Ding et al., 2022; Joslin et al., 2003; Kang, McAlinden, & Wildsoet, 2017; Mathur & Atchison, 2009), compromising low-contrast vision even when high-contrast

acuity remains stable. Similarly, multifocal and dual-focus lenses typically induce positive spherical aberration that degrades low-contrast visual acuity (Fedtke et al., 2020; Huang et al., 2022; Lipson, Boland, & McAlinden, 2022; Papadogiannis et al., 2022). Ultimately, the stability of the baseline CSF observed in this pediatric group indicates that children begin from a highly robust functional foundation before facing the optical degradation inherent to these myopia-control treatments.

Effective Field of View (UFOV)

The UFOV task provided critical insights into how these children process peripheral information. Consistent with previous reports (Chui et al., 2005), acuity thresholds increased (worsened) as stimuli moved further into the periphery (from 4° to 16°) for all participants. Interestingly, participants with MYOP demonstrated persistently higher (worse) UFOV Threshold Size than those with emmetropia across all tested eccentricities. Because the central foveal target and the peripheral target were always the exact same size and scaled together simultaneously, this task required active, distributed spatial resolution. The lack of a significant Group × Eccentricity interaction for the threshold indicates that the functional gap between MYOP and EM is relatively constant across the visual field. The MYOP visual system appears to suffer from a generalized depression in simultaneous central-peripheral discrimination. This could be attributed to the retinal stretching that accompanies axial elongation, which decreases the spatial density of peripheral photoreceptors and ganglion cells (Chui et al., 2005; Curcio & Allen, 1990). While previous studies have utilized the UFOV paradigm within the context of MYOP, they have predominantly focused on assessing the visual impact of optical interventions rather than evaluating baseline anatomical or

refractive differences. For example, investigations by Gao et al. demonstrated that wearing highly aspherical lenslets spectacles did not significantly degrade UFOV performance or peripheral visual processing in myopic individuals when compared to standard single-vision lenses (Gao et al., 2021). However, to the best of our knowledge, there are no previous studies that have directly compared the UFOV Threshold Size and temporal processing strategies between children with MYOP and EM.

The most noticeable psychophysical finding emerged from the UFOV temporal data. Importantly, this task did not measure user reaction time; instead, it dynamically tracked the threshold stimulus duration required for accurate identification (correct versus incorrect responses) of whether the targets shared the same identity. Children in each refractive group employed fundamentally different temporal strategies to process these peripheral stimuli. Children with EM exhibited a clear accuracy-driven adaptation: as the target moved to the far periphery (16°), the minimum stimulus duration required for them to accurately discriminate the targets increased significantly and progressively (from 0.055 s at 4° to 0.085 s at 8°, reaching 0.260 s at 16°). This suggests that young children with emmetropia can reliably scale their required processing time to match the increased cognitive and sensory demands of far-peripheral tasks, a well-documented compensatory mechanism in visual search and spatial attention paradigms (Carrasco et al., 1995).

In contrast, participants with MYOP demonstrated a non-monotonic temporal profile across eccentricities. Rather than requiring progressively longer stimulus exposures to manage the hardest targets, their median threshold stimulus durations peaked at 8° (0.260 s) before dropping abruptly at 16° (0.100 s). This significant interaction indicates that myopes fail to

appropriately allocate additional processing time to the most challenging far-peripheral stimuli. Instead of utilizing longer stimulus exposure times to extract difficult information at 16°, myopes attempted to process these far-peripheral targets with the same brief temporal exposures as central targets. This is an inefficient and erratic spatial-temporal strategy that likely contributes heavily to their elevated, and therefore worse, peripheral thresholds.

A review of current literature reveals that while the UFOV paradigm and peripheral temporal assessments are frequently utilized to evaluate older adult driving safety (Owsley et al., 1998), cognitive load under simulated myopic defocus (Michaud, Giraudet, & Roumes, 2021), or general athletic performance (Murphy & Spencer, 2017), there is a distinct lack of studies directly reporting baseline UFOV threshold stimulus durations across eccentricities in children with MYOP.

Because direct comparisons of pediatric temporal processing are absent from the literature, these findings offer novel evidence that, even prior to optical intervention, the young myopic visual system exhibits fundamentally altered temporal processing and compromised adaptive stimulus duration strategies when confronted with complex visual tasks (Mohanraj & Karthikeyan, 2017; Vera-Diaz, Moore, & Bex, 2018).

Longitudinal Trends and Limitations in Peripheral Processing

In the exploratory longitudinal subset of participants with MYOP that completed three visits (n=3), central UFOV Threshold Size (4°) showed slight improvement, while far-peripheral threshold (16°) remained stable. Concurrently, response times stayed consistent at 4° and 8° but slowed notably at 16° (+0.117 s increase from Visit 1 to Visit 3). This localized slowing

of UFOV response times implies that far-peripheral visual tasks may be uniquely sensitive to longitudinal shifts in attentional demand, cognitive fatigue, or search strategies.

However, these findings must be interpreted strictly as descriptive trends because the longitudinal data reflects only three participants and exhibits substantial variability. Therefore, these results do not currently provide evidence of a reliable visit effect. Once a larger cohort completes their follow-up visits, a formal repeated-measures framework, such as mixed-effects modeling, can be conducted to separate true within-subject longitudinal changes from standard between-subject variance.

Clinical Implications for Myopia Control

The visual performance tests in this study reveal an important contrast in the early myopic visual system: basic contrast vision is completely preserved, but there are already significant weaknesses in peripheral vision and attention. Recognizing which visual functions are normal and which are impaired provides a vital framework for predicting how children will adapt to myopia treatments.

First, our findings confirm that the fundamental neural mechanisms governing contrast perception appear to remain intact in young children with early-to-moderate MYOP (Vera-Diaz et al., 2025). Once the physical length of the eye is accounted for, there are no significant differences between participants with MYOP and those with EM on any overall measure of central or peripheral CS (Chui et al., 2005). This absence of a neural deficit establishes a highly resilient clinical baseline. Unlike young adults, who often experience a noticeable drop in low-contrast vision when exposed to the increased HOAs caused by

orthokeratology and multifocal contact lenses (Ding et al., 2022; Joslin et al., 2003; Kang, McAlinden, & Wildsoet, 2017; Lipson, Boland, & McAlinden, 2022; Mathur & Atchison, 2009), children in this study began treatment with a strong, healthy visual foundation. Understanding that their baseline contrast sensitivity is primarily limited by ocular anatomy rather than an inherent neural impairment allows clinicians to safely monitor how a child neurally adapts to the intentional optical degradation required for myopia control.

In contrast to their preserved foundational vision, significant behavioral differences emerge when evaluating the peripheral visual system and higher-order visual attention. As detailed earlier, children with MYOP not only exhibit a generalized depression in threshold size at 4 and 8 degrees but also utilize a fundamentally altered, inefficient temporal processing strategy (Mohanraj & Karthikeyan, 2017; Vera-Diaz, Moore, & Bex, 2018). Unlike their EM peers, participants with MYOP failed to adopt an adaptive duration-scaling strategy and instead process demanding far-peripheral targets at the same rapid pace used for simple central targets, thereby compromising their ability to extract complex peripheral information even before optical treatment begins (Carrasco et al., 1995).

This combination of strong central contrast vision but compromised side vision and processing timing would directly influence how a child will respond to optical therapies. As discussed above, treatments such as orthokeratology, multifocal soft contact lenses, and highly aspheric spectacle lenses function precisely by intentionally altering peripheral image quality and inducing myopic defocus to slow eye growth (Ding et al., 2022; Huang et al., 2022; Kang, McAlinden, & Wildsoet, 2017; Lipson, Boland, & McAlinden, 2022; Mathur & Atchison, 2009; Nti & Berntsen, 2020; Papadogiannis et al., 2022; Song et al., 2021). If a

young MYOP visual system already starts from a depressed functional baseline in the periphery and lacks the adaptive strategy to slow down for challenging peripheral stimuli, imposing additional peripheral blur could further exacerbate their impaired spatial awareness or visual search behaviors. Understanding this split between intact basic contrast processing and pre-existing behavioral weaknesses in the periphery will be crucial for predicting which children might struggle to adapt to specific optical interventions, ultimately paving the way for more personalized myopia control strategies.

9. General Discussion

The primary aim of this thesis was to characterize ocular structure and visual function in children with early-to-moderate myopia before and after they enroll in myopia-control treatment, and to explore whether baseline anatomical or functional features might help explain subsequent treatment-related changes. Although the study was designed as a prospective longitudinal investigation, the limited number of participants completing repeated follow-up visits means that the most robust conclusions are derived from the baseline comparisons between the myopic and emmetropic cohorts. Even with that limitation, the combined structural, optical, electrophysiological, and psychophysical data provide an integrated view of how early pediatric myopia differs from emmetropia before substantial treatment exposure.

9.1. Pediatric myopia is marked by elongation, no overall structural compromise

Across the biometric analyses, the most consistent anatomical difference between groups was axial elongation. Children with myopia showed longer axial dimensions centrally and at the measured nasal and temporal eccentricities, indicating that eye growth in this cohort was already detectable not only on-axis but also within the near peripheral retina. In contrast, anterior segment dimensions such as central corneal thickness, anterior chamber depth, and lens thickness remained largely comparable between refractive groups. Similarly, posterior corneal eccentricity, posterior corneal volume, and CH did not differ significantly at baseline, although posterior corneal astigmatism showed greater variability in the myopic group. Together, these findings suggest that early pediatric myopia in this sample was defined

primarily by elongation of the globe rather than by broad disruption of anterior segment architecture or corneal biomechanics.

This structural pattern extended to the posterior segment. Wide-field OCT showed the expected eccentricity-dependent topography for both choroidal and retinal thickness, but no statistically reliable baseline differences between myopic and emmetropic children. The choroid and retina therefore appeared topographically normal, despite the longer AXL of the myopic eyes. When considered together with the preserved pERG responses described below, these findings support the view that early-to-moderate pediatric myopia is not yet characterized by gross posterior tissue attenuation. Rather, substantial retinal and choroidal thinning may emerge later, as a consequence of more advanced or prolonged axial stretching.

9.2. Optical quality differences were selective and spatially organized

The optical data showed that the visual consequences of early myopia were not uniform across metrics. DEF was the clearest baseline optical discriminator between groups: myopic eyes showed higher DEF overall, and the magnitude of the difference depended on retinal area. This indicates that the off-axis optical environment of the myopic eye is already spatially distinct in childhood, even before long-term treatment follow-up can be evaluated. Because many myopia-control interventions act by modifying peripheral image quality, this regional organization of baseline DEF is clinically important. It suggests that children do not enter treatment with identical peripheral optics, and that baseline optical geometry may shape how a given intervention is experienced by the visual system.

The higher-order aberration findings were more nuanced. Horizontal coma showed only weak evidence of an overall group effect and no area-dependent interaction, while primary SA varied by retinal area but did not differ significantly between refractive groups. The Strehl metrics added another layer: Strehl Ratio inclusive of all aberrations showed significant effects of group, area, and their interaction, with the emmetropic group generally demonstrating higher overall Strehl ratios, a difference that grew more pronounced moving from the temporal to the nasal retina. Conversely, Strehl Ratio including only high-order aberrations did not show a main refractive-group effect, but it did show a strong Group × Area interaction. Differences in the high-order Strehl ratio were complex and region-specific: the myopic group exhibited superior high-order optical quality in the near temporal periphery, but poorer quality in the nasal periphery.

Taken together, these results suggest that optical quality in early myopia is not simply globally degraded. Instead, it is redistributed across the visual field in a location-dependent way, with different metrics capturing different aspects of that redistribution. This distinction is important. The optical profile of the myopic eyes in this cohort cannot be reduced to a single statement such as “poorer optical quality” or “more aberrations”. A more accurate conclusion is that early myopia was associated with selective, regional changes in peripheral defocus and Strehl-based image quality, whereas foundational high-order aberrations remained broadly similar between groups. That pattern is more compatible with a spatial reorganization of optics than with generalized optical failure.

9.3. Neural encoding of contrast appeared preserved, unlike peripheral vision processing

A major strength of this thesis is that it did not stop at anatomy and optics, but also evaluated how these differences relate to visual function. The electrophysiological data indicated that retinal neural encoding remained largely intact in early pediatric myopia. In the pERG experiment, response density declined with eccentricity as expected, but there was no significant main effect of refractive group and no group-by-eccentricity interaction. Latency also showed no significant group difference. Thus, despite axial elongation and regional optical differences, the retina's electrophysiological response to the naturalistic stimulus remained comparable between groups at baseline.

The contrast sensitivity results were similarly reassuring. The central CSF model adjusted only for age detected a group difference in CSF acuity, but that effect disappeared once AXL was added to the models. No robust group differences were detected in broader central or peripheral CSF metrics. In practical terms, this suggests that contrast processing in these children was largely preserved, and that any apparent central acuity reduction was better explained by anatomical elongation than by a broader sensory deficit. The functional foundation of the myopic visual system therefore appears relatively intact in early disease.

The clearest functional group differences instead emerged in the UFOV task. Children with myopia showed worse peripheral acuity thresholds overall, and their temporal response pattern differed from that of emmetropes. Emmetropic children slowed substantially at 16°, suggesting a speed–accuracy trade-off when the peripheral discrimination demand increased. Myopic children, in contrast, showed relatively stable response times across eccentricities,

despite worse acuity thresholds. This pattern suggests that the main behavioral difference in this cohort was not a generalized slowing or a broad sensory loss, but a different peripheral processing strategy. That interpretation has direct clinical relevance, because myopia-control optics often deliberately degrade or redistribute peripheral image quality. A child who already shows reduced peripheral discrimination or less adaptive temporal allocation may respond differently to such treatments than a child whose peripheral processing is more flexible.

9.4. An integrated interpretation: preservation centrally, vulnerability peripherally

When the findings from all chapters are considered together, a coherent pattern emerges. Central and foundational aspects of ocular function were largely preserved in early pediatric myopia: anterior segment morphology was stable, retinal and ChT profiles were not significantly altered, pERG responses remained intact, and contrast sensitivity was broadly comparable once AXL was accounted for. At the same time, the periphery appeared to be the domain in which group differences were most evident. AXL differences extended off-axis, peripheral DEF and Strehl profiles differed by location, and behavioral performance during peripheral visual tasks was reduced and strategically different in the myopic group.

This distinction between preserved central function and altered peripheral structure-optics-behavior may be especially important for myopia control. Current interventions are typically designed around peripheral image manipulation, yet the present findings suggest that the peripheral visual system in children with myopia is not equivalent to that of emmetropic children even before treatment. Accordingly, treatment efficacy and adaptation may depend not only on the imposed optical design, but also on the child's pre-existing peripheral optical

profile and perceptual strategy. The present data do not yet prove predictive utility, but they provide a rationale for treating these baseline peripheral measures as candidate biomarkers of treatment response.

9.5. Longitudinal observations were suggestive, but remain preliminary

The longitudinal component of the thesis offers useful early observations, but it must be interpreted carefully. In the myopic cohort, AXL increased descriptively over follow-up, while most broad ocular structural measures remained statistically stable. The one parameter that did show a significant longitudinal effect in formal modeling was posterior corneal eccentricity, which decreased modestly over time. This result suggests that some subtle anterior segment remodeling may accompany progression and treatment, but the effect should not be overstated given the limited number of repeated observations.

The same caution applies to the optical and psychophysical longitudinal findings. In the subset with three visits, DEF decreased descriptively over time, SA showed a small upward trend, SR including all aberrations improved slightly, and UFOV response times at 16° became slower at follow-up. These patterns are interesting and qualitatively consistent with treatment-related optical changes and altered peripheral processing demands, but they remain descriptive only. With follow-up data dropping from 11 participants at baseline to 5 at 6 months and 3 at 12 months for several analyses, the study was underpowered to determine whether these trajectories reflect true treatment effects, normal developmental variability, treatment heterogeneity, or selective return of specific participants.

For that reason, the longitudinal data in this thesis are best viewed as pilot signals rather than confirmatory evidence. They indicate where treatment-related changes may occur first, particularly in peripheral optics and behavior, but they do not yet allow strong statements about efficacy, mechanism, or causality.

9.6. Predictive implications

A secondary goal of the thesis was to assess whether baseline ocular or functional characteristics might help predict treatment effectiveness. At this stage, the available data do not support a reliable predictive role for the baseline structural metrics that were tested. No significant correlations were found between baseline biometric or corneal variables and subsequent axial elongation. However, the absence of significant predictors should not be interpreted as evidence that prediction is impossible. Rather, it more likely reflects the combination of modest sample size, attrition, treatment heterogeneity, and limited longitudinal power.

Even so, the current results point to more promising candidates for future predictive models. The regional organization of peripheral DEF, the location-dependent Strehl differences, the greater variability in posterior corneal astigmatism, and the altered UFOV strategy all represent biologically plausible markers of how an individual child may experience and adapt to myopia-control optics. These measures may prove more informative than gross baseline anatomy alone once larger treatment-specific datasets are available.

9.7. Limitations

Several limitations must be acknowledged. First, the study was feasibility-driven and the final sample sizes were small, particularly for longitudinal analyses. Attrition was substantial, and the number of returning myopic participants was reduced to five at 6 months and three at 12 months in several chapters. This sharply limited power to detect within-subject change. Second, the emmetropic group completed only one visit, so normal developmental or repeat-testing changes could not be separated from treatment-related changes in longitudinal comparisons. Third, the myopia group was heterogeneous with respect to treatment modality, and orthokeratology was represented by very few participants, limiting any modality-specific interpretation. Fourth, some measures were only available in subsets of participants, such as off-axis biometry in a smaller emmetropic sample, which constrains the generalizability of some baseline comparisons. Finally, the emmetropic cohort was assembled across two recruitment periods and from somewhat different data sources, which may have introduced additional variability even though the protocols were aligned as closely as possible.

9.8. Future directions

Future work should prioritize larger, better-retained cohorts with balanced longitudinal follow-up and sufficient numbers within each treatment modality to permit treatment-specific modeling. The most valuable next step will likely be an integrated longitudinal framework in which axial growth, regional optics, posterior structure, and peripheral visual behavior are analyzed together rather than in isolation. Such an approach would be well suited to testing

whether children with particular peripheral optical profiles or behavioral strategies adapt more successfully to specific myopia-control designs.

A second important direction is to refine the concept of functional biomarkers. The present thesis suggests that peripheral temporal strategy and spatially organized optical measures may be more sensitive than gross baseline anatomy for understanding individual response to treatment. Future studies should therefore examine whether these measures are reproducible, whether they predict adherence or adaptation, and whether they can guide more personalized selection of optical versus pharmacological therapies.

10.Conclusions

In summary, this thesis shows that early-to-moderate pediatric myopia is characterized primarily by axial elongation and region-dependent changes in peripheral optics, while much of the eye's gross structure, retinal thickness profile, corneal biomechanics, contrast sensitivity, and retinal electrophysiological function remain preserved. The most prominent functional differences were observed not in central neural integrity, but in peripheral visual performance and temporal processing strategy. These findings suggest that the early myopic eye is not broadly compromised, but selectively different in ways that are highly relevant to therapies that act through peripheral optical manipulation. Although the longitudinal component was limited, the combined results provide a useful framework for understanding how baseline ocular structure and peripheral visual function may contribute to individual variation in adaptation to myopia-control treatment.

11. Bibliography

Alonso-Caneiro, D., Read, S.A., & Collins, M.J. (2011). Speckle reduction in optical coherence tomography imaging by affine-motion image registration. Journal of Biomedical Optics, 16(11): 116027.

Amorim-de-Sousa, A., Pauné, J., Silva-Leite, S., Fernandes, P., González-Méijome, J.M., & Queirós, A. (2023). Changes in Choroidal Thickness and Retinal Activity with a Myopia Control Contact Lens. Journal of Clinical Medicine, 12(11): 3618.

An, W., Wei, S., Li, S.M., Cao, K., Hu, J., Lin, C., et al. (2025). Significant Loss of Coordination Among Astigmatism Components in Young Chinese Adults with High Myopia. Translational Vision Science and Technology, 14(5): 26.

Atchison, D.A., Pritchard, N., & Schmid, K.L. (2006). Peripheral refraction along the horizontal and vertical visual fields in myopia. Vision Research, 46(8-9): 1450-1458.

Atchison, D.A., Pritchard, N., Schmid, K.L., Scott, D.H., Jones, C.E., & Pope, J.M. (2004). Eye shape in emmetropia and myopia. Investigative Ophthalmology and Visual Science, 45(10): 3380-3386.

Bao, J., Yang, A., Huang, Y., Li, X., Pan, Y., Ding, C., et al. (2022). One-year myopia control efficacy of spectacle lenses with aspherical lenslets. British Journal of Ophthalmology, 106(8).

Berntsen, D.A. (2018). Retinal image quality after orthokeratology. Investigative Ophthalmology and Visual Science, 59(9).

Carrasco, M., Evert, D.L., Chang, I., & Katz, S.M. (1995). The eccentricity effect: target eccentricity affects performance on conjunction searches. Perception and Psychophysics, 57(8): 1241-1261.

Chan, H.H.L., Choi, K.Y., Ng, A.L.K., Choy, B.N.K., Chan, J.C.H., Chan, S.S.H., et al. (2022). Efficacy of 0.01% atropine for myopia control in a randomized, placebo-controlled trial depends on baseline electroretinal response. Scientific Reports, 12(1): 11588.

Chang, P.Y., Chang, S.W., & Wang, J.Y. (2010). Assessment of corneal biomechanical properties and intraocular pressure with the Ocular Response Analyzer in childhood myopia. British Journal of Ophthalmology, 94(7): 877-881.

Chen, D., Lam, A.K., & Cho, P. (2009). A pilot study on the corneal biomechanical changes in short-term orthokeratology. Ophthalmic and Physiological Optics, 29(4): 464-471.

Chen, J.C., Brown, B., & Schmid, K.L. (2006). Delayed mfERG responses in myopia. Vision Research, 46(8-9): 1221-1229.

Chen, Y., Zheng, C., Zhu, R., Dong, L., Cen, J., Yu, J., et al. (2022). Assessing the efficacy of myopia control in monocular orthokeratology treated unilateral myopic children. BMC Ophthalmology, 22(1).

Chui, T.Y.P., Yap, M.K.H., Chan, H.H.L., & Thibos, L.N. (2005). Retinal stretching limits peripheral visual acuity in myopia. Vision Research, 45(5): 593-605.

Cooper, J., Eisenberg, N., Schulman, E., & Wang, F.M. (2013). Maximum atropine dose without clinical signs or symptoms. Optometry and Vision Science, 90(12).

Corpus, G., & Piñero, D.P. (2022). Short-Term Effect of Wearing of Extended Depth-of-Focus Contact Lenses in Myopic Children: A Pilot Study. Applied Sciences, 12(1).

Curcio, C.A., & Allen, K.A. (1990). Topography of ganglion cells in human retina. Journal of Comparative Neurology, 300(1): 5-25.

Ding, C., Chen, Y., Li, X., Huang, Y., Chen, H., & Bao, J. (2022). The associations of accommodation and aberrations in myopia control with orthokeratology. Ophthalmic and Physiological Optics, 42(2).

Faria-Ribeiro, M., Queirós, A., Lopes-Ferreira, D., Jorge, J., & González-Méijome, J.M. (2013). Peripheral refraction and retinal contour in stable and progressive myopia. Optometry and Vision Science, 90(1): 9-15.

Fedtke, C., Bakaraju, R.C., Ehrmann, K., et al. (2020). Visual performance of single vision and multifocal contact lenses in myopic children. Contact Lens and Anterior Eye, 43(3): 264-272.

Fernandes, P., Marinho, B., Alves-de-Carvalho, R.S., & González-Méijome, J.M. (2026). Short-Term Changes in Retinal Activity With Four Myopia Control Spectacle Lenses. Translational Vision Science and Technology, 15(3): 11.

Fontaine, M., Gaucher, D., Sauer, A., & Speeg-Schatz, C. (2017). Choroidal thickness and ametropia in children: A longitudinal study. European Journal of Ophthalmology, 27(6): 730-734.

Gao, Y., Lim, E.W., Yang, A., Drobe, B., & Bullimore, M.A. (2021). The impact of spectacle lenses for myopia control on visual functions. Ophthalmic and Physiological Optics, 41(6): 1320-1331.

González-Méijome, J.M., Villa-Collar, C., Queirós, A., Jorge, J., & Parafita, M.A. (2008). Pilot study on the influence of corneal biomechanical properties over the short term in response to corneal refractive therapy for myopia. Cornea, 27(4): 421-426.

Gupta, S.K., Chakraborty, R., & Verkicharla, P.K. (2022). Electroretinogram responses in myopia: a review. Documenta Ophthalmologica, 145.

Ha, A., Kim, S.J., Shim, S.R., Kim, Y.K., & Jung, J.H. (2022). Efficacy and Safety of 8 Atropine Concentrations for Myopia Control in Children: A Network Meta-Analysis. Ophthalmology, 129(3).

Han, X., Xu, D., Ge, W., Wang, Z., Li, X., & Liu, W. (2018). A Comparison of the Effects of Orthokeratology Lens, Medcall Lens, and Ordinary Frame Glasses on the Accommodative Response in Myopic Children. Eye and Contact Lens, 44(4).

Ho, W.C., Kee, C.S., & Chan, H.H. (2012). Myopia progression in children is linked with reduced foveal mfERG response. Investigative Ophthalmology and Visual Science, 53(9): 5320-5325.

Holden, B.A., Fricke, T.R., Wilson, D.A., Jong, M., Naidoo, K.S., Sankaridurg, P., et al. (2016). Global Prevalence of Myopia and High Myopia and Temporal Trends from 2000 through 2050. Ophthalmology, 123(5): 1036-1042.

Hoseini-Yazdi, H., Vincent, S.J., Collins, M.J., Read, S.A., & Alonso-Caneiro, D. (2019). Wide-field choroidal thickness in myopes and emmetropes. Scientific Reports, 9(1): 3474.

Hu, Y., Wang, Y., Du, Z., Zhu, S., Xiong, L., Fang, X., et al. (2025). Correlations of anterior and posterior corneal parameters in Chinese myopic patients: a retrospective multicenter study. Quantitative Imaging in Medicine and Surgery, 15(1): 88-102.

Huang, Y., Li, X., Ding, C., Chen, Y., Mao, X., Chen, H., et al. (2022). Comparison of peripheral refraction and higher-order aberrations between orthokeratology and multifocal soft contact lens designed with highly addition. Graefe's Archive for Clinical and Experimental Ophthalmology, 260(5).

Jin, P., Zou, H., Zhu, J., et al. (2016). Choroidal and Retinal Thickness in Children with Different Refractive Status Measured by Swept-Source Optical Coherence Tomography. American Journal of Ophthalmology, 168: 164-176.

Joslin, C.E., Wu, S.M., McMahon, T.T., & Kaupke, C. (2003). Higher-order wavefront aberrations in corneal refractive therapy. Optometry and Vision Science, 80(12): 805-811.

Kader, M.A. (2012). Electrophysiological study of myopia. Saudi Journal of Ophthalmology, 26(1): 91-99.

Kang, P., McAlinden, C., & Wildsoet, C.F. (2017). Effects of multifocal soft contact lenses used to slow myopia progression on quality of vision in young adults. Acta Ophthalmologica, 95(1).

Koh, V., Tan, C., Nah, G., Zhao, P., Yang, A., Lin, S.T., et al. (2014). Correlation of structural and electrophysiological changes in the retina of young high myopes. Ophthalmic and Physiological Optics, 34(6): 658-666.

Lam, C.S.Y., Tang, W.C., Qi, H., Radhakrishnan, H., Hasegawa, K., To, C.H., et al. (2020). Effect of defocus incorporated multiple segments spectacle lens wear on visual function in myopic chinese children. Translational Vision Science and Technology, 9(9).

Lee, S.H., Tsai, P.C., Chiu, Y.C., Wang, J.H., & Chiu, C.J. (2025). Impact of orthokeratology and low-dose atropine on corneal biomechanics and myopia progression in children. Ophthalmic and Physiological Optics, 45(2): 565-576.

Li, X., Huang, Y., Liu, C., Chang, X., Cui, Z., Yang, Q., et al. (2025). Myopia control efficacy of spectacle lenses with highly aspherical lenslets: results of a 5-year follow-up study. Eye and Vision, 12(1): 10.

Lian, Y., Shen, M., Huang, S., et al. (2023). Comparison of visual performance between peripheral gradient high-addition multifocal soft contact lenses and orthokeratology. Ophthalmic and Physiological Optics, 43(4): 874-884.

Lipson, M.J., Boland, B., & McAlinden, C. (2022). Vision-related quality of life with myopia management: A review. Contact Lens and Anterior Eye, 45.

Lu, Y., Lin, Z., Wen, L., Gao, W., Pan, L., Li, X., et al. (2020). The Adaptation and Acceptance of Defocus Incorporated Multiple Segment Lens for Chinese Children. American Journal of Ophthalmology, 211: 207-216.

Mathur, A., & Atchison, D.A. (2009). Effect of orthokeratology on peripheral aberrations of the eye. Optometry and Vision Science, 86(5).

Michaud, L., Giraudet, G., & Roumes, C. (2021). Increased visual and cognitive demands emphasize the importance of meeting visual needs at all distances while driving. PLoS One, 16(2): e0247254.

Mohanraj, M., & Karthikeyan, T. (2017). Comparison of visual reaction time in myopic patients with emmetropic patients. National Journal of Physiology, Pharmacy and Pharmacology, 7(2): 196-199.

Murphy, C.P., & Spencer, N.D. (2017). The field of view is more useful in golfers than regular exercisers. Advances in Cognitive Psychology, 13(1): 64-69.

Mutti, D.O., Sinnott, L.T., Reuter, K.S., Walline, J.J.; Bifocal Lenses In Nearsighted Kids (BLINK) Study Group. (2019). Peripheral refraction and eye lengths in myopic children in the Bifocal Lenses In Nearsighted Kids (BLINK) study. Translational Vision Science and Technology, 8(2): 17.

National Academies of Sciences, Engineering, and Medicine. (2024). Myopia: causes, prevention, and treatment of an increasingly common disease. Washington (DC): The National Academies Press.

Nickla, D.L., & Wallman, J. (2009). The multifunctional choroid. Progress in Retinal and Eye Research, 29(2): 144.

Nti, A.N., & Berntsen, D.A. (2020). Optical changes and visual performance with orthokeratology. Clinical and Experimental Optometry, 103.

Owsley, C., Ball, K., McGwin, G. Jr., Sloane, M.E., Roenker, D.L., White, M.F., & Overley, E.T. (1998). Visual processing impairment and risk of motor vehicle crash among older adults. JAMA, 279(14): 1083-1088.

Panorgias, A., Aigbe, S., Jeong, E., Otero, C., Bex, P.J., & Vera-Diaz, F.A. (2021). Retinal Responses to Simulated Optical Blur Using a Novel Dead Leaves ERG Stimulus. Investigative Ophthalmology and Visual Science, 62(10): 1.

Papadogiannis, P., Romashchenko, D., Vedhakrishnan, S., Persson, B., Lindskoog Pettersson, A., Marcos, S., et al. (2022). Foveal and peripheral visual quality and accommodation with multifocal contact lenses. Journal of the Optical Society of America A, 39(6): B39.

Park, S., Kim, S.H., Park, T.K., & Ohn, Y.H. (2013). Evaluation of structural and functional changes in non-pathologic myopic fundus using multifocal electroretinogram and optical coherence tomography. Documenta Ophthalmologica, 126(3): 199-210.

Piñero, D.P., & Alcón, N. (2015). Corneal biomechanics: a review. Clinical and Experimental Optometry, 98(2): 107-116.

Plakitsi, A., O'Donnell, C., Miranda, M.A., Charman, W.N., & Radhakrishnan, H. (2011). Corneal biomechanical properties measured with the Ocular Response Analyser in a myopic population. Ophthalmic and Physiological Optics, 31(4): 404-412.

Polling, J.R., Kok, R.G.W., Tideman, J.W.L., Meskat, B., & Klaver, C.C.W. (2016). Effectiveness study of atropine for progressive myopia in Europeans. Eye, 30(7).

Queirós, A., Pereira-Da-mota, A.F., Costa, J., Amorim-De-sousa, A., Fernandes, P.R.B., & González-Méijome, J.M. (2020). Retinal response of low myopes during orthokeratology treatment. Journal of Clinical Medicine, 9(8).

Read, S.A., Alonso-Caneiro, D., & Vincent, S.J. (2017). Longitudinal changes in macular retinal layer thickness in pediatric populations: Myopic vs non-myopic eyes. PLoS One, 12(6): e0180462.

Romashchenko, D., Rosén, R., & Lundström, L. (2020). Peripheral refraction and higher order aberrations. Clinical and Experimental Optometry, 103(1): 86-94.

Sachidanandam, R., Ravi, P., & Sen, P. (2017). Effect of axial length on full-field and multifocal electroretinograms. Clinical and Experimental Optometry, 100(6): 668-675.

Sankaridurg, P., Tahhan, N., Kandel, H., Naduvilath, T., Zou, H., Frick, K.D., et al. (2021). IMI impact of myopia. Investigative Ophthalmology and Visual Science, 62.

Schmid, K.L., Gifford, K.L., & Atchison, D.A. (2023). The effect of concentric and aspheric multifocal soft contact lenses on binocular vision in young adult myopes. Contact Lens and Anterior Eye, 46(1).

Shen, M., Fan, F., Xue, A., Wang, J., Zhou, X., & Lu, F. (2008). Biomechanical properties of the cornea in high myopia. Vision Research, 48(21): 2167-2171.

Song, Y., Congdon, N., Li, L., Zhou, Z., Choi, K., Lam, D.S., et al. (2008). Corneal hysteresis and axial length among Chinese secondary school children: the Xichang Pediatric Refractive Error Study (X-PRES) report no. 4. American Journal of Ophthalmology, 145(5): 819-826.

Song, Y., Zhu, S., Yang, B., Wang, X., Ma, W., Dong, G., et al. (2021). Accommodation and binocular vision changes after wearing orthokeratology lens in 8- to 14-year-old myopic children. Graefe's Archive for Clinical and Experimental Ophthalmology, 259(7).

Spaide, R.F., Koizumi, H., & Pozzoni, M.C. (2008). Enhanced depth imaging spectral-domain optical coherence tomography. American Journal of Ophthalmology, 146(4): 496-500.

Summers, J.A. (2013). The Choroid as a Sclera Growth Regulator. Experimental Eye Research, 114: 120.

Troilo, D., Smith, E.L., Nickla, D.L., Ashby, R., Tkatchenko, A.V., Ostrin, L.A., et al. (2019). IMI – Report on experimental models of emmetropization and myopia. Investigative Ophthalmology and Visual Science, 60(3).

Vera, J., Redondo, B., Galan, T., Machado, P., Molina, R., Koulieris, G.A., et al. (2023). Dynamics of the accommodative response and facility with dual-focus soft contact lenses for myopia control. Contact Lens and Anterior Eye, 46(1).

Vera-Diaz, F.A., Dhungel, D., McCullough, A., Kerber, K.L., & Bex, P.J. (2025). Longitudinal measures of peripheral optical quality in young children. Ophthalmic and Physiological Optics, 45(2): 550-564.

Vera-Diaz, F.A., Liang, C., Curtin, S., & Panorgias, A. (2023). Effect of Atropine Eye Drops on Retinal Responses to Clear and Blurred Images. Poster presented at: ARVO; 2023 April 23-27; New Orleans, LA.

Wan, K., Cheung, S.W., Wolffsohn, J.S., Orr, J.B., & Cho, P. (2018). Role of corneal biomechanical properties in predicting of speed of myopic progression in children wearing

orthokeratology lenses or single-vision spectacles. BMJ Open Ophthalmology, 3(1): e000204.

Weng, R., Lan, W., Bakaraju, R., Conrad, F., Naduvilath, T., Yang, Z., et al. (2022). Efficacy of contact lenses for myopia control: Insights from a randomised, contralateral study design. Ophthalmic and Physiological Optics, 42(6).

Wildsoet, C.F., Chia, A., Cho, P., Guggenheim, J.A., Polling, J.R., Read, S., et al. (2019). IMI – Interventions myopia institute: Interventions for controlling myopia onset and progression report. Investigative Ophthalmology and Visual Science, 60.

Zhang, J.S., Li, J., Wang, J.D., Xiong, Y., Cao, K., Li, M., et al. (2024). The Association of Myopia Progression with Changes in Retinal Thickness among Primary School Students with Myopia. Journal of Ophthalmology, 2024: 1055700.

Zhu, X., Liu, Y., Gao, Y., Zhang, Y., Zhang, Y., & Zhao, Y. (2023). Choroidal thickness in relation to diopter and axial length among myopic children. Frontiers in Medicine, 10: 1241352.

12.Appendix

Table A. 1 IOLMaster 700 biometry results for all participants at each visit. (Corneal Central Thickness = CCT, Anterior Chamber Depth = ACD, Lens Thickness = LT, Central Axial Length = AXL-C, Axial Length at 10° Temporal = AXL-T10, Axial Length at 10° Nasal = AXL-N10). All units are in mm.

Participant ID	Visit 1 (Baseline)					
	CCT	ACD	LT	AXL-C	AXL-T10	AXL-N10
MCC02	0.57	3.75	3.29	24.30	24.27	24.54
MCC03	0.54	3.92	3.31	25.07	24.77	24.91
MCC04	0.53	3.91	3.34	24.78	24.92	24.63
MCC05	0.53	4.23	3.26	26.32	25.91	26.38
MCC06	0.60	3.83	3.17	24.10	23.95	24.17
MCC07	0.53	3.92	3.01	26.04	N/A	N/A
MCC08	0.56	4.39	2.98	25.00	24.49	24.80
MCC09	0.52	3.87	3.26	25.01	24.92	24.90
MCC12	0.62	3.88	3.35	24.20	23.97	24.24
MCC13	0.50	4.03	3.24	25.23	25.13	25.41
MCC14	0.50	3.64	N/A	23.94	23.63	24.17
MCC15	0.53	4.18	3.45	25.26	24.83	25.29
MCC16	0.58	3.53	3.45	24.15	23.73	23.87
EMM07	0.57	3.69	3.58	23.75	23.73	23.71
EMM08	0.55	3.83	3.25	22.40	22.35	22.39
EMM09	0.56	3.38	3.66	23.73	23.63	23.81
EMM10	0.54	3.78	3.69	23.77	23.74	23.80
	Visit 2 (6-month post treatment)					
MCC02	0.57	3.81	3.24	24.26	24.19	24.20
MCC03	0.53	3.93	3.30	25.12	24.83	25.17
MCC05	0.54	4.23	3.30	26.41	26.17	26.43
MCC06	0.60	3.84	3.23	24.35	24.18	24.45
MCC08	0.55	4.42	2.98	25.13	24.90	24.82
	Visit 3 (12-month post treatment)					
MCC02	0.57	2.86	3.21	24.43	24.31	24.60
MCC03	0.54	3.96	3.29	25.27	24.95	25.24
MCC05	0.52	4.25	3.25	26.42	26.13	26.73

Table A. 2 Baseline corneal biomechanical properties and intraocular pressure measurements. Values represent the average of three readings obtained using the Ocular Response Analyzer® G3 for emmetropic and myopic participants at Visit 1.

Note: IOPcc = Corneal Compensated Intraocular Pressure; IOPg = Goldmann-correlated Intraocular Pressure; CH = Corneal Hysteresis; CRF = Corneal Resistance Factor. All measurements are in millimeters of mercury (mmHg).

Participant ID	Visit 1 (Baseline)			
	IOPcc	IOPg	CH	CRF
MCC02	15.70	16.30	11.30	11.40
MCC03	14.50	15.10	11.40	11.10
MCC04	14.30	11.90	9.10	8.20
MCC05	16.40	17.70	11.70	12.20
MCC06	12.80	17.10	14.70	14.50
MCC08	21.00	22.80	11.60	13.70
MCC09	14.30	14.70	11.30	10.90
MCC12	12.10	16.20	14.50	14.10
MCC13	20.40	19.80	9.80	11.20
MCC14	11.40	10.90	11.00	9.60
MCC15	14.70	15.60	11.70	11.60
MCC16	19.70	23.60	13.40	15.40
EMM01	14.00	15.00	11.90	11.50
EMM02	17.60	21.70	13.90	15.30
EMM04	23.20	25.90	12.10	15.00
EMM05	13.10	15.70	13.20	12.90
EMM06	14.70	15.80	11.80	11.60
EMM07	13.60	15.80	12.90	12.60
EMM08	16.20	16.80	11.20	11.50
EMM09	14.00	14.20	11.30	10.80
EMM10	13.90	13.70	10.90	10.30